

**ENGINEERING A HIGH AFFINITY EXTRACELLULAR ATP SENSOR
FOR STUDYING PURINERGIC SIGNALING**

by

Daniel J. Cholger

A Dissertation

Submitted to the Faculty of Purdue University

In Partial Fulfillment of the Requirements for the degree of

Doctor of Philosophy



Department of Chemistry

West Lafayette, Indiana

August 2019

**THE PURDUE UNIVERSITY GRADUATE SCHOOL
STATEMENT OF COMMITTEE APPROVAL**

Dr. Mathew Tantama, Chair

Department of Chemistry

Dr. Jason Cannon

College of Health and Human Sciences

Dr. Estuardo Robles

Department of Biology

Dr. Angeline Lyon

Department of Chemistry

Approved by:

Dr. Christine Hrycyna

Head of the Graduate Program

I dedicate this dissertation to my favorite doctor, Jozlyn Clasman, and our two kitties Independence (Indy) and St. Patrick (Paddy). Without each other and our two kitties, this dissertation might not have been possible. I also would like to dedicate this thesis to my parents for all their help and support over the years as Jozlyn and I went on this grand scientific adventure together.

ACKNOWLEDGMENTS

First, I would like to acknowledge Dr. Mathew Tantama for his guidance and mentorship through this process of cradle to grave sensor design and testing. Second, committee members Dr. Jason Cannon, Dr. Estuardo Robles, and Dr. Angeline Lyon acknowledged for their insightful feedback and guidance through the years. I am thankful for and acknowledge the support from all my fellow Tantama lab members; Dr. Megha Rajendran, Dr. Jason Conley, Dr. Alex French, Dr. Keelan Trull, Dr. Stevie Norcross, Emily Haynes, Saranya Radhakrishnan, Steve Valentino, Jake Norley and Sehong Min. I am particularly thankful for Dr. Jason Conley's patience with me in training me in microscopy and dissection techniques, and his guidance in experiment design. I cannot thank Dr. Megha Rajendran, Dr. Stevie Norcross, Keelan Trull and Emily Haynes enough for their emotional support through this venture. Saranya was willing to help me out with finishing up dissections or viral productions if I could not be present for a part of the protocol, and for that I cannot thank her enough. I thank Keelan, Steve and Jake for their many stimulating discussions about creative problem solving.

Where do I begin for acknowledgements outside of the lab? This entire process has been such a roller coaster ride of ups and downs with support from so many different people over the years. First and foremost is my fiancé Dr. Jozlyn Rose Clasman who graduated a couple months before me and has been with me through this graduate school journey every step of the way. Over halfway through the process and after both of us passed our PULSe preliminary examinations, Jozlyn and I received a new fuzzy little resident in our household; our orange tabby cat Independence (Indy). Indy needed a friend, and Jozlyn and I adopted our second tabby cat shortly after, Saint Patrick. Pat survived a traumatic head injury this past spring 2019, bringing a surprising

amount of personal relevance to the studies described in Chapters 4 and 5. Without Jozlyn, Patty and Indy, I am certain that I would not have persevered through the remainder of the program.

My parents have supported my education for as long as I can remember. I cannot thank them enough for their continuous support through my bachelor's degree and now my doctorate degree. I believe my tenacious work ethic and light-hearted curiosity comes from them and gives me the motivation to keep moving forward in science.

TABLE OF CONTENTS

LIST OF TABLES.....	9
LIST OF FIGURES	10
LIST OF ABBREVIATIONS.....	12
ABSTRACT.....	13
CHAPTER 1. INTRODUCTION	15
1.1 Purinergic Signaling in the Brain.....	15
1.2 Traumatic Brain Injury and Pathologies	17
1.2.1 Mechanical Stimulation and Injury	17
1.2.2 Swelling and Edema	18
1.2.3 Ischemia.....	18
1.2.4 Seizure-like Excitotoxicity	19
1.3 Genetically-Encoded Fluorescent Protein Sensors	19
CHAPTER 2. INCREASING AFFINITY FOR ATP USING CYCLIC MUTANT ANALYSIS	23
2.1 Introduction.....	23
2.2 Materials and Methods.....	25
2.2.1 Q5 Site-directed Mutagenesis.....	25
2.2.2 Protein Expression and Purification	26
2.2.3 Protein Solution ATP dose-response Assays.....	27
2.2.4 Determining Fluorescence Lifetime	27
2.2.5 HEK293A Cell Line Maintenance.....	27
2.2.6 Live-cell Fluorescent Microscopy and Analysis	27
2.2.7 Statistical Analysis.....	29
2.3 Results.....	29
2.3.1 The R103A/R115A double mutant of ATeam3.10 is a high ATP binding affinity mutant	29
2.3.2 Mutation of R103 and R115 can fine tune ATP binding affinity	33
2.3.3 Mutational analysis of ATeam1.03 and ATeamYEMK	34

2.3.4 Fine-tuning ATeam sensor ATP affinity is functionally relevant for live-cell imaging	43
2.4 Discussion	46
CHAPTER 3. EXTRACELLULAR ATEAM OPTIMIZATION	48
3.1 Introduction	48
3.2 Materials and Methods	49
3.2.1 Cloning ER/K Linkers into pMinDis-ecATEam3.10-R103A/R115A	49
3.2.2 Neuro2A Cell Culture and Transfection	49
3.2.3 Live-cell Fluorescent Microscopy and Analysis	51
3.2.4 Statistical Analysis	52
3.3 Results	52
3.4 Discussion	61
CHAPTER 4. ATP RELEASE IN CELLULAR MODEL OF EDEMA	63
4.1 Introduction	63
4.2 Materials and Methods	64
4.2.1 HEK293A Cell Line Maintenance	64
4.2.2 Calcium Phosphate Transfection	65
4.2.3 Live-cell Fluorescent Microscopy	67
4.2.4 Statistical Analysis	68
4.3 Results	68
4.4 Discussion	72
CHAPTER 5. PRIMARY CELL MODELS OF TBI	74
5.1 Introduction	74
5.2 Materials and Methods	76
5.2.1 Cloning Sensors into Lentiviral and Adenoviral Production Plasmids	76
5.2.2 HEK293A Cell Culture and Adenovirus Production	77
5.2.3 HEK293FT Cell Culture and Lentivirus Production	78
5.2.4 Microdissection of Hippocampal Neurons and Cortical Astrocytes	78
5.2.5 Primary Cell Culture of Astrocytes and Neuron-Astrocyte Co-culture	79
5.2.6 Live Cell Fluorescent Microscopy and Analysis	80
5.2.7 Statistical Analysis	81

5.3 Results.....	82
5.3.1 Mechanical stimulation of Cortical Astrocytes	82
5.3.2 Hypo-osmotic shock of Cortical Astrocytes shows ATP release	88
5.3.3 Hypo-osmotic shock of Neuron-Astrocyte Co-culture.....	98
5.3.4 KCN Ischemia	104
5.3.5 Seizure-like Excitotoxicity Models cause no detectable ATP release.....	106
5.4 Discussion.....	109
CHAPTER 6. CONCLUSIONS AND FUTURE PERSPECTIVES	113
6.1 Protein Engineering Perspectives	113
6.2 Using ECATS2 to Study Purinergic Signaling.....	115
REFERENCES	117
VITA	122
PUBLICATIONS.....	125

LIST OF TABLES

Table 1 Mutagenesis Primers for Cyclic Mutant Analysis of ATeam Constructs.....	26
Table 2 ATP affinity of the ATeam3.10 sensor and its mutants	31
Table 3 ATP affinity of the ATeam1.03 sensor and its mutants	37
Table 4 Purinergic Receptors in the Brain.....	114

LIST OF FIGURES

Figure 1.1 Machinery for Purinergic Signaling in the Synapse.....	16
Figure 1.2 Example Structure of the ATeam Family of FRET Sensors	21
Figure 1.3 Diagram Demonstrating Strategy for Targeting ATeam3.10 to the Membrane	22
Figure 2.1 Structure of ATP binding domain in ATeam family of sensors.....	25
Figure 2.2 ATP-dose responses for the ATeam3.10 sensor and its mutants at room temperature	32
Figure 2.3 Mutant cycle analysis of the ATeam3.10 sensor and its mutants.....	34
Figure 2.4 ATP-dose response curves for ATeam1.03 mutants	36
Figure 2.5 ATP-dose response curves for ATeam1.03(YEMK) mutants.....	39
Figure 2.6 Time-resolved CFP donor fluorescence lifetime distribution analysis of ATeamYEMK and its mutants	42
Figure 2.7 Steady-state YFP acceptor fluorescence polarization for ATeamYEMK and its mutants in the absence and presence of ATP	43
Figure 2.8 Live-cell imaging of YEMKwt vs YEMK115E.....	45
Figure 2.9 The lower affinity mutant ATeamYEMK(R115E) is more sensitive to mild metabolic inhibition with deoxyglucose only	46
Figure 3.1 Diagram Demonstrating Approach to Distinguish Two Species of ATeam	50
Figure 3.2 The R103A/R115A Double-Mutant does not Increase Extracellular ATP Affinity ..	53
Figure 3.3 ECATS1 has Similar Affinity and Better Dynamic Range than DM-10nm ER/K.....	55
Figure 3.4 DM-20nm ER/K shows Increased ATP Affinity over ECATS1.....	57
Figure 3.5 Double-Mutant with 30nm ER/K linker shows slight Increase in ATP Affinity	58
Figure 3.6 DM-20nm ER/K mutant shows slightly increased ADP Affinity over ECATS1	60
Figure 4.1 Diagram Demonstrating Methods of Distinguishing Two Species of ATeam.....	66
Figure 4.2 ATP release detected from HEK293A cells using ECATS2.....	70
Figure 4.3 A 50% HOS causes an ATP release and cAMP response in HEK293A cells expressing P2Y11	72
Figure 5.1 Poke Injury Shows ATP-release from Damaged Astrocyte	83
Figure 5.2 Poke of Neighboring Cells Shows No Detectable ATP Release.....	85
Figure 5.3 Scratch Injury Shows ATP Release Detectable by ECATS2	87

Figure 5.4 ECATS2 Detects ATP Release in Cortical Astrocytes in Response to 50% HOS in Presence of 100 μ M ARL	89
Figure 5.5 Second Experiment using ECATS2 Detects ATP Release in Cortical Astrocytes in Response to 50% HOS in Presence of 100 μ M ARL	91
Figure 5.6 Third Experiment using ECATS2 Detects ATP Release in Cortical Astrocytes in Response to 50% HOS without ARL.....	94
Figure 5.7 50% HOS Reveals ATP Release by use of the ECATS2 Sensor	96
Figure 5.8 HOS in Neuron-Astrocyte Co-culture	100
Figure 5.9 HOS causes calcium oscillations in neurons and astrocytes	102
Figure 5.10 KCN Induced Ischemia shows ATP release detected by ECATS2 in Cortical Astrocytes	105
Figure 5.11 Seizure-like Excitotoxicity Model does not show ATP signaling.....	107
Figure 6.1 ATP Signaling Concentrations and Current Extracellular ATP Sensors	113

LIST OF ABBREVIATIONS

ATP	=	Adenosine Triphosphate
ADP	=	Adenosine Diphosphate
AMP	=	Adenosine Monophosphate
AT	=	ATeam
cAMP	=	cyclic adenosine monophosphate
CFP	=	cyan fluorescent protein
DM	=	double-mutant referring to R103A/R115A mutations
ECATS	=	extra-cellular ATP sensor
ECATS1	=	extra-cellular ATP sensor generation 1 or ecATeam3.10
ECATS2	=	extra-cellular ATeam3.10-R103A/R115A-20nm ER/K linker
FP	=	fluorescent protein
FRET	=	Förster Resonance Energy Transfer
HOS	=	hypo-osmotic shock
NB	=	Non-ATP-binding control of ECATS2
PDGFR	=	Platelet-derived growth factor receptor
RFP	=	Red fluorescent protein
TBI	=	Traumatic Brain Injury
VACCs	=	Voltage activated calcium channels
VRACs	=	Volume-Regulatory Anion Channels
YFP	=	Yellow fluorescent protein

ABSTRACT

Author: Cholger, Daniel J. PhD

Institution: Purdue University

Degree Received: August 2019

Title: Engineering A High Affinity Extracellular ATP Sensor for Studying Purinergic Signaling

Committee Chair: Mathew Tantama

Adenosine Triphosphate (ATP) can be released as a signal between cells in an autocrine and paracrine manner that bind purinergic receptors. Highly conserved, purinergic receptors expressed on the cell surface of neurons and astrocytes are capable of being activated across eight orders of magnitude from hundreds of nanomolar ATP to millimolar. Genetically encoded fluorescent protein biosensors have been used to detect ATP outside the cell, but a high affinity extracellular ATP sensor is required to study the ATP signaling dynamics from nanomolar to micromolar magnitudes. Previously, our lab developed a first generation sensor of extracellular ATP called ECATS1 (Conley et al.). To develop an improved sensor, we carried out site-directed mutagenesis of the sensor's ATP-binding site and identified a mutant that exhibited 4-fold increase in ATP binding affinity in solution. We then optimized the membrane-tethering of the sensor to achieve the 4-fold increase in extracellular ATP binding affinity when measured on live cells. This second-generation sensor was dubbed ECATS2. As a proof-of-concept application, we sought to detect ATP release from cells using *in vitro* models of edema. We subjected HEK293A cells to hypo-osmotic shock (HOS), revealing ATP release at micromolar levels. Then we tested HOS in cultured cortical astrocytes, also revealing micromolar ATP release. However, when we tested neuron-astrocyte co-cultures, we no longer observed ATP release in response to HOS. Interestingly, this implies that co-culture either entirely prevented ATP release from astrocytes or dampened it into the nanomolar range below the limit of ECATS2 detection. Thus, we have

validated the development of a higher affinity, second generation sensor and used it to discover that ATP release from astrocytes after HOS can be affected by the presence of neurons.

CHAPTER 1. INTRODUCTION

1.1 Purinergic Signaling in the Brain

The thought that adenosine 5'-triphosphate (ATP) acted as a signaling molecule was first proposed in the 1970's (Burnstock). Until then, it was widely accepted that ATP released into the extracellular space was only a result of some form of insult or damage to the membrane (Burnstock). The concept that ATP acts as a signaling molecule is now widely accepted, and it is known that ATP is packaged in secretory vesicles in neurons along with neurotransmitters as a co-transmitter and neuromodulator (Burnstock; Engel et al.; Praetorius and Leipziger). Ectonucleotidases in the extracellular space hydrolyze ATP to adenosine 5'-diphosphate (ADP), then to adenosine 5'-monophosphate (AMP) and finally adenosine (Zhao et al.).

In order for extracellular ATP to act as a purinergic signal, receptors that bind ATP and its hydrolysis products must be present on the membrane. There are four types of adenosine receptor (A1, A2A, A2B, A3), seven subtypes of P2X ion channel receptors (P2X₁-P2X₇), and eight subtypes of P2Y G protein-coupled receptors (P2Y₁, P2Y₂, P2Y₄, P2Y₆, P2Y₁₁, P2Y₁₂, P2Y₁₃, and P2Y₁₄) expressed throughout the body (Jacobson and Muller; Burnstock; Guzman and Gerevich). Astrocytes have been demonstrated to express the ion-channel receptors P2X₁ (EC₅₀ ~100-700 nM ATP), P2X₂ (EC₅₀ ~2-8 μM ATP), P2X₃ (EC₅₀ ~1 μM ATP), P2X₄ (EC₅₀ ~1-10 μM ATP), and P2X₇ (EC₅₀ ~2-4 mM ATP) (Jacobson and Muller; James and Butt). Astrocytes also express the G protein-coupled receptors P2Y₁ (EC₅₀ ~ 10 μM ADP), P2Y₂ (EC₅₀ ~ 100 nM ATP or ~10 nM UTP), P2Y₄ (EC₅₀ ~1 μM UTP), and P2Y₆ (EC₅₀ ~300 nM UTP) (Jacobson and Muller; Guzman and Gerevich; James and Butt). Neurons are known to express P2Y₁, P2Y₂, P2Y₄, P2Y₁₂ and P2Y₁₃ in their presynaptic terminals that close voltage-activated calcium channels (VACCs) and inhibit

further glutamate release from the presynaptic neuron (Guzman and Gerevich). Astrocytes surround and support synapse function of neurons, and the machinery is in place for ATP and its hydrolysis products to modulate neurotransmission in both physiological and pathological states.

See Figure 1.1 for our model of neuron-astrocyte synapse purinergic machinery.

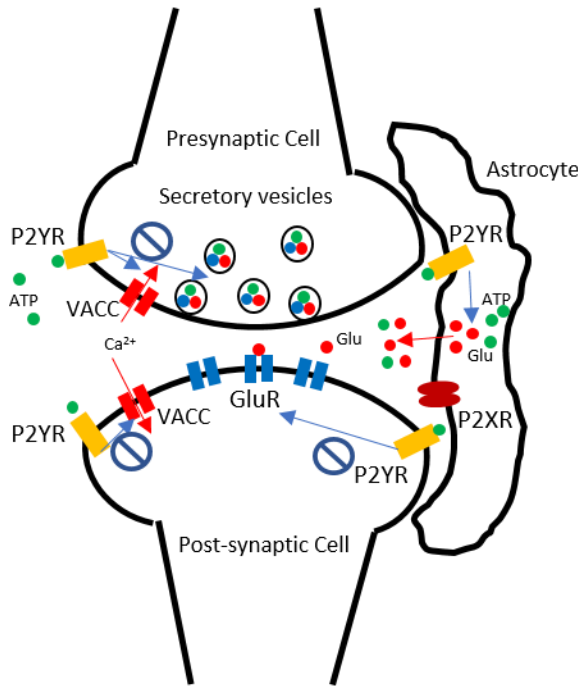


Figure 1.1 Machinery for Purinergic Signaling in the Synapse

G protein-coupled purinergic receptors (P2YR) and ion-channel purinergic receptors (P2XR) are expressed in both astrocytes and neurons. ATP activation of P2YRs in the presynaptic and post-synaptic neurons inhibits calcium influx from voltage activated calcium channels (VACCs), inhibits further vesicular release from the presynaptic cell, and inhibits glutamate excitation in the post-synaptic cell. P2YR activation in astrocytes can lead to ATP and glutamate release from astrocytes. (Guzman and Gerevich)

Purines such as ATP are capable of being released into the extracellular space by channels or secretory vesicles by both astrocytes and neurons in response to a variety of stimuli in the brain (Mulligan and MacVicar; Kimelberg et al.; Darby et al.). Released purines such as ATP act in an autocrine and paracrine manner by binding ionotropic and metabotropic P2 receptors (Wang et al.; Burnstock; Jacobson and Muller; Guzman and Gerevich). Several of these receptors have been revealed to have EC₅₀ values in the nanomolar (P2Y₂ EC₅₀ ~100 nM ATP) and low micromolar

ranges ($\text{P2X}_2 \text{ EC}_{50} \sim 2\text{-}8 \mu\text{M ATP}$), driving cellular responses to signals at concentrations at least three orders of magnitude smaller than inside the cell (Imamura et al.; Jacobson and Muller; Guzman and Gerevich; Zhao and Yang). The receptor with the lowest ATP affinity, P2X_7 ($\text{EC}_{50} \sim 2\text{-}4 \text{ mM ATP}$), has been shown to activate apoptosis or necrosis pathways in response to ATP release from membrane damage and is conserved across most cell types (Jacobson and Muller; Y. Zhang et al.; Burnstock). Thus, in order to thoroughly study purinergic signaling in regard to extracellular ATP concentrations that can activate purinergic receptors, tools capable of detecting dynamic changes in ATP across eight orders of magnitude are required.

1.2 Traumatic Brain Injury and Pathologies

Traumatic Brain Injury (TBI) can occur from a variety of stimuli and insults. Following a TBI, a variety of mechanisms can cause ATP release activating purinergic receptors (Burda et al.; Kimelberg et al.; Z. Zhang et al.; Y. Zhang et al.). The primary biological mechanisms of interest in this dissertation pertains to purinergic signaling of ATP in response to *in vitro* models of TBI such as mechanical injury, ischemia, excitotoxicity and edema.

1.2.1 Mechanical Stimulation and Injury

Mechanical stimulation and injury of brain tissues can release ATP in the extracellular space by rupturing the plasma membrane and allowing cytosolic ATP to spill out acting in an autocrine and paracrine manner. Previous studies have demonstrated that ATP released near the ruptured membrane can reach millimolar concentrations, which is sufficient to activate P2X_7 receptors that trigger apoptosis and necrosis pathways (Y. Zhang et al.; Jacobson and Muller; Neary et al.). Among the mechanical injury models tested that exhibit ATP releases are the poke, stretch and scratch models (Neary et al.; Y. Zhang et al.). It is expected that even despite the

massive ATP release, the signal is diluted beyond detection only 100 μm away, most likely from diffusion (Y. Zhang et al.). Membrane tethered cell surface sensors are required for more accurate measurements of ATP signaling for both spatial resolution and local ATP concentration ranges.

1.2.2 Swelling and Edema

Brain swelling, or edema, is a common symptom in TBIs, where excess water enters the brain. Without space to expand in the skull, the excess water causes neurons and astrocytes within the brain to swell. When cells are exposed to excess water, it is a form of hypo-osmotic shock (HOS) where the osmolality of the surrounding solution suddenly drops. Water rushes into astrocytes in an aquaporin dependent mechanism, which in turn causes volume regulated anion channels (VRACs) to open (Thrane et al.). VRACs are conserved across most cell types as nearly all mammalian cell types require some form of volume control. VRACs release many types of negatively charged molecules into the extracellular space in response to intracellular volume increase (Wang et al.). The predominant anion carrying the negative current is chloride, while ATP and negatively charged excitatory amino acids such as glutamate are released as well (Kamelberg et al.; Mulligan and MacVicar).

1.2.3 Ischemia

Lack of oxygen in the brain can result from local causes such as the rupturing or occlusion of blood vessels in stroke, or global causes such as hypoxia or cardiac arrest. In the case of TBI, the extent of the injury and damage to blood vessels creates a local ischemic environment in the brain tissue around the injury (Burda et al.). Neurons are much more sensitive to ischemic stress than astrocytes, and purinergic signaling mechanisms between astrocytes and neurons may play an important protective role (Rossi et al.). Astrocytes are reported to experience a fusion of lysosomes with the plasma membrane, releasing lysosome components into the extracellular space

in response to acute ischemic stress. ATP in lysosomes can reach millimolar concentrations, indicating lysosomal fusion from acute ischemic stress can lead to activation of P2X and P2Y receptors (Z. Zhang et al.; Rossi et al.). In cases of long-term ischemia, astrocytes begin to swell and can release ATP in the same mechanisms described in 1.2.2.

1.2.4 Seizure-like Excitotoxicity

Seizures and epilepsy are caused by a myriad of genetic and environmental factors. Patients that experience a TBI may experience seizures depending on the brain region and severity of their injury (Engel et al.; Burda et al.). During a seizure, neurons are overly active and increase their firing activity. Increased neuronal activity has been reported to increase extracellular ATP levels (Burnstock; Engel et al.), but whether the ATP originates in neurons, astrocytes or both is not well known.

1.3 Genetically-Encoded Fluorescent Protein Sensors

In all of the aforementioned TBI-associated pathologies, understanding the role of purinergic signaling could benefit from better technology to measure extracellular ATP. One of the first methods that forged the path for detection of ATP for the study of metabolism and purinergic signaling was the use of firefly luciferase (Beigi et al.; Gould and Subramani). Providing an incredibly bright signal upon use of ATP to oxidize its substrate luciferin, firefly luciferase can detect even small ATP release events. Even current end-point ATP detection kits like the ATPlite assay (PerkinElmer Cat# 6016943) use a version of firefly luciferase to produce a signal from ATP in solution. While incredibly useful, luciferase requires the addition of the substrate luciferin to produce a signal and consumes ATP to produce its signal. The consumption of ATP could prove to be a confounding variable in studies that aim to understand purinergic signaling mechanisms in real-time and their downstream implications.

Genetically encoded fluorescent protein biosensors provide a reagent-free solution to the problem. While the addition of luciferin is no longer needed, a method for delivering the DNA of the desired sensor into the target cell type is a major consideration when constructing the sensor and choosing its delivery vector. For example, a sensor required to be expressed in mammalian cells will require a vector possessing the sequences for making mammalian transcription possible. Several such vectors for purchase come with features that can modify the protein product with N- and C-terminal domains such as secretion sequences or transmembrane domains.

ATeam is a ratiometric Förster Resonance Energy Transfer (FRET) based ATP sensor, consisting of a cyan fluorescent protein (CFP) and a yellow fluorescent protein (YFP) connected by an ATP binding domain. Developed by the Imamura lab, ATeam has three variants consisting of three different ATP binding domains from different species of *Bacillus* bacteria. ATeam3.10 derived its ATP binding domain from the epsilon subunit of the F₀F₁-ATP synthase in *Bacillus PS3*. ATeam1.03 and its variant ATeam1.03-YEMK both derive their ATP binding domain from *Bacillus subtilis* (Imamura et al.). An example of ATeam structure is shown in Figure 1.2 below.

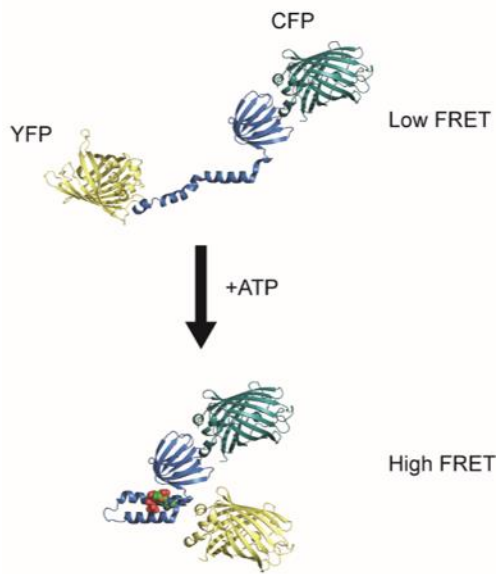


Figure 1.2 Example Structure of the ATeam Family of FRET Sensors

Top: The unbound, low ATP, low FRET apo-state shows increased space between the YFP and CFP. Bottom: The ATP bound, high FRET state reduces space between the YFP and CFP increasing FRET.

Conversion of ATeam3.10 from a cytosolic sensor into an extracellular sensor was done prior to this study (Conley et al.). The strategy employed the addition of an N-terminal IgK leader sequence and a C-terminal transmembrane tethering domain from the platelet-derived growth factor receptor (PDGFR). The addition of these two domains tethers the sensor to the membrane and directs it for secretion to the extracellular side of the plasma membrane (Coloma et al.; Gronwald et al.; Conley et al.). An example of the extracellular ATeam3.10 sensor (ecATeam3.10; ECATS1) is shown in Figure 1.3 below.

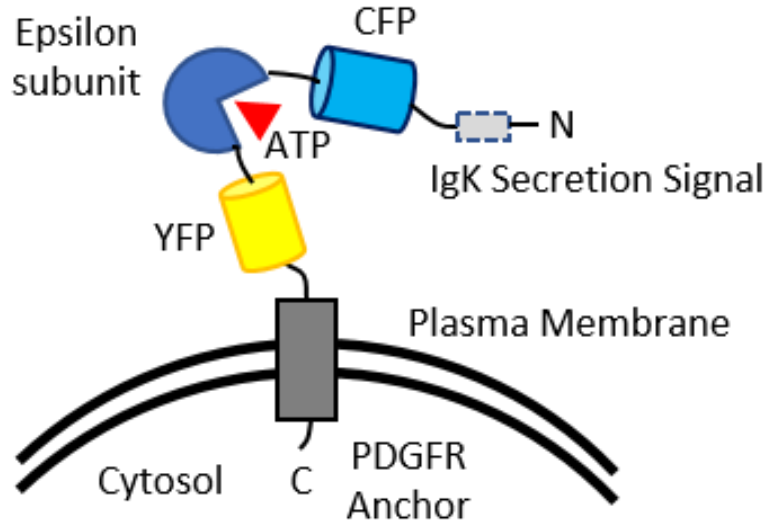


Figure 1.3 Diagram Demonstrating Strategy for Targeting ATeam3.10 to the Membrane
 From C-terminus to N-terminus: transmembrane PDGFR tether, mVenus as the yellow fluorescent protein (YFP), the ATP binding domain of the epsilon subunit of the F₀F₁-ATP synthase, CFP, then finally the IgK secretion signal.

In the following studies, we describe the modulation of ATP binding affinity by mutation of the epsilon subunit from two different species of *Bacillus* to tailor ATP affinity across the several orders of magnitude necessary for studying purinergic signaling. We specifically focused on the development and testing of the highest affinity sensor when displayed on the cell surface. After mutating the epsilon subunit and optimizing the length of the linker between the sensor and the PDGFR anchor, we successfully developed an increased affinity sensor that we dubbed extracellular ATeam3.10 sensor 2 (ECATS2).

CHAPTER 2. INCREASING AFFINITY FOR ATP USING CYCLIC MUTANT ANALYSIS

2.1 Introduction

ATP plays a vital role in signaling and metabolism both inside and outside cells. Within prokaryotic and eukaryotic cells, ATP is the product of central energy metabolism, and it is a universal energy currency found at millimolar concentrations in the cytosol (Zhao et al.). Intracellular ATP also has important roles in signaling because it is a major phosphate donor in the phosphorylation of proteins and other biomolecules, which is a key regulatory modification. Furthermore, ATP acts outside of cells as one of the most widespread autocrine and paracrine signals (Burnstock). Extracellular ATP can be released via channels or secretory vesicles, and extracellular ATP directly activates metabotropic and ionotropic purinergic receptors. Activation of these receptors occurs over a wide range of concentrations from nanomolar to millimolar levels (Jacobson and Muller; Zhao et al.; Burnstock; Guzman and Gerevich; Engel et al.). Within secretory vesicles, it has also been estimated that ATP levels can reach up to 100 mM concentrations (Engel et al.). Thus, the functions of ATP are incredibly diverse and ubiquitous, and this diversity is reflected in the very broad range of physiologically relevant concentrations that span nearly eight orders of magnitude.

To understand the function of ATP in signaling and metabolism, genetically encoded fluorescent protein-based sensors, such as the Perceval and ATeam sensors, have been especially useful for measuring real-time ATP dynamics in live cells (Tantama et al.; Imamura et al.). For example, the ATeam sensors originally engineered by Imamura and co-workers have been used extensively to study energy metabolism in bacteria, yeast, flies, and mammalian cells, and they have also been re-engineered to study extracellular ATP and purinergic signaling (Conley et al.).

These sensors are composed of an ATP-binding domain flanked by a cyan fluorescent protein (CFP) and yellow fluorescent protein (YFP). The CFP and YFP act as a Förster-type resonance energy transfer (FRET) donor-acceptor pair. The ATP-binding domain is derived from an epsilon subunit of a bacterial F₀F₁-ATPase, which undergoes an ATP-dependent conformational change that causes an increase in FRET between the CFP-YFP pair (Imamura et al.).

Although the ATeam sensors have proven valuable in the measurement of ATP dynamics, they are still limited in the ranges over which they can detect changes in ATP concentration. In the original development of the ATeam sensors, four affinity variants were reported based on sensors constructed from epsilon subunits from different *Bacilli* species. The ATeam3.10 and ATeam3.10^{MGK} variants utilized the *Bacillus sp. PS3* epsilon subunit and exhibit micromolar ATP affinities. The ATeam1.03, ATeam1.03YEMK variants utilize the *Bacillus subtilis* epsilon subunit and exhibit millimolar ATP affinities. The ATeam1.03NL variant also has millimolar ATP affinity and was rationally engineered by examining contacts between the N-terminal and C-terminal domains in the ATP-bound crystal structure (Zhao and Yang). Thus, with the one exception of the ATeam1.03NL mutant, there has little exploration of other ATP binding determinants that could be exploited.

To expand the range of sensors with different affinities, it is important to use a range of different protein engineering strategies. Recently, Kato-Yamada experimentally demonstrated that a mutant of the *Bacillus sp. PS3* epsilon subunit with two arginine-to-alanine mutations near the ATP binding site has increased ATP affinity, and Krah and co-workers computational studies suggest that these two residues are generally important secondary ATP binding determinants found across epsilon subunits from different species (Krah et al.; Kato-Yamada). Thus, in this study we

carried out a systematic mutational analysis of these two arginine residues in the context of the ATeam sensors to test whether they are fruitful sites for fine-tuning the ATP affinity of the sensors.

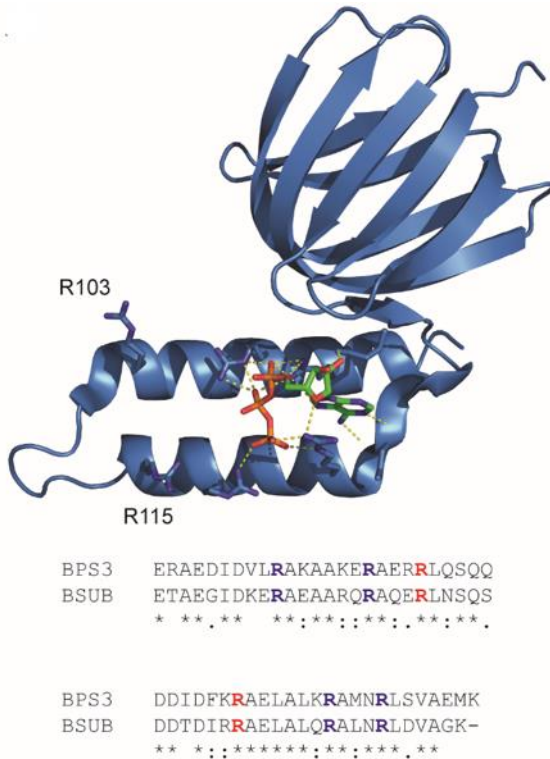


Figure 2.1 Structure of ATP binding domain in ATeam family of sensors

Top: Crystal structure of the ATP-bound *Bacillus* sp. PS3 epsilon subunit. PDB: 2E5Y. Arginine residues R103 and R115 that are studied in this work are labeled. Bottom: Sequence alignment of the *Bacillus* PS3 and *Bacillus subtilis* epsilon subunits, which are the ATP-binding domains for ATeam3.10 and ATeam1.03. R103 and R115 are shown in red. Arginine residues that form direct interactions with ATP (R92, R99, R122 and R126) are shown in blue.

2.2 Materials and Methods

2.2.1 Q5 Site-directed Mutagenesis

All chemicals and cell culture reagents were purchased from Sigma Aldrich and ThermoFisher. Template vectors pRSetB-ATeam3.10 (from H. Imamura), pRSetB-ATeam1.03 and pRSetB-ATeam1.03-YEMK were used to generate mutants using the primers in **Table 1** and the NEB Q5 site-directed mutagenesis kit. All mutants were sequence verified by Sanger sequencing at Genewiz (South Plainfield, NJ).

Table 1 Mutagenesis Primers for Cyclic Mutant Analysis of ATeam Constructs

pRset-AT1.03 and pRset-AT1.03YEMK	Sequence
nt0819_B.subtilis_eps_R103A_F	GGCCCAGGAGGCCCTGAACCTCTCAATC
nt0820_B.subtilis_eps_R103A-E_R	CTCTGTCTTGCAGGCTTCT
nt0821_B.subtilis_eps_R103E_F	GGCCCAGGAGGAGCTGAACCTCTC
nt0822_B.subtilis_eps_R115A_F	CGATATTGCGCTGCCGAGCTGG
nt0823_B.subtilis_eps_R115A-E_R	GTGTCATCGGATTGAGAG
nt0824_B.subtilis_eps_R115E_F	CGATATTGCGAGGCCGAGCTG
<hr/>	
pRset-AT3.10	Sequence
nt0693_BsPS3epsilon_R103A_F	GGCGGAGCGCGCCCTGCAAAGCC
nt0694_BsPS3epsilon_R103A-E_R	CGCTCTTCGCCGCTTG
nt0695_BsPS3epsilon_R103E_F	GGCGGAGCGCGAGCTGCAAAGCC
nt0696_BsPS3epsilon_R115A_F	CGACTTCAAAGCAGCCGAACGGCGTTAAAC
nt0697_BsPS3epsilon_R115A-E_R	ATGTCGTCCTGCTGGCTT
nt0698_BsPS3epsilon_R115E_F	CGACTTCAAAGAGGCCGAACGGCG

2.2.2 Protein Expression and Purification

BL-21 strain E. coli cells expressing pRSetB-ATeam3.10 was cultured in Auto Induction Media (AIM) at 37 °C for 12h then at room temp for 36h. Cells were then pelleted, resuspended in lysis buffer (25 mM Sodium Phosphate Buffer [pH 7.8], 500 mM NaCl, 10 mM Imidazole, 5% Glycerol, 0.1% Triton X-100, 1 mM PMSF, 1 mM DTT, and 0.2 mg/mL Lysozyme), and lysed by sonication. Lysate was then centrifuged at 30,000xg for 30 minutes at 4°C, and passed through a 0.45 µm syringe. The sample was then run over a Ni column (GE Chelating Sepharose column charged with Ni²⁺). The column was then washed with wash buffer A (25 mM Sodium Phosphate Buffer [pH 7.8], 500 mM NaCl, 20 mM Imidazole, 5% Glycerol), wash buffer B (25 mM Sodium Phosphate Buffer [pH 7.8], 500 mM NaCl, 40 mM Imidazole, 5% Glycerol), then elution buffer (25 mM Sodium Phosphate Buffer [pH 7.8], 500 mM NaCl, 150 mM Imidazole, 5% Glycerol). The fractions containing purified ATeam3.10 were dialyzed in storage buffer (5 mM MOPS Buffer [pH 7.3], 300 mM NaCl, 10% Glycerol), with two changes at 4°C and stored at -80 °C until use.

2.2.3 Protein Solution ATP dose-response Assays

Protein concentration was determined using Beer's Law and chromophore denaturation in 1M NaOH, wavelength: 448nm, $\epsilon=44000\text{ L}^*\text{mol}^{-1}\text{cm}^{-1}$. The protein was diluted to 0.125 μM in assay buffer (50 mM MOPS-KOH, pH 7.3, 50 mM KCl, 0.5 mM MgCl₂, and 0.05% Triton X-100) and fluorescence was measured using a BioTek Synergy H4 microplate reader at room temperature, in the absence and presence of dose-response of ATP concentrations. For all filter-based measurements, a 420/50 nm excitation and 485/20 and 528/20 nm emission filters were used.

2.2.4 Determining Fluorescence Lifetime

Fluorescence lifetime was determined using the Edinburgh Instruments Spectrofluorometer FS5. Lifetime measurements were done by Mathew Tantama.

2.2.5 HEK293A Cell Line Maintenance

HEK293A cells were cultured in Dulbecco's modified Eagle's medium (DMEM) containing 4.5 g/L glucose, 3.7g/L sodium bicarbonate, 4mM glutamine, 0.1mM Non-essential Amino Acids (NEAA) and supplemented with 10% cosmic calf serum. Cells were maintained at 37°C and 5% CO₂ in a humidified incubator and passed three times weekly once confluence reached 80% or higher.

2.2.6 Live-cell Fluorescent Microscopy and Analysis

Cells were prepared for microscopy by exchanging cell growth media for imaging solution consisting of 15 mM HEPES, 1.25 mM NaH₂PO₄, 10 mM glucose, 130 mM NaCl, 3 mM KCl, 2 mM CaCl₂, 1 mM MgCl₂, and 3 mM NaHCO₃ (pH 7.3) and cells were equilibrated at room temperature for at least 20 min prior to imaging. Osmotic shock solution was prepared as imaging

solution consisting of 15 mM HEPES, 10 mM glucose, 2 mM CaCl₂ and 1 mM MgCl₂. All microscopy experiments were performed at ambient room temperature in a static bath. Cells were imaged using an Olympus IX83 fluorescence microscope with a 20X/0.75 NA objective illuminated by a Lumencor SpectraX light engine and equipped with an Andor Zyla 4.2 sCMOS camera. ATeam sensor activity was measured by examining the fluorescence intensities in CFP, CFP-YFP FRET, and YFP channels. Specifically, the ATeams were excited in the CFP and CFP-YFP FRET channels using a 438/29 nm bandpass filter, and emission was collected through 470/24 and 540/30 nm bandpass filters for the CFP and CFP-YFP FRET channels, respectively. The fluorescence in the YFP channel was excited using a 510/10 nm bandpass filter and emission was collected through a 540/30 nm bandpass filter. The fluorescence in the RFP channel was excited using a 575/25 nm bandpass filter and emission was collected through a 631/28 nm bandpass filter. Excitation light from all fluorescence channel measurements was blocked by the ET-ECFP/EYFP/mCherry multiband beamsplitter (Chroma 69008bs). The microscope components and image acquisition were controlled by the Andor iQ3 software and the ImageJ/FIJI software package was used to analyze all images for each experiment, as specified. For fluorescence images, the mean and standard deviation of background intensities were measured for each channel in each field of view. For each fluorescence channel, the mean background intensity was subtracted from every image of the associated imaging set. Background masks were then created with minimum thresholds of two times the mean background intensity. The background masks were applied to the fluorescence intensity images and fluorescence ratio images were created by pixel-by-pixel division of the background masked individual fluorescence channels. Regions of interest that encompassed whole cells or cell membranes, as indicated, were drawn and the mean fluorescence ratios of pixels within each region of interest were calculated.

2.2.7 Statistical Analysis

All statistical analysis was done using OriginPro2017 64-bit software. Since our primary goal was improving ATP affinity compared to the first-generation sensor, we report the results of the unpaired 2-tailed student's t-test comparing specific mutants to the control. Differences were deemed significant if $p < 0.05$. Data in this chapter is reported as the mean \pm standard deviation.

2.3 Results

2.3.1 The R103A/R115A double mutant of ATeam3.10 is a high ATP binding affinity mutant

Kato-Yamada recently demonstrated that the R103A/R115A double mutant of the *Bacillus sp. PS3* epsilon subunit results increases the ATP binding affinity from 4 μM to 50 nM (Kato-Yamada). Subsequently, Krah et al. carried out molecular dynamics simulations and bioinformatics analysis predicting that both the double mutant and the individual single mutations would affect ATP binding affinity by increasing protein-ligand hydrogen bonding and electrostatic interactions (Krah et al.). We therefore carried out a mutational analysis of these two arginines in the ATeam3.10 sensor, which utilized the *Bacillus sp. PS3* epsilon subunit, to determine if substitution of these residues could be used to fine-tune the ATP affinity of the sensor. The changes in K_{app} for ATeam3.10 for ATP can be seen in Table 2.

We first determined whether the reported arginine-to-alanine charge neutralization double mutation would increase the ATP binding affinity of the ATeam3.10 sensor because of important differences between the reported mutant protein and the sensor. The wildtype and reported double mutant were tested using the purified epsilon subunit with a Q107C mutation for conjugation to a Cy3 reporter dye (Kato-Yamada). The Q107 residue is found in the hairpin loop between the two C-terminal α -helices that comprise the ATP binding site. In contrast, the ATeam sensor harbors

the wildtype Q107 residue in its epsilon domain, but the epsilon domain is flanked by the two bulky fluorescent proteins. While it is likely that R103A/R115A double mutation would have the same or similar effect in the sensor, these differences make it important to directly test. Indeed, we found that the ATeam3.10(R103A/R115A) double mutation causes an approximate 4-fold increase in ATP binding affinity from 800 ± 300 nM (n=9) to 200 ± 100 nM (n=4) (mean \pm stdev, p=0.004, 2-tail t-test) at room temperature (Figure 2.2), and a similar increase was observed at 37 °C (not shown).

Table 2 ATP affinity of the ATeam3.10 sensor and its mutants

Table 2. ATP affinity of the ATeam3.10 sensor and its mutants	
	ATP Affinity, K_D^{app} mean \pm std (95% conf. int.)
ATeam3.10	800 \pm 300 (200) nM
R103A	800 \pm 300 (200) nM
R103E	600 \pm 300 (200) nM
R115A	600 \pm 200 (200) nM
R115E	300 \pm 100 (60) nM *
R103A/R115A	200 \pm 100 (90) nM *
R103A/R115E	200 \pm 100 (70) nM *
R103E/R115A	700 \pm 300 (200) nM
R103E/R115E	800 \pm 400 (200) nM

* Significantly different from ATeam3.10, p<0.01, 2-tail t-test.

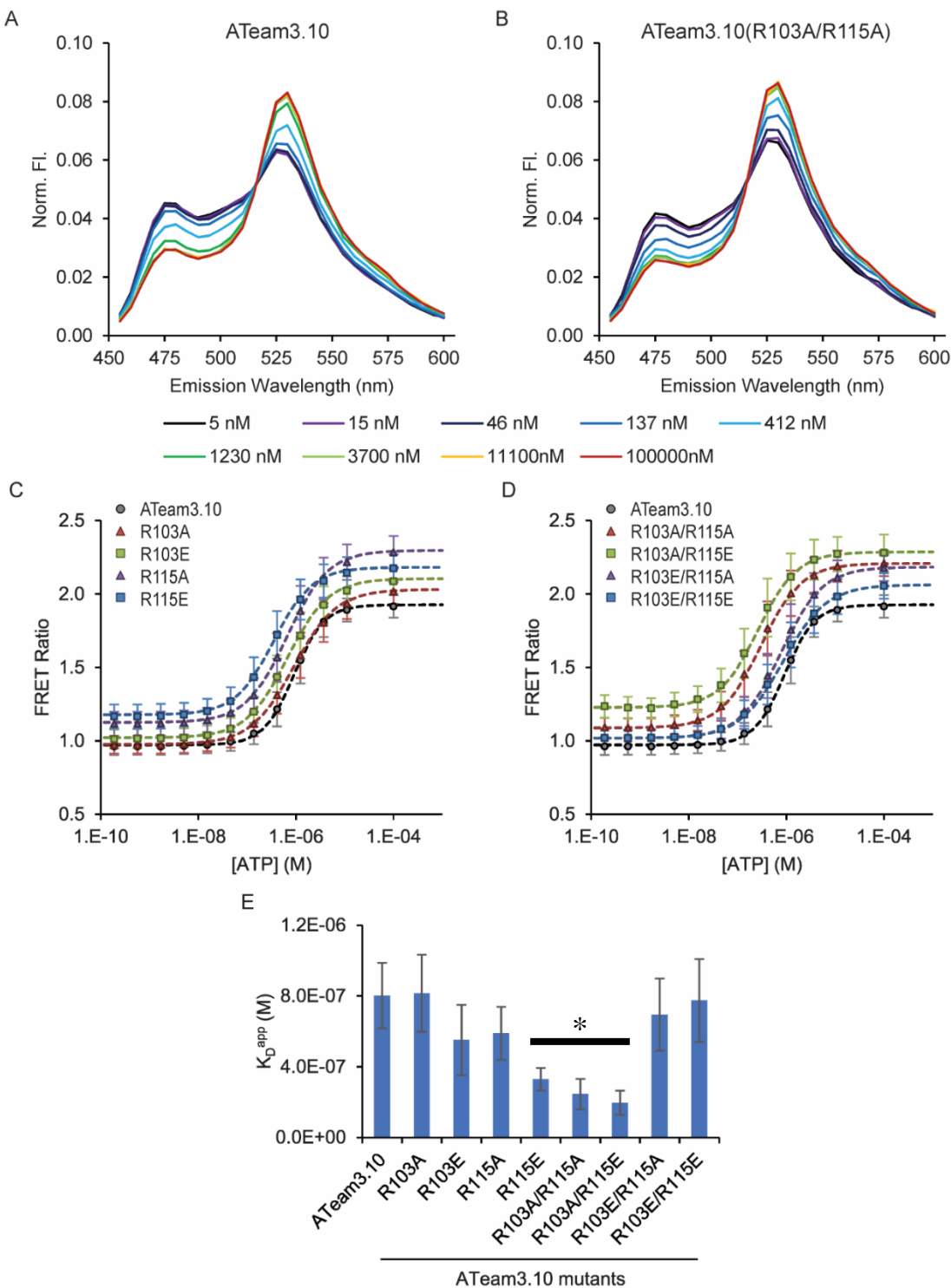


Figure 2.2 ATP-dose responses for the ATeam3.10 sensor and its mutants at room temperature. See Table 1 for affinities. ATP-dependent fluorescence emission spectra of the A) wildtype ATeam3.10 protein and B) R103A/R115A mutant protein. ATP-dose response curves for the C) single-site mutant proteins and D) double mutant proteins. The same data for the wildtype response is shown in both C) and D) for comparisons. E) Summary of the apparent ATP binding affinities. Mean \pm 95% confidence interval ($n=4-9$). * $p<0.005$, 2-tail t-test of mutant vs ATeam3.10.

2.3.2 Mutation of R103 and R115 can fine tune ATP binding affinity

We next investigated whether substitutions other than the double alanine mutations at the R103 and R115 residues could fine-tune the ATP binding affinity of the ATeam3.10 sensor. To do so, we generated a combinatorial library of single and double mutants, consisting of arginine-to-alanine charge neutralization and arginine-to-glutamate charge reversal mutations at the R103 and R115 residues. Contrary to the computational prediction by Krah and Bond (2018), we found that neither the R103A single mutation nor the R115A single mutation significantly increases ATP binding affinity in the context of the ATeam3.10 sensor (Figure 2.2, Table 1). Surprisingly, however, we found that the single R115E charge reversal mutation significantly increases the ATP binding affinity to 300 ± 100 nM compared to the parent sensor ($n = 4$, $p=0.004$, 2-tail t-test). Furthermore, the R103A/R115E double mutant exhibited an increase in ATP binding affinity to 200 ± 100 nM ($n = 4$), similar to the R103A/R115A double mutant (Figure 2.2, Table 1).

Given the differences in apparent ATP affinity for the single and double mutants, we asked whether the measured binding constants indicated strong interactions between the sites by carrying out a double-mutant cycle analysis (Horovitz). The analysis confirmed our qualitative observations that non-linear energetic interactions could occur between the sites. However, the interaction energies are small and do not suggest that strong direct interactions between residues at positions 103 and 115 (Figure 2.3).

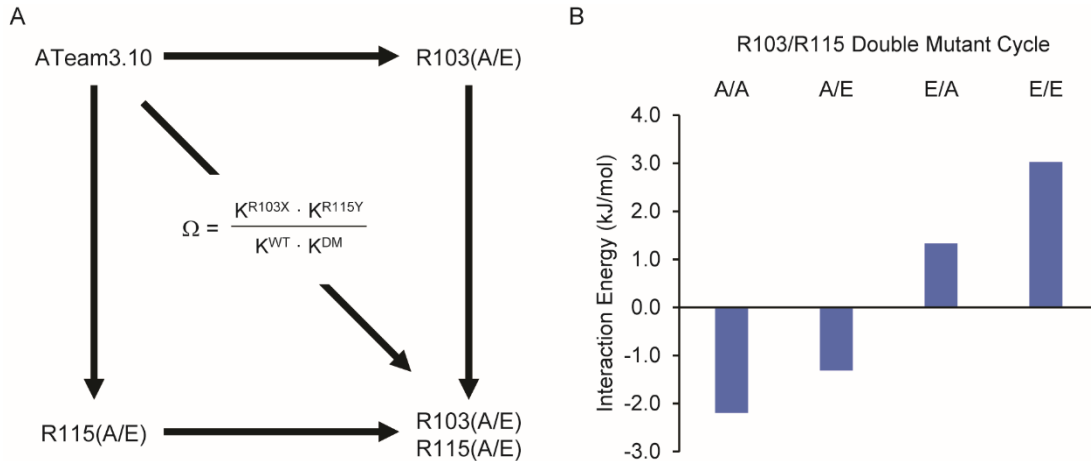


Figure 2.3 Mutant cycle analysis of the ATeam3.10 sensor and its mutants.
A) Mutant cycle interaction energy diagram for the R103 and R115 residues. B) The calculated interaction energies using the apparent ATP affinities.

2.3.3 Mutational analysis of ATeam1.03 and ATeamYEMK

We next hypothesized that mutagenesis of the R103 and R115 residues in the ATeam1.03 sensor could also fine tune the ATP affinity for this sensor. The ATeam1.03 sensor uses the *Bacillus subtilis* epsilon subunit and exhibits near millimolar ATP affinity at room temperature. The *Bacillus subtilis* and *Bacillus* sp. PS3 epsilon subunits share conserved arginine residues at the 103 and 115 sites, and additionally share the conserved R92, R99, R122, and R126 arginine residues involved in protein-ATP direct interactions (Figure 2.1). While these key arginines are conserved, the portions of the epsilon subunits used in ATeam3.10 (*B. PS3*) and ATeam1.03 (*B. subtilis*) have an overall 68.67% identical DNA sequence determined by the NCBI BLASTn 2-sequences alignment. An X-ray crystal structure of the *Bacillus subtilis* epsilon subunit is not available, but we generated a model using the I-TASSER server with the *Bacillus* sp. PS3 epsilon subunit as a template to confirm that there are no major structural differences predicted for the ATP-binding fold (not shown). We again generated a combinatorial library of single and double

R103 and R115 mutants in the ATeam1.03 sensor. Interestingly, all single and double mutants resulted in a loss of ATP binding over the measured concentration range (Figure 2.4, Table 2).

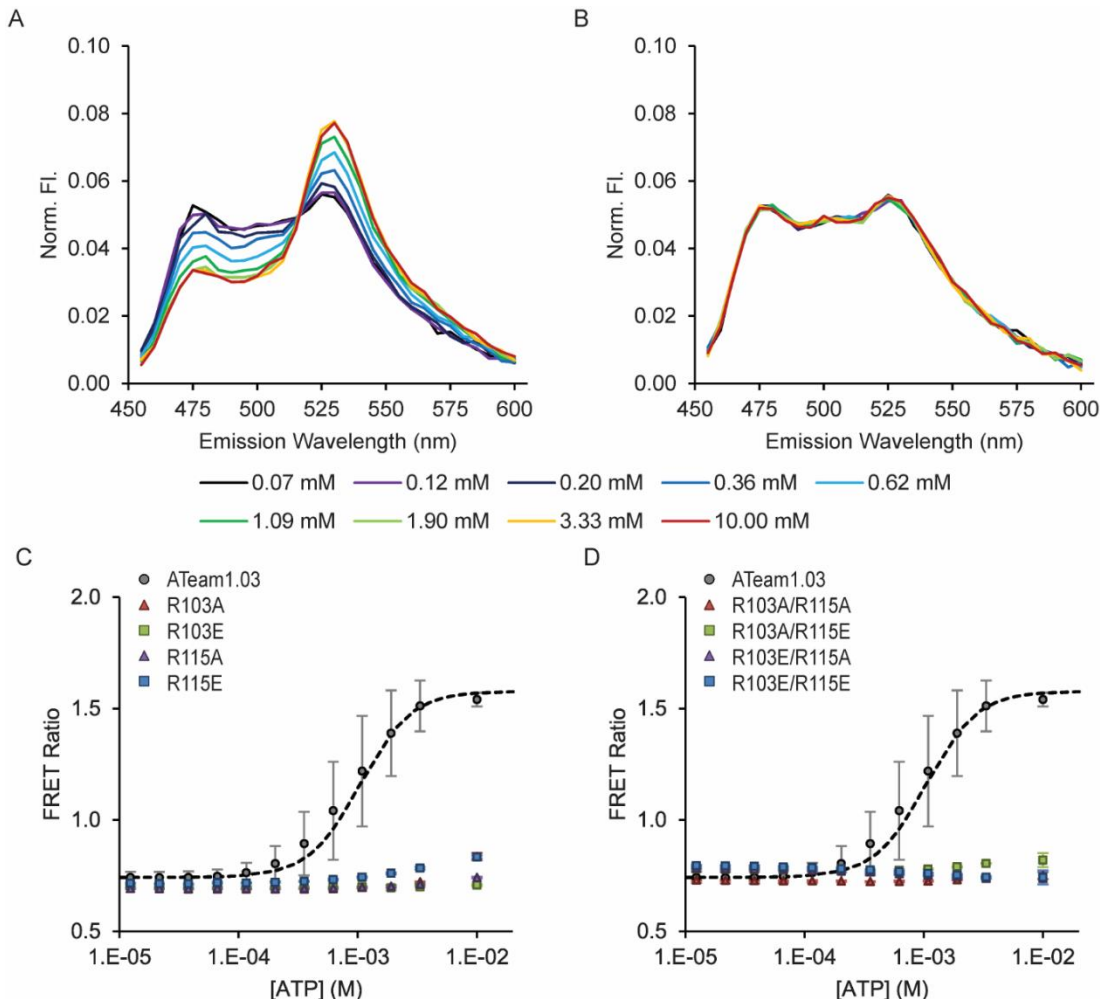


Figure 2.4 ATP-dose response curves for ATeam1.03 mutants

See Table 2 for affinities. Spectra for wildtype and AA mutant (A) ATeam1.03 wild-type spectra (B) ATeam1.03 A/A spectra (C) single mutants dose response (D) double mutants dose response.

Table 3 ATP affinity of the ATeam1.03 sensor and its mutants

Table 3. ATP affinity of the ATeam1.03 sensor and its mutants.			
	ATP Affinity, K_D^{app} mean ± std (95% conf. int.)		ATP Affinity, K_D^{app} mean ± std (95% conf. int.)
ATeam1.03	1.0 ± 0.5 (0.3) mM	ATeamYEMK*	0.2 ± 0.1 (0.09) mM
R103A	Non-binding	R103A	Non-binding
R103E	Non-binding	R103E	ND **
R115A	Non-binding	R115A	1.8 ± 0.5 (0.5) mM
R115E	Non-binding	R115E	0.7 ± 0.2 (0.2) mM
R103A/R115A	Non-binding	R103A/R115A	Non-binding
R103A/R115E	Non-binding	R103A/R115E	1.9 ± 0.2 (0.2) mM
R103E/R115A	Non-binding	R103E/R115A	1.9 ± 0.2 (0.2) mM
R103E/R115E	Non-binding	R103E/R115E	2.2 ± 0.3 (0.3) mM

ATeamYEMK refers to ATeam1.03(YEMK)

** The ATeamYEMK(R103E) mutation resulted in truncated protein over several expression attempts and was not tested.

Given these results, it was not clear if the arginine residues at positions 103 and 115 are absolutely required for ATP binding in *Bacillus subtilis* epsilon subunit, and therefore we studied the same mutations in the ATeam1.03(YEMK) sensor variant, abbreviated ATeamYEMK for clarity here. The ATeamYEMK sensor utilizes the *Bacillus subtilis* epsilon subunit but with the C-terminal residues mutated to match the *Bacillus sp. PS3* epsilon subunit C-terminus. Imamura et al. originally demonstrated that the mutated C-terminus results in increased ATP affinity relative to the ATeam1.03 sensor (Imamura et al.), and we used that to our advantage here. Given the loss of binding in the ATeam1.03 sensor, we hypothesized that mutations at the R103 and R115 positions in the ATeamYEMK sensor would lead to diminished ATP affinity that might be now

detectable because of a higher starting affinity using the ATeamYEMK scaffold. Indeed, we measured decreased binding affinity in five of the eight single and double mutants (Figure 2.5, Table 2). Thus, like the ATeam3.10 sensor and *Bacillus sp. PS3* epsilon subunit, the R103 and R115 residues can be mutated to fine tune the ATP affinity of the *Bacillus subtilis* epsilon subunit in ATeamYEMK. However, contrary to the effect in the ATeam3.10 sensor, alanine and glutamate substitutions decrease ATP binding affinity to the ATeam1.03 and ATeamYEMK sensors.

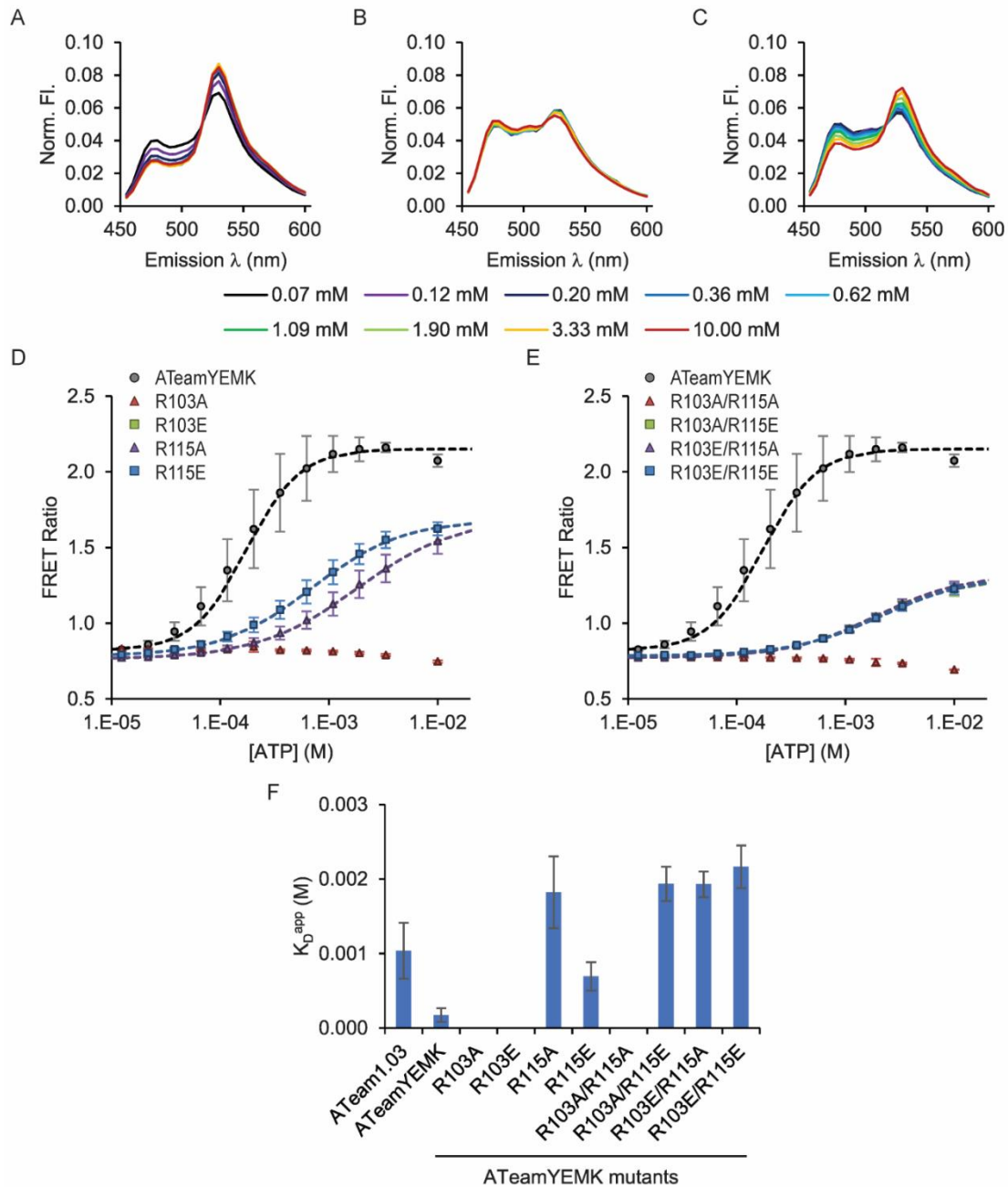


Figure 2.5 ATP-dose response curves for ATeam1.03(YEMK) mutants
 See Table 2 for affinities. Spectra for wildtype, 103A, 103A/115A, 103A/115E A) ATeamYEMK wt spectra B) 103A spectra C) 103A/115E spectra D) Kapp summary bar graph E) single mutants dose response F) double mutants dose response.

Given that mutation of the 103 and 115 positions caused such drastic loss of ATP binding to the ATeam1.03 and ATeamYEMK sensors, we asked whether the non-binding mutations might cause a larger scale disruption of the epsilon subunit C-terminal domain structure. We focused on one interesting pair of mutants in particular, the ATeamYEMK(R103A) single mutant and ATeamYEMK(R103A/R115E) double mutant. The R103A single mutant exhibits loss of ATP binding that is rescued in the R103A/R115E double mutant. We initially attempted to analyze the protein structure of the sensors and mutants using circular dichroism, but the signal from the fluorescent proteins and epsilon subunit N-terminal domain overwhelmed the spectra (not shown). We therefore examined the donor fluorescence lifetime distribution and acceptor fluorescence polarization.

Yagi et al. used nuclear magnetic resonance (NMR) to determine solution structures of the *Bacillus sp. PS3* epsilon subunit, showing that the C-terminal domain has α -helical secondary structure (Yagi et al.). In the absence of ATP, the C-terminal domain behaves like two α -helices connected by a flexible hinge, and it exhibits a large range of conformational freedom. In contrast, ATP binding results in a compact helix-turn-helix conformation. We would therefore predict that the ATeamYEMK(R103A) non-binding mutation would have large conformational freedom even in the presence of ATP, which is validated by our steady-state measurements that show the ATeamYEMK(R103A) does not exhibit any increase in FRET with the addition of ATP (Figure 2.5). However, we were curious if the R103A mutation caused any additional disorder or increased conformational flexibility that might not be revealed by the population average given by steady-state measurements. We therefore measured the donor fluorescence lifetime distribution using time-resolved spectroscopy. As expected, the ATeamYEMK exhibited a decrease in CFP donor lifetime with the addition of ATP because of increased donor excited state deactivation by FRET,

and the non-binding R103A mutant does not show a decrease in lifetime in the presence of ATP (Figure 2.6). However, in the absence of ATP there was no significant increase in the CFP donor fluorescence lifetime distribution for the R103A mutant compared to the ATeamYEMK parent. Similarly, we did not observe any significant differences in steady-state YFP acceptor polarization between the two proteins in the absence of ATP. These observations indicate that the R103A is not causing any additional increase in the conformational flexibility of the apo C-terminal domain (Figure 2.7).

Interestingly, we did observe that the addition of ATP caused an increase in steady-state YFP acceptor fluorescence polarization (Figure 2.7). This indicates that the YFP has decreased conformational flexibility in the more compact, ATP-bound form of the ATeamYEMK sensor, despite the expected increase in rotational diffusion caused by the change in protein shape.

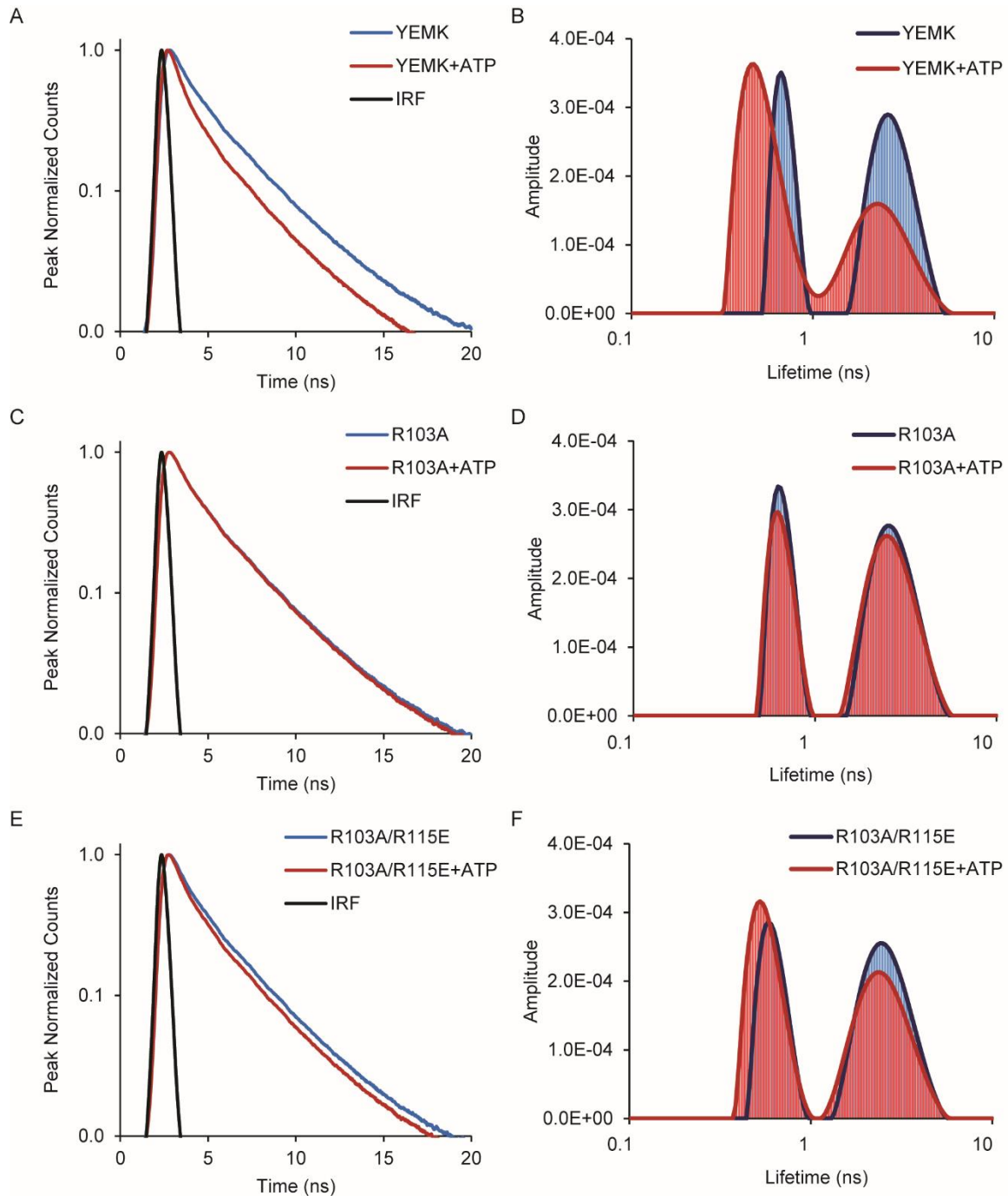


Figure 2.6 Time-resolved CFP donor fluorescence lifetime distribution analysis of ATeamYEMK and its mutants

A) Representative CFP donor fluorescence decays for the original ATeam1.03, the loss-of-function single point mutant ATeam1.03(R103A), and the partial-rescue double point mutant ATeam1.03(R103A/R115E). (B) Lifetime distribution analysis using the maximum entropy method. See Table 5.

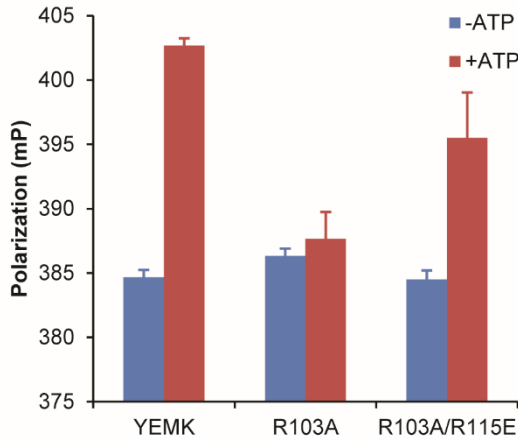


Figure 2.7 Steady-state YFP acceptor fluorescence polarization for ATeamYEMK and its mutants in the absence and presence of ATP

2.3.4 Fine-tuning ATeam sensor ATP affinity is functionally relevant for live-cell imaging

Finally, we tested if these mutations might have any repercussions for sensor expression in mammalian cells by validating that we could detect functional differences caused by affinity tuning. As a test case, we expressed the ATeamYEMK(R115E) mutant in HEK293A cells and compared its properties to the ATeamYEMK parent sensor. To do so, we carried out live-cell fluorescence imaging during metabolic inhibition of the cells. To enable paired comparisons between the two sensors, we imaged them simultaneously by co-expressing nuclear-targeted mApple with the parent ATeamYEMK sensor as a marker. We chose the ATeamYEMK(R115E) mutant because it has an affinity similar to the ATeam1.03 sensor, which has been effective for monitoring changes in ATP levels in mammalian cells. At room temperature, the ATeamYEMK sensor has a high affinity for ATP ($K_D = 0.2 \text{ mM}$) relative to cytosolic concentrations of ATP (2–10 mM), and we would expect the ATeamYEMK sensor to remain ATP-saturated in a high FRET state unless ATP levels are severely depleted by strong metabolic inhibition. The ATeamYEMK(R115E) mutant has decreased ATP affinity ($K_D = 0.7 \text{ mM}$), similar to the ATeam1.03 sensor, which has been used to monitor ATP changes in mammalian cells under

metabolic inhibition (Imamura et al.). We first imaged cells in the presence of the mitochondrial substrates glutamine and pyruvate with or without a high concentration of glucose (10 mM). Under either fuel condition, both sensors exhibited a decrease in FRET with strong metabolic inhibition using a combination of 2-deoxyglucose (DG) to attenuate glycolysis and trifluoromethoxy carbonylcyanide phenylhydrazone (FCCP) plus oligomycin to attenuate mitochondrial ATP production. As expected, the absence of glucose caused greater ATP depletion with either glycolytic, mitochondrial, or combined inhibition, and the presence of glucose was able to attenuate ATP depletion by DG addition (Figure 2.8). Overall, we observed that the ATeamYEMK(R115E) mutant did show higher sensitivity to metabolic inhibition, and the largest difference was detected under combination glycolytic and mitochondrial inhibition in the presence of glucose.

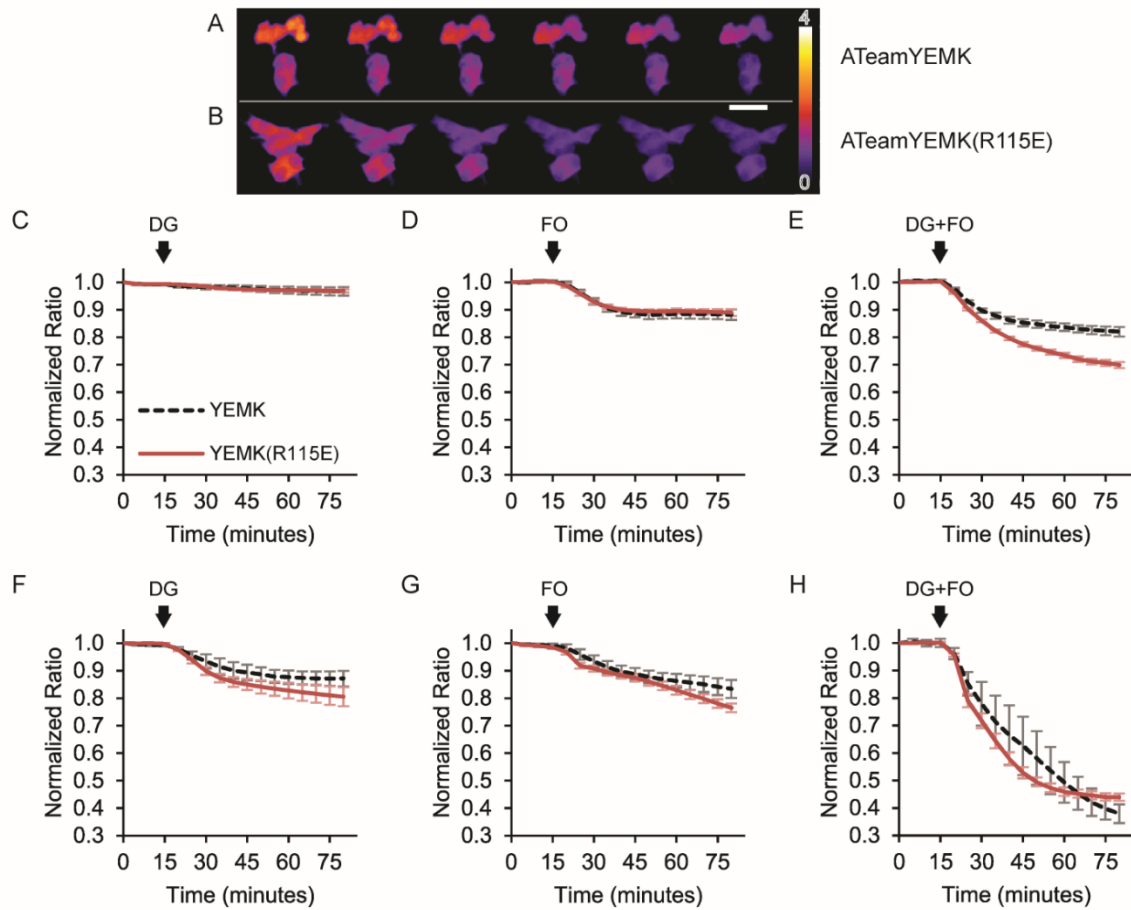


Figure 2.8 Live-cell imaging of YEMKwt vs YEMK115E

A) and B) show ratio images of both species of sensor. C) and D) 10 mM glucose plus 5 mM glutamine and 1 mM pyruvate. F)-H) 5 mM glutamine and 1 mM pyruvate without glucose. 10 mM 2-deoxyglucose (DG). 2 μ M FCCP plus 2.5 μ M oligomycin (FO).

Given our observation that high glucose is able to sustain ATP production under these conditions, we hypothesized that ATeamYEMK(R115E) would be more sensitive to mild ATP depletion than the parent ATeamYEMK sensor. We validated this hypothesis by monitoring ATP depletion in the presence of lowered glucose concentration (2mM) with glycolytic inhibition by DG addition only and observed that the parent ATeamYEMK sensor did not report any changes,

but the ATeamYEMK(R115E) mutant was more sensitive and did report mild depletion of ATP (Figure 2.9).

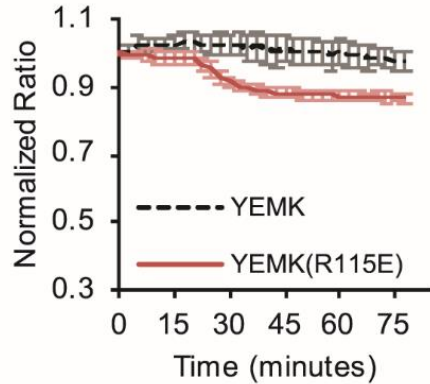


Figure 2.9 The lower affinity mutant ATeamYEMK(R115E) is more sensitive to mild metabolic inhibition with deoxyglucose only

Our cell imaging results demonstrate that fine-tuning the affinity of these sensor can provide functional advantages to detecting different regimes of ATP depletion, and that mutations do not affect the stability of the sensor in cells.

2.4 Discussion

In this study we demonstrated that mutagenesis of the R103 and R115 residues near the *Bacillus* ATP synthase epsilon subunit ATP binding site provides an important new strategy for semi-rational fine tuning of the ATeam sensors' ATP affinity. In terms of sensor development, this provides a significant new strategy for diversifying the toolbox of available sensors to match the ATP concentrations ranges encountered inside and outside cells. Our work also provides experimental data that, in combination with future computational studies (Krah et al.), could provide important new insights into the ATP-dependent regulatory roles of prokaryotic epsilon subunits.

We limited our mutagenesis in this study to alanine and glutamate substitutions because these residues have a propensity to form helices (Sivaramakrishnan and Spudich; Swanson and Sivaramakrishnan). We first validated that the R103A/R115A double mutation reported by Kato-Yamada would result in increased ATP affinity of the ATeam3.10 sensor. We did indeed measure a 4-fold increase in affinity, however this was a small increase in affinity compared to Kato-Yamada (Kato-Yamada). The difference in affinity shift is likely caused by the differences between the protein used. Kato-Yamada used the isolated *Bacillus sp.* PS3 epsilon subunit with a single Q107C mutation for labeling with a Cy3 fluorescent dye (Kato-Yamada). It is possible that the conjugated Cy3 contributed additional binding energy for this system, but the Q107C site is distant from the ATP binding site. It is more likely that in the context of the ATeam3.10 sensor, the bulky YFP and CFP that flank the epsilon subunit decrease the energetic stability of the ATP-bound state either through steric hindrances or other weak interactions between the fluorescent proteins. Similarly, Krah and co-workers used molecular dynamics simulations to predict that single mutation of the R103 or R115 residues would result in a comparable increase in ATP affinity relative to the wildtype and double mutant (Krah et al.). Although we did observe that the R115E single mutant caused an increase in ATP affinity, we did not measure significant increases in ATP affinity for the R103A or R115A single mutants, contrary to Krah's prediction. It is possible that our observation is confound by the steric bulk of the fluorescent proteins, making our observations specific to the ATeam3.10 sensor. However, given the agreement between the ATeam3.10 and isolated epsilon(Q107C) protein for the R103A/R115A double mutant, we hypothesize that our results reflect a diminished or absent effect of the single mutants on the isolated epsilon subunit. In the future, it will be of interest to test this by making the single mutants in the isolated epsilon subunit.

CHAPTER 3. EXTRACELLULAR ATEAM OPTIMIZATION

3.1 Introduction

The extracellular environment of a cell is a complicated matrix of protein channels, receptors, saccharides and other biomolecules. Loaded into secretory vesicles and capable of passing through a variety of channels, ATP is readily released into the extracellular space. ATP released into the extracellular environment acts in an autocrine and paracrine manner, binding metabotropic and ionotropic purinergic receptors (James and Butt). These receptors can respond to a wide range of ATP concentrations spanning nanomolar to millimolar magnitudes (Jacobson and Muller). Detecting ATP extracellularly is difficult to do due to low concentration release events, degradation by enzymes, and rapid diffusion away from the release site.

One of the long-standing methods for detecting extracellular ATP uses the bioluminescence given off by firefly luciferase when it reacts with its substrate luciferin and ATP (Gould and Subramani; Beigi et al.). The firefly luciferase systems consume ATP to produce its signal and requires the addition of a reagent which can confound results in sensitive signaling systems. The alternative to luciferase and luminescence systems largely consists of genetically encoded fluorescent protein biosensors. Several such ATP sensors have been developed for various cellular compartments including the mitochondria, cytosol and the membrane for extracellular detection. Among the extracellular ATP detection sensors are iATPSnFR^{1.0}, iATPSnFR^{1.1}, and ecATEam3.10 (Conley et al.; Lobas et al.). While tools like these can measure the middle and higher ends of the range of expected extracellular ATP, further development was needed to investigate ATP signaling closer to the nanomolar levels of ATP release.

We initially hypothesized that making affinity improving mutations discovered in Chapter 2 would increase ATP-binding affinity of ecATEam3.10, which we rename ECATS1 here for

convenience. As described in our results, this hypothesis was proven false, and we began to question if the physical constraints of tethering a cytosolic sensor to the membrane would limit its freedom of movement thereby limiting the FRET response. We then hypothesized that the membrane-tether was restraining the sensor and restoring freedom of movement would rescue ATP-binding affinity. To test this hypothesis, we created a small linker library of three lengths including ten, twenty and thirty nanometer linkers. These linkers were based of the alpha-helical structure of four glutamates following by four arginine or four lysine residues (ER/K) described and defined by Sivaramakrishnan (Sivaramakrishnan and Spudich). We observed that the ten-nanometer linker reduced sensor dynamic range, the twenty-nanometer linker restored affinity and improved dynamic range, while the thirty-nanometer linker restored affinity only.

3.2 Materials and Methods

3.2.1 Cloning ER/K Linkers into pMinDis-ecATeam3.10-R103A/R115A

The R103A/R115A double-mutation was applied to pMinDis-ecATeam3.10 (ECATS1) using the mutagenic primers described in Chapter 2.2.1 Table 1. Cloning of the double-mutant and the ER/K linker library was performed by Jason Conley and Elaine Colomb.

3.2.2 Neuro2A Cell Culture and Transfection

N2A cells (ATCC CCL-131) were cultured in Dulbecco's modified Eagle's medium containing 4.5 g/L glucose, 2 mM glutamine, and supplemented with 10% cosmic calf serum and were maintained at 37°C and 5% CO₂ in a humidified incubator. N2A cells were confirmed to be mycoplasma free as assessed by the Universal Mycoplasma Testing Kit (ATCC). Cells were transfected with plasmid DNA for expression of ecATeam sensors by living cells using the Effectene (Qiagen) transfection reagent as described in the manufacturer's protocol. Wild-type

ecATeam3.10 received co-transfection with an H2B-mApple construct to distinguish the mutant ecATeam3.10-R103A/R115A-20nm ER/K from wild-type within the same field-of-view as demonstrated in Figure 3.1. For imaging experiments, a mixture of wild-type ecATeam3.10/H2B mApple and ATeam3.10-R103A/R115A-20nm ER/K mutant expressing cells were then seeded, as indicated, onto nitric acid-cleaned and washed 18-mm #1.5 coverslips.

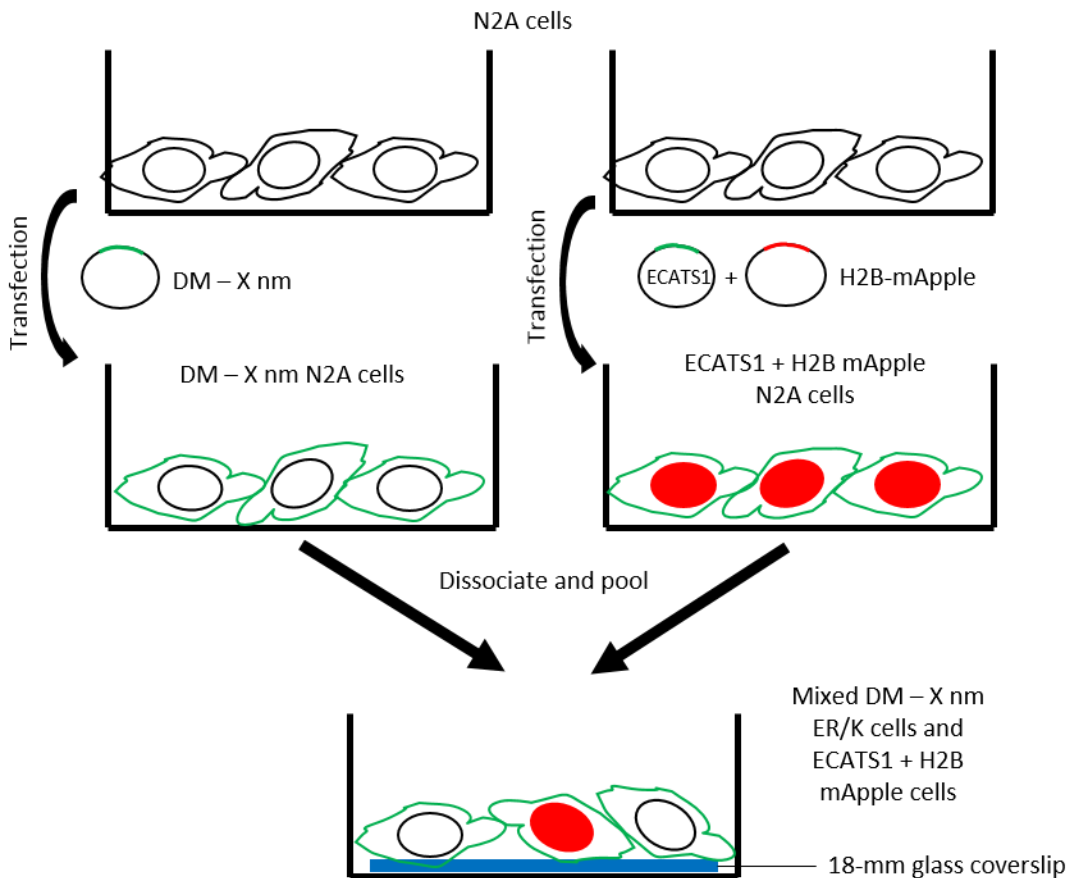


Figure 3.1 Diagram Demonstrating Approach to Distinguish Two Species of ATeam
 DM = R103A/R115A double-mutant. X nm = 10, 20 or 30 nm ER/K linkers. ECATS1 + H2B mApple is present as a reference and control to ATP responses in the presence of a spectrally identical mutant.

3.2.3 Live-cell Fluorescent Microscopy and Analysis

Cells were prepared for microscopy by exchanging cell growth media for imaging solution consisting of 15 mM HEPES, 1.25 mM NaH₂PO₄, 10 mM glucose, 130 mM NaCl, 3 mM KCl, 2 mM CaCl₂, 1 mM MgCl₂, and 3 mM NaHCO₃ (pH 7.3) and cells were equilibrated at room temperature for at least 20 min prior to imaging. Osmotic shock solution was prepared as imaging solution consisting of 15 mM HEPES, 10 mM glucose, 2 mM CaCl₂ and 1 mM MgCl₂. All microscopy experiments were performed at ambient room temperature, using either continuous perfusion (~ 1.5 mL/min flow rate) of imaging solution, static bath, or a mixture of static and perfusion steps. Cells were imaged using an Olympus IX83 fluorescence microscope with a 20X/0.75 NA objective illuminated by a Lumencor SpectraX light engine and equipped with an Andor Zyla 4.2 sCMOS camera. ECATS2 sensor activity was measured by examining the fluorescence intensities in CFP, CFP-YFP FRET, and YFP channels. Specifically, the ATeams were excited in the CFP and CFP-YFP FRET channels using a 438/29 nm bandpass filter, and emission was collected through 470/24 and 540/30 nm bandpass filters for the CFP and CFP-YFP FRET channels, respectively. The fluorescence in the YFP channel was excited using a 510/10 nm bandpass filter and emission was collected through a 540/30 nm bandpass filter. The fluorescence in the RFP channel was excited using a 575/25 nm bandpass filter and emission was collected through a 631/28 nm bandpass filter. Excitation light from all fluorescence channel measurements was blocked by the ET-ECFP/EYFP/mCherry multiband beamsplitter (Chroma 69008bs). The microscope components and image acquisition were controlled by the Andor iQ3 software and the ImageJ/FIJI software package was used to analyze all images for each experiment, as specified. For fluorescence images, the mean and standard deviation of background intensities were measured for each channel in each field of view. For each fluorescence channel, the mean background intensity was subtracted from every image of the associated imaging set. Background

masks were then created with minimum thresholds of two times the mean background intensity. The background masks were applied to the fluorescence intensity images and fluorescence ratio images were created by pixel-by-pixel division of the background masked individual fluorescence channels. Regions of interest that encompassed whole cells or cell membranes, as indicated, were drawn and the mean fluorescence ratios of pixels within each region of interest were calculated.

3.2.4 Statistical Analysis

All statistical analysis was done using OriginPro2017 64-bit software. Since our primary goal was improving ATP affinity compared to the first-generation sensor, we report the results of the unpaired 2-tailed student's t-test comparing specific linkers to the control (ECATS1). Differences were deemed significant if $p < 0.05$. Data in this chapter is reported as the mean \pm standard deviation.

3.3 Results

All work done in this chapter was in collaboration with Jason Conley. The first hypothesis tested was that making the R103A/R115A mutations to the epsilon subunit of ecATeam3.10 would increase ATP binding affinity as observed in solution. This hypothesis was proven false as seen by the similar affinities (ecAT3.10 $K_{app} = 12 \pm 5 \mu\text{M}$; ecAT3.10-(A/A) $K_{app} \sim 12 \mu\text{M}$) and slight loss of dynamic range (ecAT3.10 = 1.2 versus ecAT3.10-(A/A) = 0.87) observed in the double mutant in Figure 3.2. At all concentrations of ATP (3 μM ATP ECATS1 vs A/A mutant $p=0.619$; 10 μM ATP ECATS1 vs A/A mutant $p=0.975$; 300 μM ATP ECATS1 vs A/A mutant $p=0.075$ determined by unpaired 2-tailed student's t-test) there were no significant differences between ecAT3.10 and the R103A/R115A double mutant when directly comparing responses to ATP.

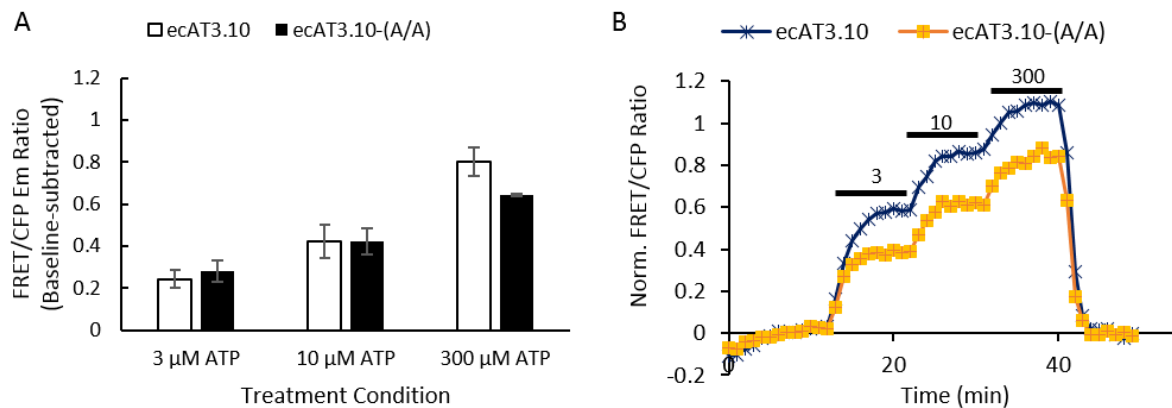


Figure 3.2 The R103A/R115A Double-Mutant does not Increase Extracellular ATP Affinity
 A) Data represents the mean \pm SEM of averaged data from cells from three different dates where $n=31$ ECATS1 cells and $n=69$ double-mutant expressing cells. B) Representative single cell traces during perfusion ATP dose-response. Black bars indicate the concentration of ATP being perfused in micromolar (μM). No significant differences in response were detected between ecAT3.10 and the R103A/R115A double-mutant ($p>0.05$ at all ATP concentrations) when responses to the same ATP concentrations were compared. Data courtesy of Jason Conley.

Since our first hypothesis was proven false by the data in Figure 3.2, we hypothesized that the surface membrane tether reduces ATP binding affinity. This alternative hypothesis would be consistent with our observation that surface tethering itself causes a loss of ATP binding affinity when ATeam3.10 is tethered to the membrane, as shown in the first-generation ECATS1 sensor (Conley et al.). To test this hypothesis, we generated a small linker library of increasing lengths. There are only 13 amino acids in between the PDGFR transmembrane domain and the YFP of ATeam in ECATS1, and therefore steric constraints could be limiting the movement of the sensor affecting ATP binding affinity. A small, semi-rigid, rotatable ER/K linker library was made of lengths ten (92 amino acids), twenty (153 amino acids) and thirty (229 amino acids) nanometers modeled after the linkers characterized by Sivaraj Sivaramakrishnan to address our hypothesis (Sivaramakrishnan and Spudich; Swanson and Sivaramakrishnan). We expected that lengthening the tether would increase ATP binding affinity by increasing the distance between the sensor and membrane while providing better freedom of movement.

The ten nanometer ER/K linker combined with the R103A/R115A double-mutant (DM-10nm) ecATeam3.10 showed no increase in ATP binding affinity (no significant differences in response to 3 μ M ATP ECATS1 vs DM-10nm $p=0.13$, and 10 μ M ATP ECATS1 vs DM-10nm mutant $p=0.30$; unpaired 2-tailed t-test) and had a reduced dynamic range (ecAT3.10 = 1.1 verses DM-10nm = 0.8) when compared to ECATS1 in N2A cells as seen in Figure 3.3. The maximum signal of the DM-10nm variant to 300 μ M ATP was significantly reduced compared to ECATS1 ($p=0.0002$ unpaired 2-tailed t-test). Contrary to our expectations, the ten-nanometer linker sensor showed no improvement in ATP affinity and had a more limited dynamic range.

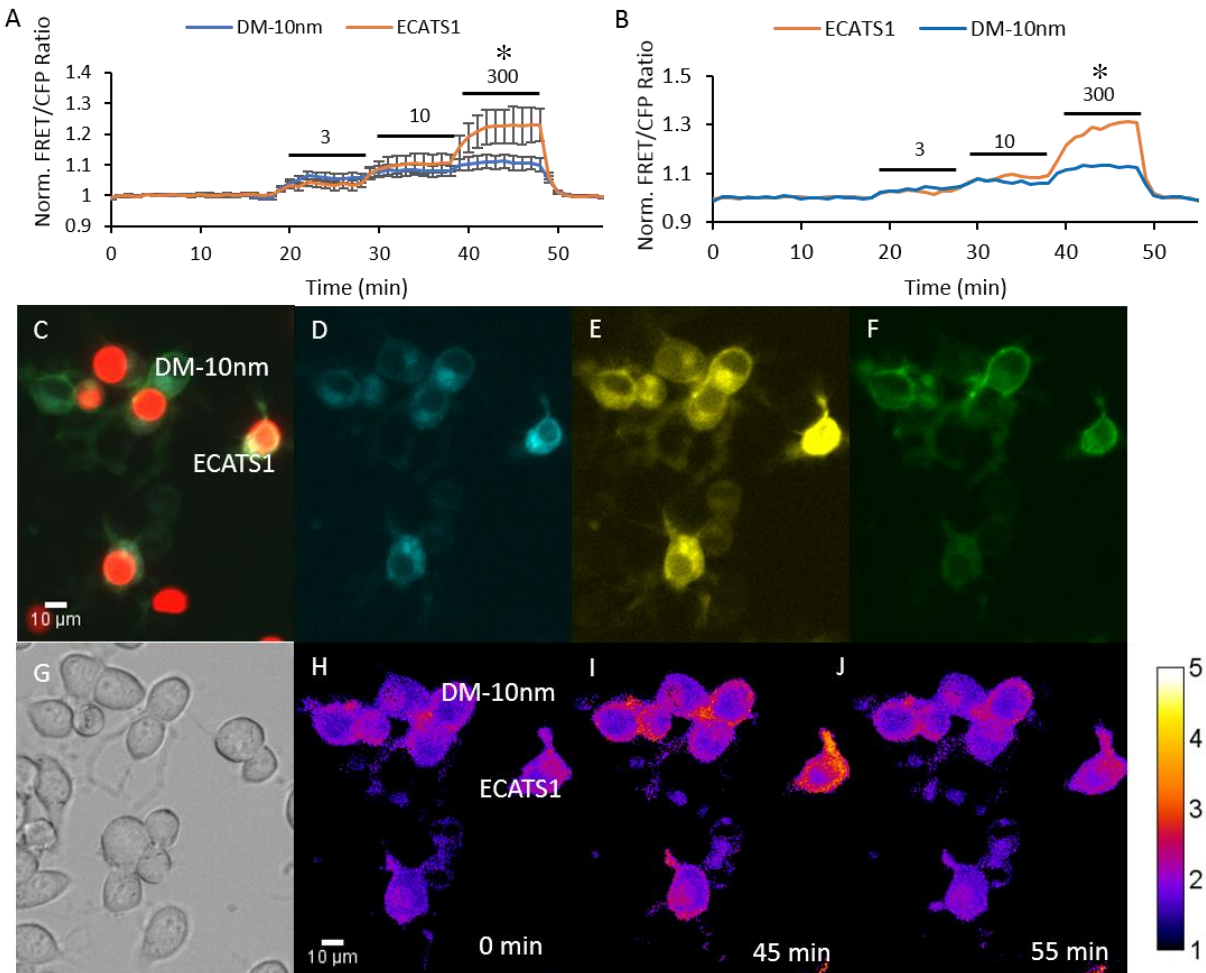


Figure 3.3 ECATS1 has Similar Affinity and Better Dynamic Range than DM-10nm ER/K

A) ECATS1 shows similar affinity to DM-10nm, while DM-10nm shows a reduced dynamic range. ECATS1 expressing cells were H2B-mApple positive to distinguish signals. ATP concentrations perfused across cells were 3, 10 and 300 μ M. DM-10nm signal is significantly lower than ECATS1 to 300 μ M ATP determined by unpaired 2-tailed student's t-test ($p=0.0002$) indicating significantly reduced dynamic range. Data shown is the normalized FRET/CFP ratio of all cells Mean \pm 95% Confidence Interval n=6 ECATS1 and n=18 DM-10nm B) Individual cell traces of ECATS1 and DM-10nm expressing N2A cells labeled and shown in images C-J. C) Merged image showing ECATS1 cells co-expressed with H2B-mApple. Individual channels D) CFP, E) CYFRET, F) YFP and G) DIC show cells expressing both sensors within the same field of view. Ratio images (H-J) show both sensors H) before ATP addition, I) response to perfused 200 μ M ATP, and J) after perfusion washout of all ATP.

The twenty nanometer ER/K linker, when combined with the R103A/R115A ecATeam3.10 (DM-20nm) showed increased ATP affinity (ECATS1 $K_{app} = 12 \pm 5 \mu\text{M}$ versus DM-20nm $K_{app} = 3.7 \pm 0.6 \mu\text{M}$) with a slight increase in dynamic range (ECATS1 = 1.4 versus DM-20nm = 1.7). Sensors ECATS1 and DM-20nm both had no response to 100 nM ATP ($p=0.818$; when comparing mean sensor response to its own baseline; unpaired 2-tailed t-test) but DM-20nm began to differ in response compared to ECATS1 as early as 500 nM ATP ($p=0.022$; when comparing 500nM ATP response in ECATS1 to DM-20nm; unpaired 2-tailed t-test). The DM-20nm variant showed increased responses to 1 μM ATP ($p=0.0008$; when comparing mean response of ECATS1 to mean response of DM-20nm at 1 μM ATP; unpaired 2-tailed t-test), 3 μM ATP ($p=5.0 \times 10^{-5}$; unpaired 2-tailed t-test), and 10 μM ATP ($p=0.0022$; unpaired 2-tailed t-test) before it returned to comparable responses with ECATS1 again at 50 μM ATP ($p=0.623$) and 300 μM ATP ($p=0.264$). In Figure 3.4, we demonstrated that the DM-20nm ER/K responds to concentrations as low as 500 nM.

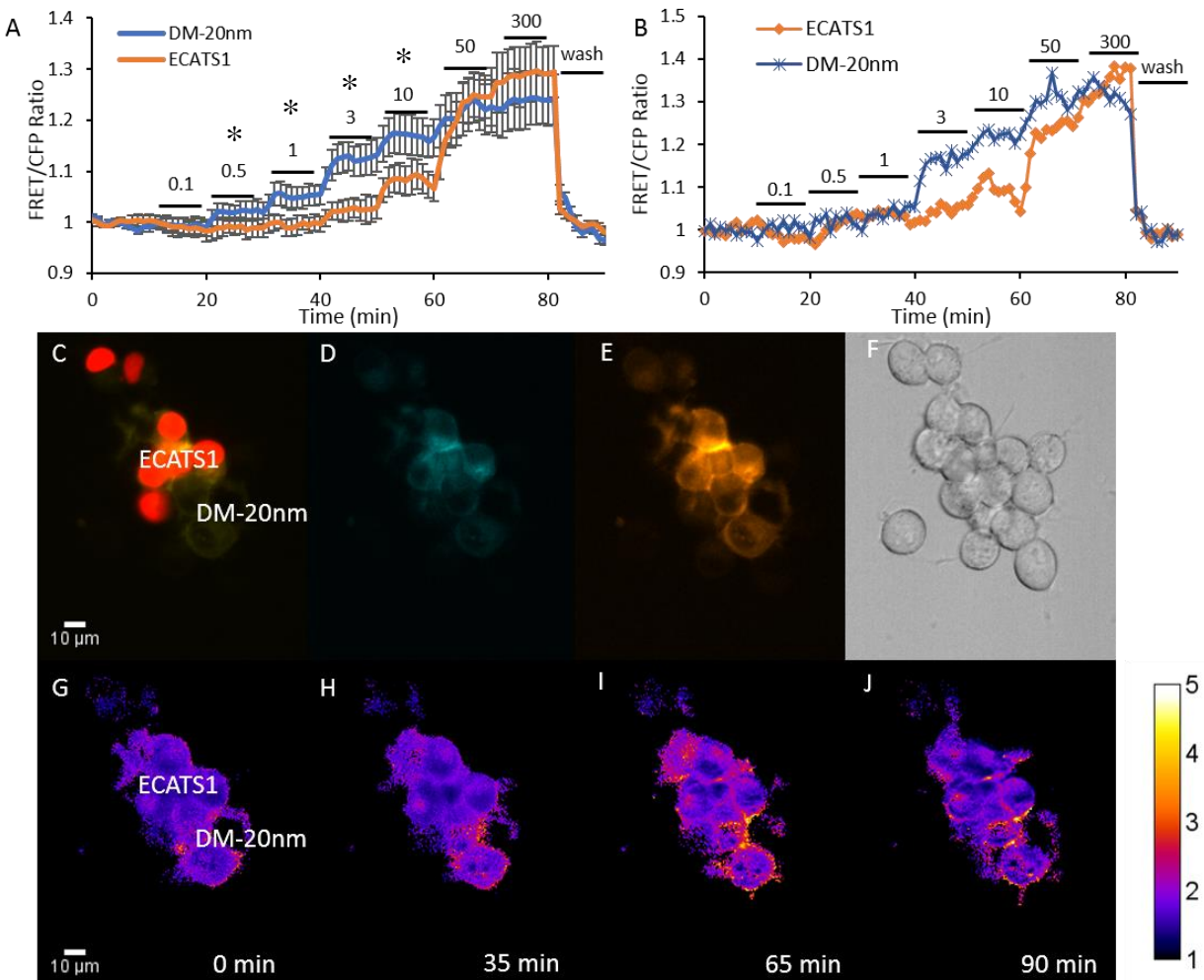


Figure 3.4 DM-20nm ER/K shows Increased ATP Affinity over ECATS1

A) DM-20nm ER/K shows increased affinity for ATP over ECATS1 with a similar dynamic range. ECATS1 cells were expressing H2B-mApple to distinguish from mutant expressing cells. ATP concentrations shown above the black bars are all in micromolar (μM). * = $p < 0.05$ as determined by unpaired 2-tailed student's t-test. Data shown is the mean \pm 95% Confidence Interval $n=12$ ECATS1 $n=18$ DM-20nm. B) Individual cell traces of each sensor type shown in images C-J. C) Merged image showing H2B-mApple channel to distinguish ECATS1 cells from DM-20nm cells. The D) CFP channel, E) FRET channel and F) DIC channels show the N2A cells expressing the sensors. G-J shows the sensors at key points during the dose-response; G) before response, H) at 35 minutes when DM-20nm started significantly responding over ECATS1, I) at 65 minutes when both sensors began to respond comparably to each other, and J) after washout of ATP.

We expected DM-30nm to provide similar results to DM-20nm if freedom of movement was the largest hindrance in ATP-binding. The DM-30nm variant showed no significant improvements in affinity or dynamic range, as it responded to all concentrations of ATP comparable with ecAT3.10 (3 μ M ATP p=0.102; 10 μ M ATP p=0.253; 300 μ M ATP p=0.749; unpaired 2-tailed t-test). While the DM-20nm data suggests that both ATP affinity and dynamic range were improved, neither the dynamic range of DM-30nm or ATP affinity was improved compared to ECATS1 as seen in Figure 3.5 (ECATS1 = 1.05 verses DM-30nm = 1.1).

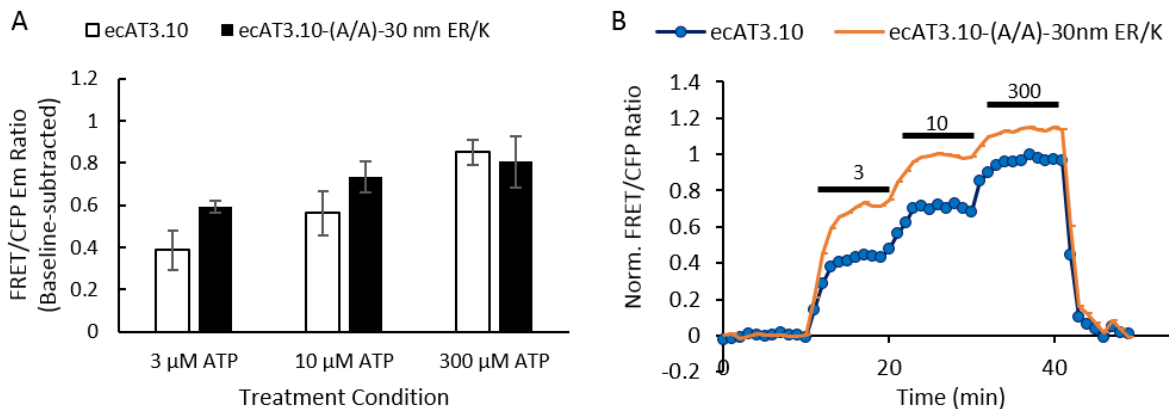


Figure 3.5 Double-Mutant with 30nm ER/K linker shows slight Increase in ATP Affinity
 A) Data represents the mean \pm SEM of averaged data from three different dates where n=29 ECATS1 cells and n=52 DM-30nm ER/K cells. B) Representative single cell traces during perfusion ATP dose-response. Black bars indicate the concentration of ATP being perfused in micromolar (μ M). No significant differences were observed by comparing ECATS1 with DM-30nm by unpaired 2-tailed t-test; all p-values>0.05. Data courtesy of Jason Conley.

Interestingly, when we screened all three linker lengths combined with our R103A/R115A double-mutant (DM), only one provided an improvement in sensor affinity. The ten-nanometer linker (DM-10nm) surprisingly created a more limited sensor than ECATS1, and we are unsure why this is the case. The twenty-nanometer linker (DM-20nm) proved successful in improving the sensor. The thirty-nanometer linker (DM-30nm) we expected to improve the sensor also, but instead DM-30nm showed less improvement over ECATS1 than the twenty-

nanometer linker. Jason Conley screened all three ER/K linker lengths in ECATS1 and found a similar trend where the twenty-nanometer provided the largest improvements (data not shown).

Having replicated our ~4-fold increase in ATP-binding affinity from protein solution at the membrane, we decided to move forward with the DM-20nm ER/K linker variant. The DM-20nm or ecATeam3.10-R103A/R115A-20nm ER/K linker will be referred to as the Extra-Cellular ATP Sensor generation 2 or ECATS2 from this point.

We know ECATS1 can respond to an ADP signal at high concentrations, and so we screened ECATS2 for its sensitivity to ADP by perfusion using the N2A cell model. ECATS2 shows an increased affinity for ADP as well (ECATS1 ADP K_{app} ~ 200 μM versus ECATS2 ADP K_{app} ~ 100 μM) seen in Figure 3.6 by ECATS2 increased response to 100 μM ADP over ECATS1 ($p=0.0026$ unpaired 2-tailed t-test). It is noted that the apparent affinity of ECATS2 for ATP is approximately twenty-five-fold greater than its affinity for ADP, and that only pathological models would even approach ADP releases capable of evoking an ECATS2 signal.

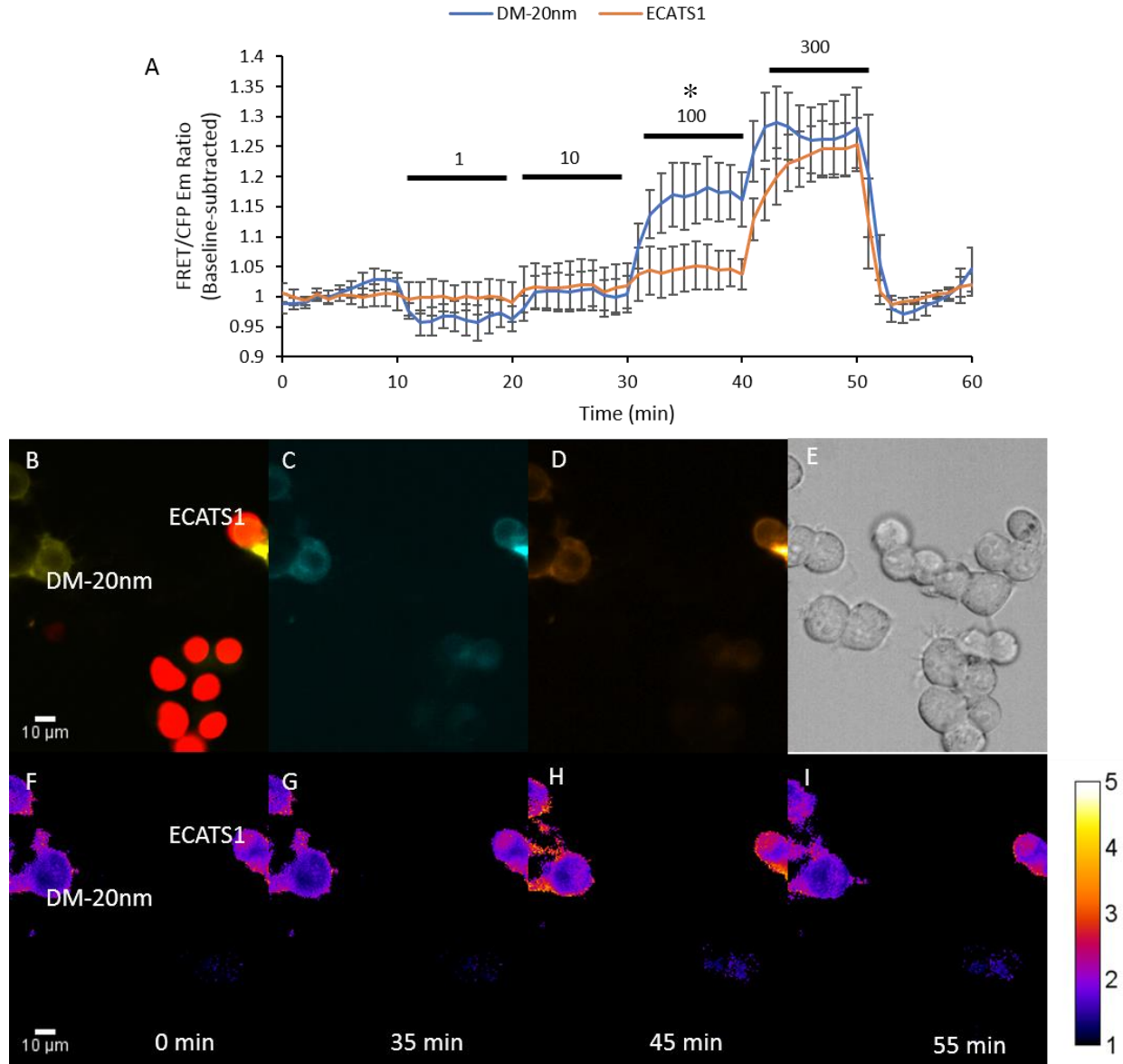


Figure 3.6 DM-20nm ER/K mutant shows slightly increased ADP Affinity over ECATS1

A) The DM-20nm ER/K mutant begins to respond to ADP at concentrations near 100 μ M before ECATS1 ($p=0.0026$; unpaired 2-tailed t-test) where their responses become comparable again when exposed to 300 μ M ADP ($p=0.400$). Data shown represents the mean \pm 95% confidence interval where $n=8$ ECATS1 cells and $n=10$ DM-20nm ER/K cells. B) Merged FRET and RFP channels to distinguish ECATS1 expression from DM-20nm cells by co-localization of H2B mApple with ECATS1. Individual channels C) CFP, D) FRET and E) DIC shows N2A expressing either sensor within same field of view. Ratio images F-I compare responses F) before ADP exposure, G) 100 μ M ADP at time 35 minutes, H) 300 μ M ADP at time 45 minutes, and I) after washout at time 55 minutes.

3.4 Discussion

In this study we first tested the hypothesis that making the R103A/R115A double-mutation within the epsilon subunit of ECATS1 would increase sensor affinity for extracellular ATP. Our results indicate this hypothesis was false, and other factors such as the cell surface environment and tethering a cytosolic sensor to the membrane could be reducing affinity. Increasing the affinity of the epsilon subunit alone did not prove enough to increase the ATP binding affinity of ECATS1.

We decided to test the secondary hypothesis that tethering a cytosolic-derived sensor to the membrane reduces its ATP affinity by limiting freedom of movement. Our lab had hypothesized previously that the addition of a surface-tether may have contributed to the 20-fold reduction in ATP binding affinity when constructing ECATS1 from the cytosolic ATeam3.10 (Conley et al.). To test this hypothesis, we cloned a small library of semi-rigid ER/K linkers of three lengths that were based off the linkers described by Sivaramakrishnan and Spudich. We screened for increased ATP affinity observed in solution for both the wild-type and the R103A/R115A double-mutant. In the wild-type, the ten-nanometer linker seemed to reduce dynamic range while the twenty and thirty nanometer linkers provided minor improvements to sensor affinity and dynamic range. This suggests that the physical constraints of membrane tethering reduce affinity when converting a FRET sensor from the cytosol.

The ten-nanometer ER/K linker combined with the R103A/R115A double-mutant provided no increase in extracellular ATP binding affinity and reduced dynamic range compared to ECATS1. The twenty-nanometer ER/K linker combined with the R103A/R115A double-mutation (DM-20nm) in the epsilon subunit provided a near 4-fold increase in ATP binding affinity, replicating our observations in protein solution in Chapter 3. These results in the double-mutant further support our observations in our ECATS1 linker library that membrane-tethering does reduce sensor affinity by restricting freedom of movement. The thirty nanometer ER/K linker

double-mutant (DM-30nm) showed a similar increase in binding affinity like DM-20nm. However, it did not seem to benefit from the slight increase in dynamic range that we observed in DM-20nm.

Having successfully increased the extracellular ATP-binding affinity by applying the double-mutation within the epsilon subunit combined with the twenty-nanometer ER/K linker in ecATeam3.10, we dubbed this new sensor ECATS2. Future work to improve ATP binding affinity and dynamic range might start at further modulation of the F₀F₁-ATP-synthase epsilon subunit, since further lengthening of the tether appears non-beneficial beyond twenty nanometers. Changing the linker lengths between the epsilon subunit and the FPs may provide improvements in dynamic range.

CHAPTER 4. ATP RELEASE IN CELLULAR MODEL OF EDEMA

4.1 Introduction

Volume regulation within cells is a critical regulatory mechanism across a variety of cell types within the human body (Hoffmann et al.). A hypo-osmotic shock (HOS) occurs when osmolality outside the cell drops below the osmolality of the cytosol, resulting in water rushing into the cell by aquaporins or passive transport (Thrane et al.). To return to a healthy cellular volume, the swollen cell must evacuate ions and amino acids such that osmotically obliged water follows (Bender et al.). In order for ions and amino acids to be readily evacuated from the cell, channels and transporters must be activated. For example, epithelial cells release ATP in response to cellular swelling that acts in an autocrine manner by binding P2 purinergic receptors (Schwiebert et al.). Binding of ATP to P2 receptors and ATP-binding cassette proteins such as Multidrug Resistance Protein (MRP) and *p*-glycoprotein activates volume-regulatory anion channels (VRACs) typically in the form of a chloride current (Darby et al.). Chloride ions are evacuated from the cell along with water, ATP, and negatively charged amino acids.

Previous studies have used membrane-attached luciferase-luciferin based methods to detect extracellular ATP, but are unable to quantify the concentration of ATP locally at the cell membrane (Darby et al.; Gould and Subramani; Beigi et al.; Y. Zhang et al.). While this is partially due to the difficult nature of detecting extracellular ATP, it is also due to the fact that, in these studies, the luminescence response is not calibrated to a known concentration of ATP in real-time systems (Darby et al.). Zhang et al. did calibrate their chemiluminescent response with a standard curve and were able to quantify ATP release following mechanical stimulation, however they could not detect release events below ten micromolar (Y. Zhang et al.). In addition, luciferase methods require the addition of the reagent luciferin and production of the signal consumes ATP.

Consumption of extracellular ATP to produce a signal could prevent or dull cellular responses elicited by P2X and P2Y receptors, confounding the signaling mechanism. P2Y receptors are believed to have relatively high affinity for extracellular ATP ($EC_{50} < 20 \mu M$) which is within the detection limits of ECATS2 (Zhao et al.; Trautmann; Jacobson and Muller). Other genetically encoded extracellular ATP fluorescent biosensors have lower ATP affinity than ECATS2 ($K_{app} = 3.7 \pm 0.6 \mu M$) such as ecATeam3.10 (ECATS1 $K_{app} = 12 \pm 5 \mu M$) and iATPSnFR^{1.0} ($K_{app} \sim 140 \mu M$) that make them less ideal to study P2Y purinergic signaling (Lobas et al.; Conley et al.).

We aimed to test the hypothesis that ATP release in response to HOS is in the range of 1-20 μM and can activate P2Y₁₁ receptors in cells. To test this hypothesis, we used our sensor ECATS2 to quantify the magnitude of ATP release in the HEK293A cellular model. As volume regulation control mechanisms are highly conserved, HEK293A cells express the necessary VRACs needed to study ATP release following HOS (Hélix et al.). Additionally, we sought to test two-color imaging paradigms using a sensor that detects cAMP to demonstrate P2Y₁₁ receptor activation, which would also orthogonally validate that ECATS2 is responding to a real ATP release following HOS. As HEK293A cells do not express endogenous P2Y₁₁ we transfected P2Y₁₁ receptor DNA into cells for two-color imaging experiments (Schachter et al.). We observed ATP release from ECATS2, as well as P2Y₁₁ receptor activation observed by the cAMP sensor Pink Flamindo in the HEK293A cellular model (Harada et al.).

4.2 Materials and Methods

4.2.1 HEK293A Cell Line Maintenance

HEK293A cells were cultured in Dulbecco's modified Eagle's medium (DMEM) containing 4.5 g/L glucose, 3.7g/L sodium bicarbonate, 4 mM glutamine, 0.1 mM Non-essential Amino Acids (NEAA) and supplemented with 10% cosmic calf serum. Cells were maintained at

37°C and 5% CO₂ in a humidified incubator and passed three times weekly once confluence reached 80% or higher.

4.2.2 Calcium Phosphate Transfection

Prior to transfection cells were washed with 1X DPBS and fed with fresh media. Transfection of HEK293As was done using calcium phosphate with DNA density of 450ng/cm² in either a 6-well plate or directly onto nitric acid washed coverslips in a 12-well plate. 250mM Calcium chloride, sensor DNA and water were mixed with a 2X HEPES buffer solution containing 140 mM NaCl, 1.5 mM Na₂HPO₄, 50 mM HEPES, pH 7.02 at room temperature. The buffer was added dropwise slowly to the DNA mix and pipetted up and down exactly one time to mix, incubated at RT for 1 minute before adding dropwise to the cells. The volume of transfection was adjusted to be 10% of the well volume to keep 6-well and 12-well transfections as similar as possible. Transfection DNA was incubated with cells overnight and washed off the next day. Cells seeded directly onto coverslips were imaged the same day as DNA wash off following a 1-hour recovery period at 37°C in the incubator.

Transfections of ECATS2 and a non-binding sensor control (NB) were done in separate wells of a 6-well plate where H2B mApple was co-transfected with the non-binding control. H2B mApple DNA was used at a ratio of 2:1 to the non-binding control DNA to ensure all cells expressing the control sensor were H2B mApple positive to distinguish from the ECATS2 sensor expressing cells. Cells expressing ECATS2 were dissociated with trypsin, mixed 1:1 with dissociated cells expressing H2B mApple coupled with the non-binding control, and seeded at a density of 50K cells/cm² on nitric acid washed 18-mm coverslips as seen in Figure 4.1 below. The mixed cell population was given 24 hours to recover and grow before imaging.

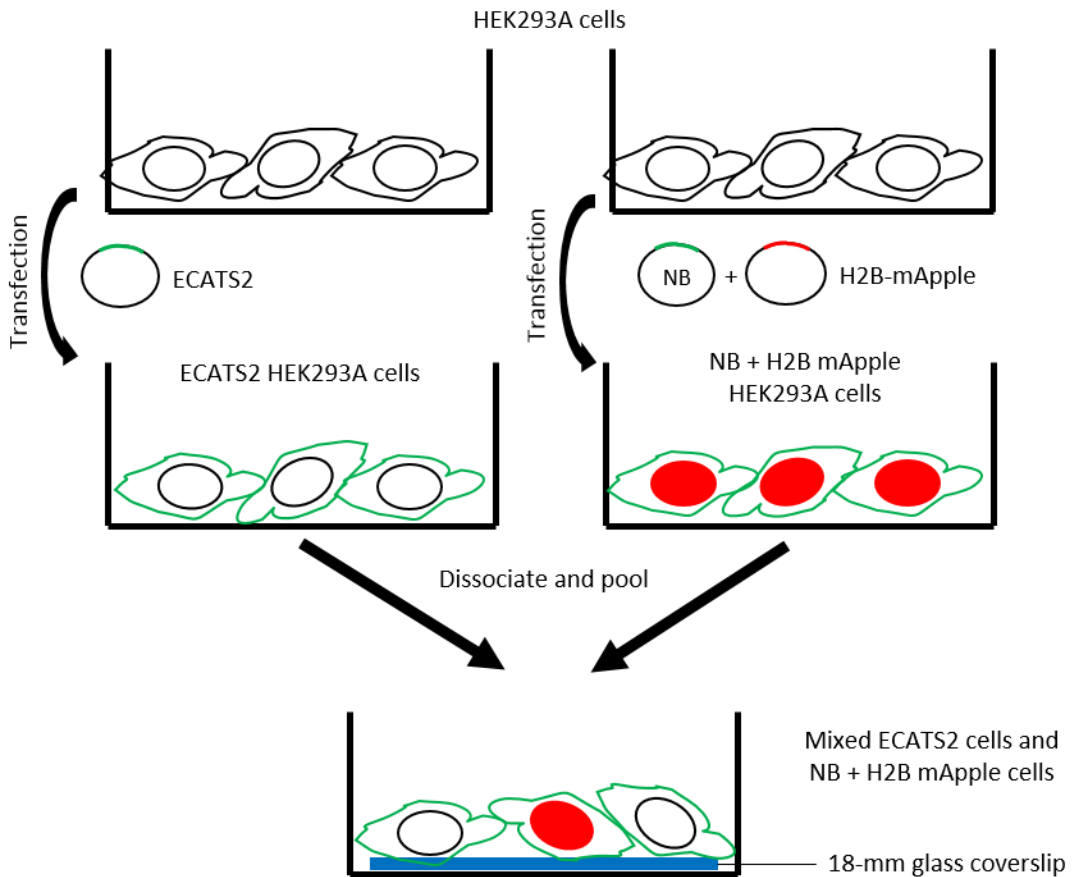


Figure 4.1 Diagram Demonstrating Methods of Distinguishing Two Species of ATeam
NB= non-binding mutant control. NB + H2B mApple is present as a non-ATP binding control.

Finally, to test spectrally compatible second messenger sensors we transfected HEK293A cells seeded on nitric acid washed 18-mm coverslips with or without the Gs-coupled P2Y₁₁ receptor, ECATS2 and Pink Flamindo at a ratio of 2:1:1 of DNA respectively. P2Y₁₁ was included such that we could see an increase in cAMP via Pink Flamindo (Harada et al.), validating ATP release by receptor activation. These experiments were repeated without P2Y₁₁ addition as a control.

4.2.3 Live-cell Fluorescent Microscopy

Cells were prepared for microscopy by exchanging cell growth media for imaging solution consisting of 15 mM HEPES, 1.25 mM NaH₂PO₄, 10 mM glucose, 130 mM NaCl, 3 mM KCl, 2 mM CaCl₂, 1 mM MgCl₂, and 3 mM NaHCO₃ (pH 7.3) and cells were equilibrated at room temperature for at least 20 min prior to imaging. 100% osmotic shock solution was prepared as imaging solution consisting of 15 mM HEPES, 10 mM glucose, 2 mM CaCl₂ and 1 mM MgCl₂. Osmotic shock and reduction of osmolality is achieved by the dilution of NaCl and KCl upon mixing imaging solution with 100% osmotic shock solution to create a 50% osmotic shock solution, which was used for all HOS experiments. All microscopy experiments were performed at ambient room temperature, using either continuous perfusion (~ 1.5 mL/min flow rate) of imaging solution, static bath, or a mixture of static and perfusion steps. Cells were imaged using an Olympus IX83 fluorescence microscope with a 20X/0.75 NA objective illuminated by a Lumencor SpectraX light engine and equipped with an Andor Zyla 4.2 sCMOS camera. ECATS sensor activity was measured by examining the fluorescence intensities in CFP, CFP-YFP FRET, and YFP channels. Specifically, the ATeams were excited in the CFP and CFP-YFP FRET channels using a 438/29 nm bandpass filter, and emission was collected through 470/24 and 540/30 nm bandpass filters for the CFP and CFP-YFP FRET channels, respectively. The fluorescence in the YFP channel was excited using a 510/10 nm bandpass filter and emission was collected through a 540/30 nm bandpass filter. The fluorescence in the RFP channel was excited using a 575/25 nm bandpass filter and emission was collected through a 631/28 nm bandpass filter. Excitation light from all fluorescence channel measurements was blocked by the ET-ECFP/EYFP/mCherry multiband beamsplitter (Chroma 69008bs). The microscope components and image acquisition were controlled by the Andor iQ3 software and the ImageJ/FIJI software package was used to analyze all images for each experiment, as specified. For fluorescence images, the mean and

standard deviation of background intensities were measured for each channel in each field of view. For each fluorescence channel, the mean background intensity was subtracted from every image of the associated imaging set. Background masks were then created with minimum thresholds of two times the mean background intensity. The background masks were applied to the fluorescence intensity images and fluorescence ratio images were created by pixel-by-pixel division of the background masked individual fluorescence channels. Regions of interest that encompassed whole cells or cell membranes, as indicated, were drawn and the mean fluorescence ratios of pixels within each region of interest were calculated. For intensiometric sensor Pink Flamindo raw intensities from ROIs were used directly for analysis.

4.2.4 Statistical Analysis

All statistical analysis was done using OriginPro2017 64-bit software. Since our primary goal was detecting ATP release in response to HOS, we report the results of the unpaired 2-tailed student's t-test comparing ECATS2 to the nonbinding (NB) control. Differences were deemed significant if $p < 0.05$ when comparing means. Data in this chapter is reported as the median \pm 95% confidence interval.

4.3 Results

In order to test the hypothesis that ATP release in response to HOS in HEK293A cells is in the range of 1-20 μM and is capable of activating P2Y receptors, we used the ECATS2 sensor. Cells were transfected separately with ECATS2 or the Non-binding (NB) mutant before being dissociated and mixed together as seen in Figure 4.1 above. The NB mutant was used as an ATP non-binding control within the same field of view of ECATS2. Since the NB-mutant is derived

from ECATS2 and occupies the same spectral space, H2B-mApple serves to distinguish NB cells from ECATS2 cells within the same experiment.

A 50% HOS achieved by a 1:1 mix of imaging solution and 100% shock solution (130 mM NaCl ~300 mosmoles → 65 mM NaCl ~150 mosmoles) shows a release of ATP ($p=3.85 \times 10^{-22}$; unpaired 2-tailed t-test comparing ECATS2 to NB) from HEK293A cells by the mean response of all time-points after HOS and before addition of a calibrating solution containing 20 μ M ATP in Figure 4.2. Perfusion wash out of ATP with 50% shock solution nearly returns to baseline in ECATS2 while the NB control has large peaks that are due to debris floating over ROIs during washing. These results show that a release of ATP from HOS in HEK293A cells is within the ideal detection range of ECATS2 and thus is also likely capable of activating P2Y receptors.

We also observed a slight increase in FRET/CFP ratio in both ECATS2 and the NB control instantly following HOS. The NB control stayed static after this initial artifact while ECATS2 proceeded to detect ATP release. While the ATeam family of sensors are known to be pH sensitive, this jump is not due to pH changes as the shock solution was pH matched to aCSF. One potential explanation is that changes in osmolality affect the dynamic range of FRET sensors.

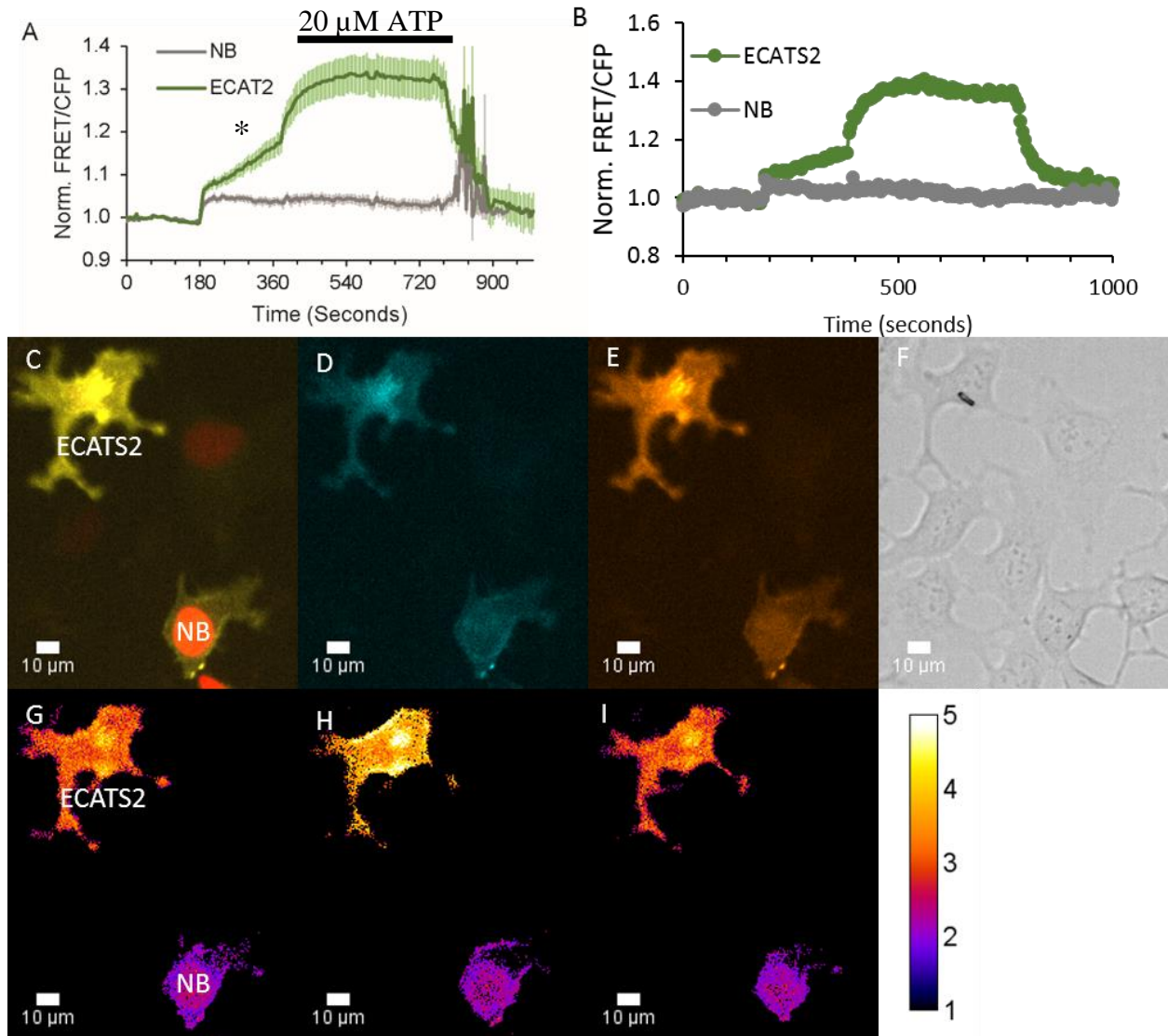


Figure 4.2 ATP release detected from HEK293A cells using ECATS2

A) Normalized FRET/CFP ratio shows an ATP release from HEK293A cells detected by ECATS2 in response to a static 50% HOS at time=180 seconds ($p<0.0001$; unpaired 2-tailed t-test comparing ECATS2 to NB control). 20 μ M ATP was added at time=380 seconds and then washed out by perfusion pump at time= 750 seconds. B) Individual cell traces of the ECATS2 and NB cells shown in C-I. C) Merged CFP/FRET/RFP color image to separate ECATS2 cells from NB cells where cells expressing NB also expressed H2B-mApple. An ECATS2+ cell is seen in the upper left while an NB+ cell is seen in the lower right. D) CFP channel, E) CYFRET channel, and F) DIC channel. CYFRET/CFP ratio images showing G) before response, H) maximal ECATS2 response after ATP addition, and I) after washout by perfusion. Scale bars are 10 μ m.

Next, in order to test the hypothesis that P2Y₁₁ receptors (EC₅₀ ~ 10 μM ATP) are activated by ATP released from HOS in HEK293A cells, we used ECATS2 and Pink Flamindo. ATP EC₅₀ values of the P2Y₁₁ receptor are near 10 μM and within the detection limit of ECATS2 (Zhao et al.; Jacobson and Muller). P2Y₁₁ is a Gs-coupled receptor, which increases cytosolic cAMP upon activation, which can be detected by the cytosolic cAMP sensor Pink Flamindo (Harada et al.). Using both ECATS2 and Pink Flamindo in tandem serves both a biological and a methodological purpose. The biological purpose demonstrated that ATP release from HOS is in the range of several micromolar, capable of activating P2Y₁₁ (EC₅₀ ~10 μM ATP) as indicated by increase in ECATS2 and Pink Flamindo signals upon HOS (Jacobson and Muller). The methodological purpose served to use Pink Flamindo signal as orthogonal validation of an ATP release. This method is similar to the concept behind Cell Neurotransmitter Fluorescent Engineered Reporter (CNiFER) cells that use G-protein coupled receptors for detection of neurotransmitters (Lacin et al.).

A 50% HOS resulted in an ATP release (ECATS2 50% HOS vs ECATS2 baseline unpaired 2-tailed t-test p=7.75x10⁻⁴²) and subsequent cAMP response (Pink Flamindo 50% HOS vs Pink Flamindo baseline unpaired 2-tailed t-test p=1.03x10⁻⁴⁶) as seen in Figure 4.3, as expected. Addition of 200 μM ATP drives both an ECATS2 and Pink Flamindo response in HEK293A cells expressing P2Y₁₁, but only an ECATS2 response in control cells without transfected P2Y₁₁. Forskolin addition was required to increase the Pink Flamindo signal in cells without P2Y₁₁, indicating little to no expression of endogenous P2Y11 in HEK293A cells (data not shown). These results further validate that two-color imaging is possible with ECATS2, making investigation of upstream and downstream purinergic receptor signaling dynamics possible, and demonstrates that ATP released in HEK293A cells in response to HOS is in the order of several micromolar capable of activating P2Y₁₁.

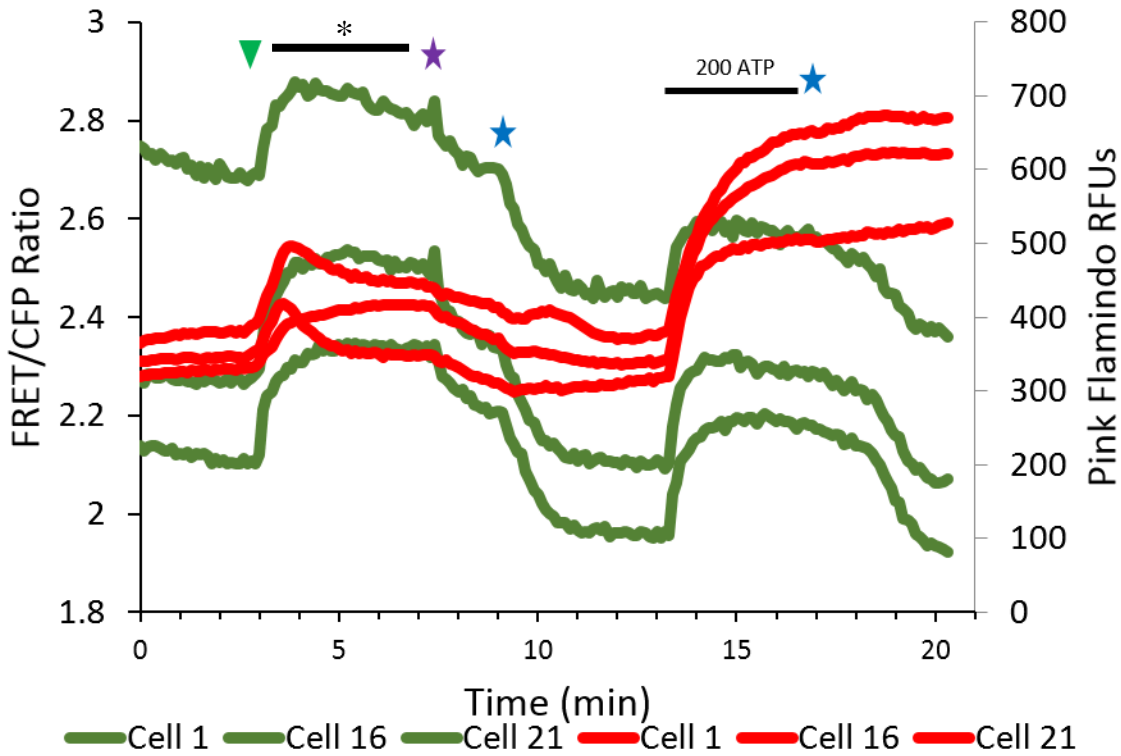


Figure 4.3 A 50% HOS causes an ATP release and cAMP response in HEK293A cells expressing P2Y₁₁

Green traces; FRET/CFP ratio of ECATS2. Red traces; intensity of Pink Flamindo. Green Triangle; 50% HOS static addition at time = 3 minutes; Purple Star; 50% Shock Solution perfusion wash at time = 7 minutes; Blue Star; iso-osmotic imaging solution washes at time = 9 minutes and 17 minutes; Black bar; perfusion pump off and 200 μ M ATP added at time = 13 minutes. Data shows individual cell traces of 3 representative cells expressing both ECATS2 and Pink Flamindo. 50% HOS resulted in a significant increase in both ECATS2 and Pink Flamindo signals (* indicates p<0.0001 unpaired 2-tailed t-test) indicating ATP release in response to HOS and P2Y₁₁ activation as seen by Pink Flamindo cAMP increases.

4.4 Discussion

Our hypothesis in this study was that ATP release from a hypo-osmotic shock (HOS) in HEK293A cells is several micromolar in magnitude and capable of activating P2Y₁₁ receptors. HEK293A cells endogenously express P2Y₁ (ADP EC₅₀ ~ 10 μ M) and P2Y₂ (ATP EC₅₀ ~ 100 nM) receptors, thus we transfected P2Y₁₁ into cells along with ECATS2 and Pink Flamindo DNA (Schachter et al.; Jacobson and Muller). P2Y₁₁ has one of the highest EC₅₀ values for ATP (EC₅₀

~ 10 μM) among the P2Y and P2X receptors, indicating that it should be among the most difficult of purinergic receptors to activate.

A HOS condition of a 50% reduction in osmolality (~300mOsm to ~150mOsm) was enough to measure an ATP release by ECATS2, signifying micromolar magnitude of ATP release from HEK293A cells. The detection of cAMP by Pink Flamindo was acute following the shock, and orthogonally validates ATP release and aligns with the timescale of P2Y₁₁ G-protein receptor signaling (Lacin et al.). Further supporting ATP release was on the order of several micromolar (~1-10 μM) is the attenuated cAMP response to the HOS when compared to the addition of 200 μM ATP (Figure 4.3). It is interesting that the HEK293A cells' ATP response changed in the presence or absence of P2Y₁₁ receptor, perhaps indicating that P2Y₁₁ autocrine and paracrine signaling play roles in regulatory volume control (Darby et al.).

This data provides the foundation that ECATS2 can be used in cellular models to quantify ATP purinergic signaling mechanisms in real-time with spectrally compatible sensors of downstream signaling events. The availability of genetically encoded fluorescent nuclear translocation probes that indicates activation of various kinase signaling cascades, such as the cAMP/PKA pathway known to be activated by purines like ATP, could be paired with ECATS2 (Duster et al.). Using spectrally compatible nuclear translocation probes with ECATS2 and second-messenger probes like Pink Flamindo could provide useful purinergic signaling information for drug targets in disease and injury models.

CHAPTER 5. PRIMARY CELL MODELS OF TBI

5.1 Introduction

Traumatic brain injury (TBI) occurs in response to a large variety of stimuli and ranges in severity. The short and long term consequences following a TBI rely on the extent of the mechanical injury, the severity of the injury, and the brain region of the injury (Burda et al.). In addition to the initial mechanical injury itself, TBI can be accompanied by local ischemia from ruptured blood vessels, suffer from edema or swelling, and in some patients seizures occur (Rossi et al.; Bender et al.; Thrane et al.; Burda et al.).

Following the initial injury, blood-flow to the damaged brain region may be impaired or cut off completely, resulting in lack of oxygen or ischemia. Neurons use a large amount of oxygen and are far more sensitive to ischemia than astrocytes, and energy management during ischemia largely falls onto the astrocytes (Rossi et al.). There are two mechanisms that ischemia can induce a release of ATP from astrocytes, an acute mechanism and a chronic mechanism. In response to acute ischemic insult, lysosomes containing ATP can fuse with the plasma membrane to release ATP into the extracellular space (Z. Zhang et al.). However, astrocytes begin to swell in response to chronic ischemia and release amino acids and purines as a result (Rossi et al.). There has been shown to be an ATP release detected by luciferase-luciferin based methods, but in either ischemic mechanisms the magnitude of local ATP release is not known (Z. Zhang et al.; Rossi et al.).

Cell swelling can be particularly damaging in body compartments that lack the elasticity to expand, such as the brain. Volume regulation and water management is the primary task of astrocytes in the brain during edema, and with the flow of water comes ions (Bender et al.). One of the primary influx routes for water to enter astrocytes during hypo-osmotic shock (HOS) is through aquaporin 4 (AQP4). While AQP4 can be held responsible for the bulk of water influx

during HOS, passive transport of water through the lipid bilayer cannot be excluded. When osmolality is reduced by thirty-percent or greater, water influx overwhelms AQP4 and passive transport results in cell swelling (Thrane et al.). As mentioned in chapter 4, volume regulation is highly conserved, and volume regulatory anion channels (VRACs) are expressed in astrocytes as well (Hoffmann et al.). ATP and glutamate exit through VRACs that open to allow anions and water out of the cell (Darby et al.; Rossi et al.). While it is known that ATP can be released from astrocytes in response to HOS, the magnitude of ATP release is not well characterized. We used ECATS2 to investigate the micromolar magnitude of ATP signaling dynamics in response to HOS and astrocyte swelling.

Severe TBIs cause non-repairable damage, and in small population of patients' epilepsy becomes a risk even after they have made their recovery. Seizures and epilepsy can arise from a variety of insults and genetic mutations, while epilepsy following TBI is thought to be mediated by pro-inflammatory cytokines (Yuen and Sander; Burda et al.). Seizures themselves can lead to further excitotoxicity, expanding the brain damage from a prior TBI in the patient's life (Burda et al.). The magnitude of ATP released in response to seizure-like excitotoxic activity is not well understood, and we used ECATS2 to quantify the micromolar range of ATP signaling to seizure-like excitotoxicity.

Herein we test the hypothesis that *in vitro* models of TBI lead to ATP release from astrocytes in the micromolar order of magnitude. We test this hypothesis by use of ECATS2 in models of mechanical stimulation, edema, ischemia, and seizure-like excitotoxicity. We also further aim to show that ECATS2 can be coupled with spectrally compatible sensors to detect intracellular responses simultaneously. We attempted to detect ATP release from TBI models of poke and stretch mechanical stimulation, ischemia, glutamate excitotoxicity, and edema. Our

observations in poke and stretch models largely agree with previous studies where ATP is released near the site of injury and quickly diffuses away. Hypo-osmotic shock (HOS) yielded ATP release in astrocytes alone, but not in neuron-astrocyte co-culture. Seizure-like excitotoxicity and ischemia did not detect ATP release by ECATS2.

5.2 Materials and Methods

5.2.1 Cloning Sensors into Lentiviral and Adenoviral Production Plasmids

Cloning jRGECO1a into Lentiviral vectors was done by Jason Conley and Elaine Colomb.

To produce ECATS2, NB control adenovirus, we first cloned the sensors into the pENTR1a vector with subsequent recombination into the pAd/CMV-V5-DEST vector as per the manufacturer's instructions (Invitrogen Cat# K4930-00 and V493-20). In place of lipofectamine transfection of constructs suggested by the manufacturer, we used calcium phosphate transfection as described in Chapter 4.2.2. Cloning of ECATS2 and NB-control into the pENTR1a vector for adenovirus production was done by restriction enzyme cloning. pMinDis-ecATeam3.10-(R103A/R115A)-20 nm ER/K or pMinDis-NB-control were double-digested with KpnI and NotI (New England Biolabs) flanking the IgK-secretion sequence and PDGFR transmembrane domain to excise ECATS2 and NB-control DNA. jRGECO1a was excised from pGP-CMV-NES-jRGECO1a by BglII and BamHI double-digest (New England Biolabs). Sensor DNA was then ligated with T4 ligase into pENTR1a. LR recombination reaction was done using LR Clonase II in pH 8 Tris-EDTA buffer at room temperature overnight using a 2:1 ratio of pAd/CMV-V5-DEST (300 ng/reaction) to pENTR1a-construct (150 ng/reaction), respectively. LR recombination was stopped by incubation with proteinase K for 10 minutes at 37°C. LR reactions were used to transform DH5a E. coli cells directly, and eight colonies were picked for mini-prep and sequencing. Sequence verified pAd/CMV-V5-Dest-construct plasmids were then digested with

PacI to prepare them for transfection of HEK293A cells as per Life Technologies ViraPowerTM Adenovirus Expression System manual.

5.2.2 HEK293A Cell Culture and Adenovirus Production

HEK293A cells were cultured in Dulbecco's modified Eagle's medium (DMEM) containing 4.5 g/L glucose, 3.7g/L sodium bicarbonate, 4 mM glutamine, 0.1 mM Non-essential Amino Acids (NEAA) and supplemented with 10% cosmic calf serum. Cells were maintained at 37°C and 5% CO₂ in a humidified incubator and passed three times weekly once confluency reached 80% or higher. All methods to produce adenovirus were adapted from the Life Technologies ViraPowerTM Adenovirus Expression System manual.

To produce adenovirus, HEK293A cells were passed and seeded into a 6-well plate at a density of 50,000 cells/cm² and given 24 hours to grow. PacI cut pAd/CMV-V5-DEST-construct DNA for ECATS2 was transfected into HEK293A cells near confluence. 48 hours post-transfection the infectious cells were expanded into a T75 flask. The infectious cells were fed HEK293A media every 2-3 days until 14 days had passed and visible cytopathic effect could be observed in the cells. Remaining cells were blasted off the T75 flask surface using a 10 mL pipette and transferred to a 15 mL falcon tube. The infected HEK293A cells and media were then frozen at -80°C for 30 minutes, then thawed in a 37°C water bath for 15 minutes a total of three times. This crude viral lysate was then spun down in a table-top centrifuge at 3000 rpm for 15 minutes to pellet cell debris. The supernatant containing the adenoviral particles were then transferred to cryovials in 1 mL aliquots labeled "crude viral lysate" and stored at -80°C.

To amplify our adenovirus stock, we seeded HEK293A cells in a T75 flask at a density of 40,000 cells/cm² and gave them 24 hours to recover before adding 1 mL of crude viral lysate. HEK293A cells were incubated for 72 hours following transduction with crude adenovirus lysate.

High titer viral lysate was isolated using the same freeze/thaw and spin down protocol described for the crude viral lysate above.

5.2.3 HEK293FT Cell Culture and Lentivirus Production

Maintenance of HEK293FT cells and production of jRGECO1a lentivirus was all done by Jason Conley.

5.2.4 Microdissection of Hippocampal Neurons and Cortical Astrocytes

Post-natal day 1 (p1) pups were dissected for primary hippocampal neurons and cortical astrocytes. Neuron-astrocyte co-cultures were isolated solely from the hippocampus. Pups were anesthetized using isoflurane gas before decapitation. Stainless steel tools were used to isolate the full brain into Hank's Buffered Saline Solution (HBSS) fortified with 1.26 mM CaCl₂, 0.49 mM MgCl₂ and 0.4 mM MgSO₄ (HBSS+). Full brains were bisected using a scalpel and the midbrain removed with forceps. Starting at the olfactory bulb, the meninges was removed, and the hippocampus and/or cortex were isolated. Isolated brain regions were diced with a scalpel before being washed three times in HBSS not fortified with divalent cations (HBSS-) before being treated with DNaseI and porcine trypsin for fifteen minutes at 37°C with occasional gentle agitation. The trypsin and DNaseI were removed with three washes of HBSS- before resuspending neurons and astrocytes in neurobasal media and astrocyte media, respectively. Fire-polished and fire-narrowed horse serum coated glass Pasteur pipettes were used to dissociate brain regions before filtering through a 0.2μm filter to remove any large chunks of debris and meninges. Primary neurons were counted and plated at a density of one-hundred thousand per centimeter squared on poly-D-lysine coated 18mm glass coverslips. A complete change of neurobasal media was done one to four hours

after plating. Due to difficulties in counting, primary astrocytes were plated one brain per 12-well plate.

5.2.5 Primary Cell Culture of Astrocytes and Neuron-Astrocyte Co-culture

Astrocytes were cultured using a mix of Dulbecco's modified Eagle's medium (DMEM) and F12 media (Gibco 12400-024) supplemented with 1.2 g/L sodium bicarbonate and 10% cosmic calf serum or fetal bovine serum. Astrocyte media was fortified with penicillin/streptomycin to protect primary culture from contamination. Astrocytes were washed with DPBS buffer to remove dead cells and fed fresh media twice weekly.

Neurobasal-A media (Gibco 10888022) was used for neuron-astrocyte co-culture and was supplemented with 5 mM glucose, 0.5 mM Glutamax-I, 0.25 mM sodium pyruvate, and antibiotics B27 and Pen/Strep to prevent contamination. Media was then syringe filtered through a 0.2 µm filter for sterilization. Neuron-astrocyte co-cultures were fed fresh media every three or four days as a 50% media change.

Neuron-astrocyte co-cultures were transduced with a mix of adenovirus containing ECATS2 DNA and lentivirus containing jRGECO1a DNA. After 2 days *in vitro* (DIV2) we performed a half media change with complete neurobasal medium and saved the conditioned media. Conditioned media was syringe filtered and kept for feeding cells after washing virus off later. On DIV3 we added a mixture of 100 µL ECATS2 adenovirus and 50 µL of jRGECO1a lentivirus in the presence of 100 µM kynurenic acid. The kynurenic acid served as a glutamate receptor inhibitor, which was required due to the glutamate present in HEK293A media the adenovirus was harvested in to prevent excitotoxicity. On DIV5 virus was washed off the co-culture with three rinses of complete neurobasal medium. The washed cells were then fed with

50% conditioned media using the medium saved from the feeding on DIV2. Imaging was done primarily on days DIV7-DIV10.

5.2.6 Live Cell Fluorescent Microscopy and Analysis

Cells were prepared for microscopy by exchanging cell growth media for imaging solution consisting of 15 mM HEPES, 1.25 mM NaH₂PO₄, 5 mM glucose, 130 mM NaCl, 3 mM KCl, 2 mM CaCl₂, 1 mM MgCl₂, 0.2 mM sodium pyruvate, 0.5 mM Glutamax and 3 mM NaHCO₃ (pH 7.3) and cells were equilibrated at room temperature for at least 20 min prior to imaging. Osmotic shock solution was prepared as imaging solution consisting of 15 mM HEPES, 5 mM glucose, 2 mM CaCl₂, 1 mM MgCl₂, 0.2 mM sodium pyruvate and 0.5 mM glutamax. All microscopy experiments were performed at ambient room temperature, using either continuous perfusion (~ 1.5 mL/min flow rate) of imaging solution, static bath, or a mixture of static and perfusion steps. Cells were imaged using an Olympus IX83 fluorescence microscope with a 20X/0.75 NA objective illuminated by a Lumencor SpectraX light engine and equipped with an Andor Zyla 4.2 sCMOS camera. The ecATgen2 sensor activity was measured by examining the fluorescence intensities in CFP, CFP-YFP FRET, and YFP channels. Specifically, the ATeams were excited in the CFP and CFP-YFP FRET channels using a 438/29 nm bandpass filter, and emission was collected through 470/24 and 540/30 nm bandpass filters for the CFP and CFP-YFP FRET channels, respectively. The fluorescence in the YFP channel was excited using a 510/10 nm bandpass filter and emission was collected through a 540/30 nm bandpass filter. The fluorescence in the RFP channel was excited using a 575/25 nm bandpass filter and emission was collected through a 631/28 nm bandpass filter. Excitation light from all fluorescence channel measurements was blocked by the ET-ECFP/EYFP/mCherry multiband beamsplitter (Chroma 69008bs). The microscope components and image acquisition were controlled by the Andor iQ3 software and the ImageJ/FIJI

software package was used to analyze all images for each experiment, as specified. For fluorescence images, the mean and standard deviation of background intensities were measured for each channel in each field of view. For each fluorescence channel, the mean background intensity was subtracted from every image of the associated imaging set. Background masks were then created with minimum thresholds of two times the mean background intensity. The background masks were applied to the fluorescence intensity images and fluorescence ratio images were created by pixel-by-pixel division of the background masked individual fluorescence channels. Regions of interest that encompassed whole cells or cell membranes, as indicated, were drawn and the mean fluorescence ratios of pixels within each region of interest were calculated. For intensiometric sensor jRGECO1a raw intensities from ROIs were used directly for analysis.

5.2.7 Statistical Analysis

In sections 5.3.1 Mechanical Stimulation of Cortical Astrocytes and 5.3.4 KCN Ischemia there are only n=1 experiment performed, and therefore no statistical analysis can be performed on these preliminary studies. While ATP release is robustly reported in the literature in response to mechanical injury, the method was cumbersome in our hands and we decided not to choose it as our model system.

To accommodate for the imaging artifact following osmotic shock, we adjusted the baseline to the first several datapoints following shock to get an adjusted normalized FRET/CFP ratio. All statistical analysis was done using OriginPro2017 64-bit software. Since our primary goal was detecting ATP release in response to HOS, we report the results of the unpaired 2-tailed student's t-test comparing ECATS2 to the nonbinding (NB) control. Differences were deemed significant if p<0.05. Data in this chapter is reported as the median \pm 95% confidence interval.

5.3 Results

5.3.1 Mechanical stimulation of Cortical Astrocytes

Since there is an abundance of literature on ATP release following injury (Y. Zhang et al.; Pérez-Ortiz et al.; James and Butt; Praetorius and Leipziger), we hypothesized ECATS2 could detect ATP released by mechanical injury of astrocytes in poke and scratch models. Our poke injury test directly on an ECATS2 astrocyte shown in Figure 5.1 showed ATP release around the site of injury. The FRET/CFP ratio around the site of injury are clearly increased in the images post-injury and slowly recover as we continued monitoring. This agrees with reports of membrane attached firefly-luciferase that estimated a millimolar release of ATP (Y. Zhang et al.). The direct injury test using ECATS2 and mouse cortical astrocytes provided validation that ECATS2 can detect membrane injury ATP release. As we only performed n=1 experiment, we did not perform a statistical analysis on our mechanical stimulation data.

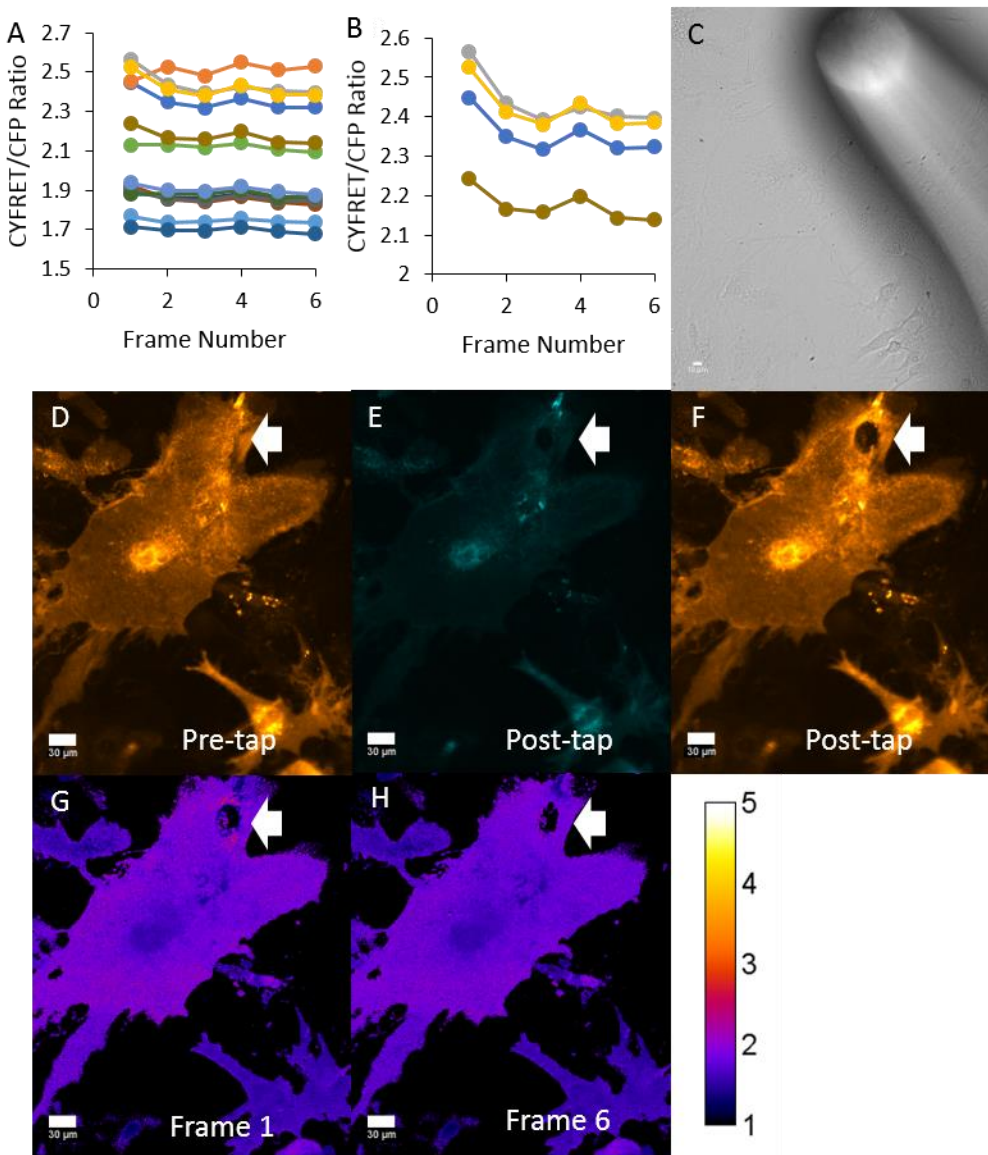


Figure 5.1 Poke Injury Shows ATP-release from Damaged Astrocyte

A) Individual ROI traces of various astrocytes across the entire field of view where $n = 11$ ROIs in the field of view B) ROIs around site of injury and of injured cell C) DIC channel showing the fire-polished rounded glass mechanical stimulation pipette over the site of injury. D) Representative pre-injury image shown as FRET channel E) CFP channel post-injury F) FRET channel post-injury showing clear poke injury G) Ratio image first image post-injury H) Ratio image after ~ 2 minutes recovery with ratio calibration bar. All white arrows indicate the site of injury. Scalebars are 30 μm .

Our test in which we poked a neighboring cell shown in Figure 5.2 showed no change in ECATS2 signal. Poking a neighboring cell did not show a measurable ATP release in the surrounding cells ~100 μm away expressing ECATS2. These results agree with previous studies using cell surface tethered firefly luciferase in astrocyte poke injury models where detection of injury ATP was lost 100 μm away from the site of injury (Y. Zhang et al.).

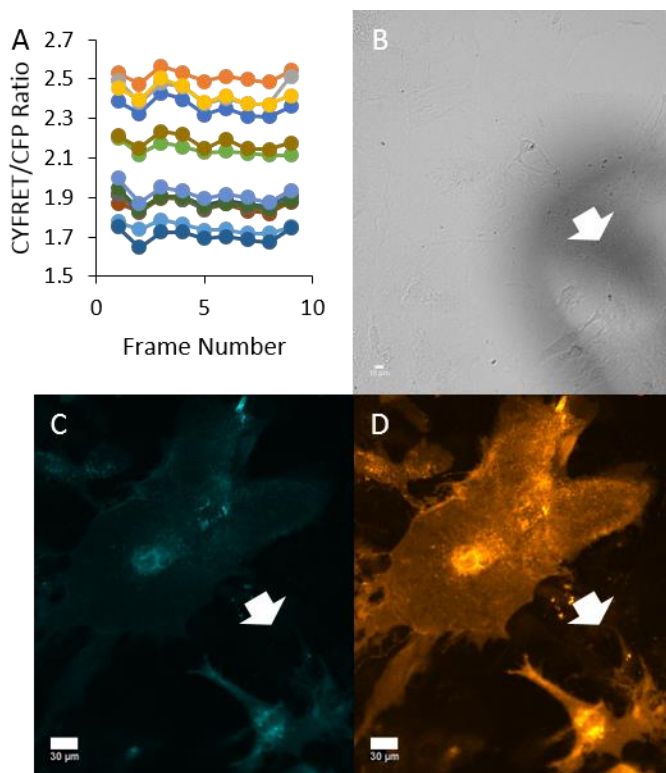


Figure 5.2 Poke of Neighboring Cells Shows No Detectable ATP Release

A) Individual ROI Traces of astrocytes surrounding the site of injury show little to no change n=11 ROIs across the field of view. B) DIC channel showing fire-polished rounded glass pipette hovering over site of injury. C) CFP and D) FRET channels with white arrows indicating injury site. Scalebars are 30 μ m.

While the poke model appears to have promising prospects for future experiments, we also qualitatively tested the scratch model. The scratch or stretch model implies ATP release *in vitro* by previous studies preventing downstream signaling by addition of exogenous apyrase (Neary et al.; Pérez-Ortiz et al.; Gao et al.). The results of our direct poke test led us to expect that ATP released during a stretch or scratch is within the detection range of ECATS2. We decided to try causing a larger injury with the stretch/scratch model. Overall, most of the surrounding cells that did not get directly injured did not detect ATP release (Figure 5.3). The injured cell showed a detectable ATP release, but the signal was quickly cleared. This data agrees with previous studies that suggest ATP release diffuses into the extracellular space quickly, and is likely in the hundreds of micromolar range or higher (Y. Zhang et al.).

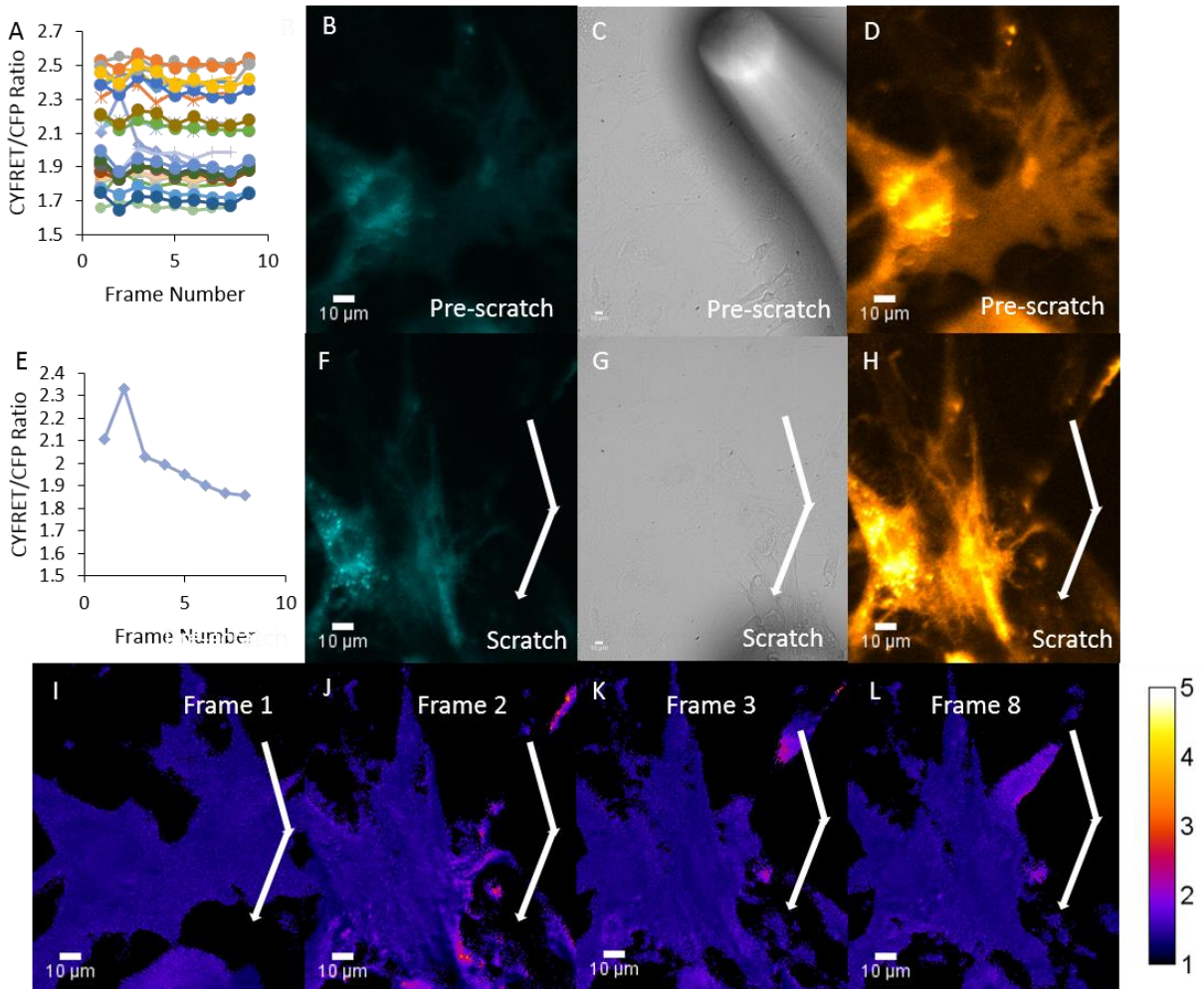


Figure 5.3 Scratch Injury Shows ATP Release Detectable by ECATS2

A) Individual ROI traces of astrocytes in field of view show mostly non-responders except for the injured cell n=X ROIs in and around astrocytes B) CFP channel pre-scratch. C) DIC channel pre-scratch. D) FRET channel pre-scratch. E) Individual ROI traces of scratched cell shown in I-J shows ATP release and a quick clearance. F) CFP channel post-scratch. G) DIC channel post-scratch H) FRET channel post-scratch. I) Ratio image frame 1 pre-scratch with scratch vector arrows J) Ratio frame 2 scratch indicates ATP release from injured cell K) Ratio frame 3 indicates a fast return to baseline within the site of injury L) Ratio frame 8 shows a mostly recovered astrocyte. White arrows represent the scratch injury vector. Scalebars are 10 μ m.

As an *in vitro* model of TBI, these results confirm our hypothesis that ECATS2 detects ATP release from mechanical injury poke, stretch, and scratch models that agrees with previous studies (Y. Zhang et al.; Pérez-Ortiz et al.; Neary et al.; Gao et al.). Our results align with previous studies that report ATP release following injury using other methods of detection (Y. Zhang et al.).

5.3.2 Hypo-osmotic shock of Cortical Astrocytes shows ATP release

The next *in vitro* model of TBI we tested was simulated edema by hypo-osmotic shock (HOS) of astrocytes. We tested the hypothesis that a 50% HOS results in an ATP release in the order of micromolar detectable by ECATS2. In cortical astrocytes cultured alone, a fifty percent reduction in osmolality caused a measurable ATP release shown in Figure 5.4, almost comparable to the 20 μM ATP added to calibrate the ECATS2 signal. A small imaging artifact was seen in the NB-mutant and ECATS2 upon osmotic shock as well. We hypothesize this artifact could be due to changes in the dynamic range of the sensor that accompany changes in osmolality of the surrounding environment. Changing the osmolality environment around the sensor could change the physical constraints on ECATS2, like our observations in chapter three when optimizing the length of the ER/K linker. We do observe some slight baseline drift over the long time-course of the experiment, but the large acute changes in ECATS2 signals are indicative of ATP dynamics near the surface of the astrocyte.

Our second HOS experiment repeated the conditions of the first and is shown in Figure 5.5. In this experiment, ECATS2 showed a stronger signal from astrocytes than in our first experiment almost comparable to the 20 μM ATP response used to calibrate the signal. This supports that ATP responses to osmotic shock are perfectly within the detection range of ECATS2 (~1-20 μM ATP). A fifty percent reduction in osmolality caused the same imaging artifact in both ECATS2 and the NB-control as we observed in the previous experiment in primary mouse cortical astrocytes.

Figure 5.4 ECATS2 Detects ATP Release in Cortical Astrocytes in Response to 50% HOS in Presence of 100 μ M ARL

A) FRET/CFP ratio signal of ECATS2 signal mean \pm 95% confidence interval where n=13 astrocytes. B) NB mutant mean \pm 95% confidence interval where n=13 astrocytes. A pH matched 200 μ M ARL osmotic shock solution was added at a 1:1 volume ratio at time=5 minutes to cause a 50% reduction in osmolality in the presence of 100 μ M ARL. Addition of 20 μ M ATP was made at time=11 minutes as indicated by the black bar and 20 over A and B. (C-J) Consist of all ECATS2 channels of a representative responding astrocyte. C) DIC channel D) CFP channel E) FRET channel F) YFP channel (G-H) FRET/CFP ratio. G) ECATS2 Ratio at time=0 minutes H) ECATS2 Ratio at time=6 minutes 40 seconds at peak of response indicated by the green triangle in A and B. I) ECATS2 Ratio at time=13 minutes 20 seconds as response to 20 μ M ATP began to peak. J) ECATS2 Ratio at time=20 minutes during perfusion washout of ATP with 50% osmotic shock imaging solution after having reached a stable baseline. (K-R) Consist of all control NB-mutant channels of a representative astrocyte. K) DIC channel L) CFP channel M) FRET channel N) YFP channel (O-R) Time-matched NB-control representations of the FRET/CFP ratio to the same conditions as ECATS2 shown in (G-H).

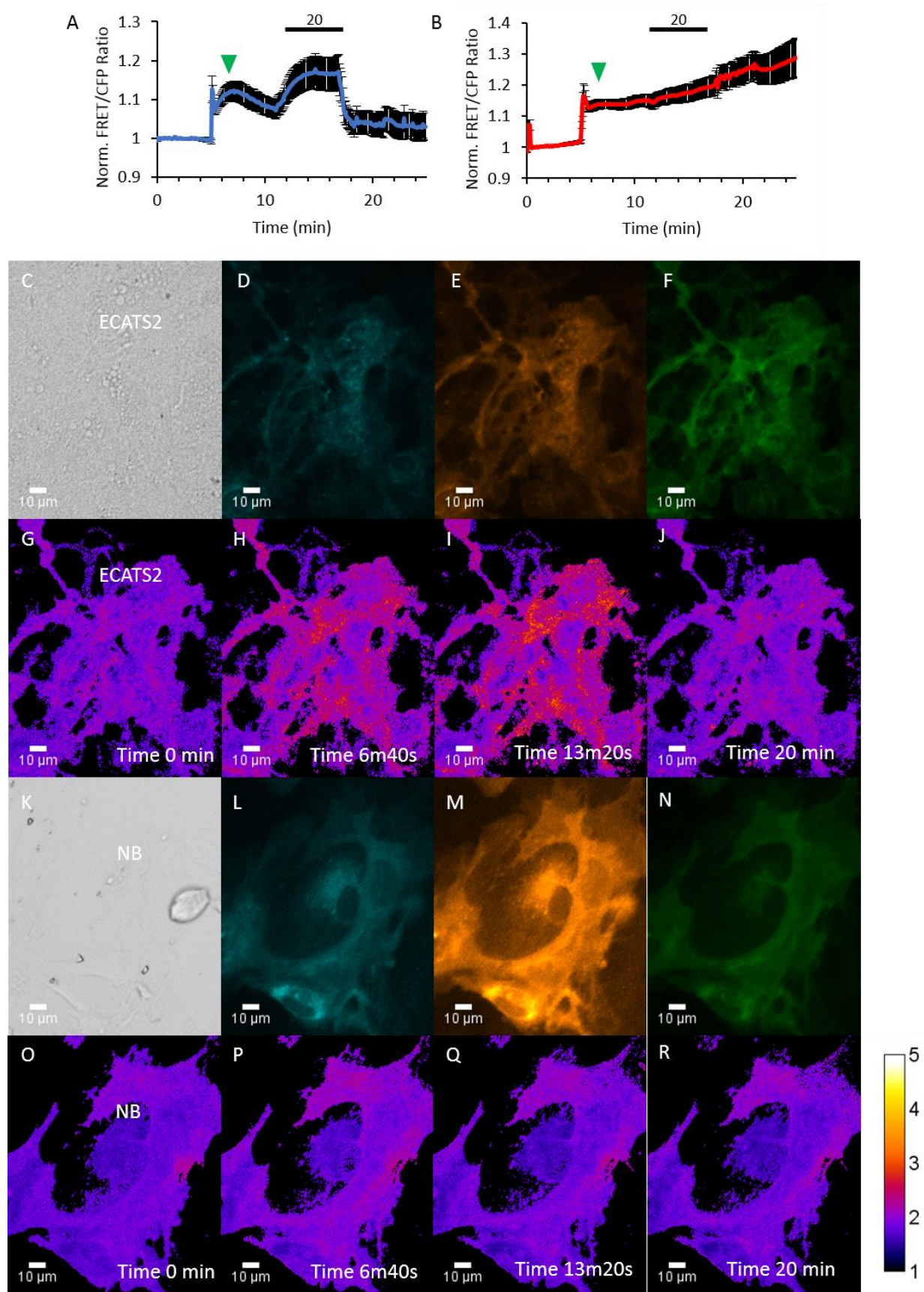
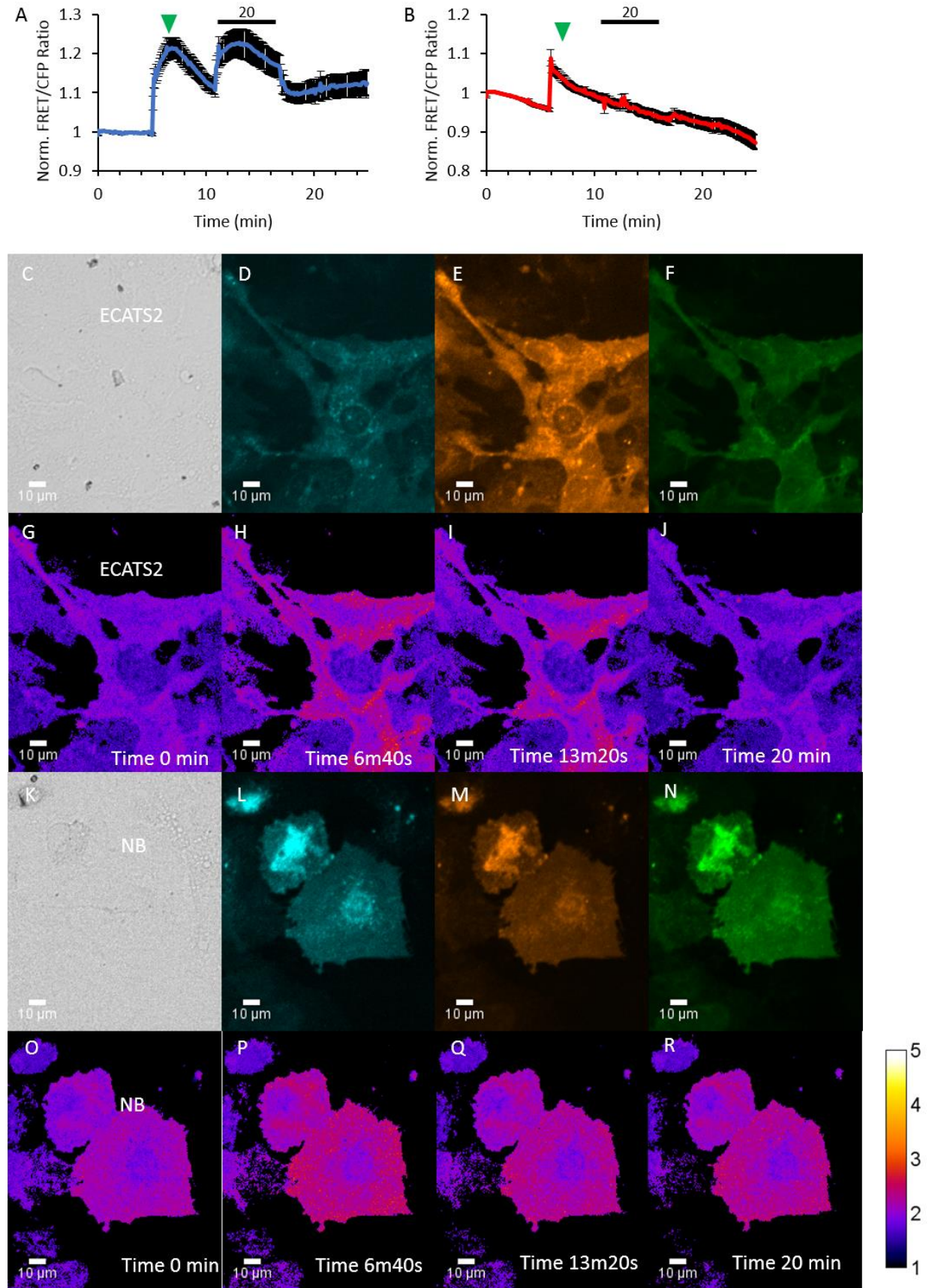


Figure 5.5 Second Experiment using ECATS2 Detects ATP Release in Cortical Astrocytes in Response to 50% HOS in Presence of 100 μ M ARL

A) FRET/CFP ratio signal of ECATS2 signal mean \pm 95% confidence interval where n=15 astrocytes. B) NB mutant mean \pm 95% confidence interval where n=13 astrocytes. A pH matched 200 μ M ARL osmotic shock solution was added at a 1:1 volume ratio at time=5 minutes to cause a 50% reduction in osmolality in the presence of 100 μ M ARL. Addition of 20 μ M ATP was made at time=11 minutes as indicated by the black bar and 20 over A and B. (C-J) Consist of all ECATS2 channels of a representative responding astrocyte. C) DIC channel D) CFP channel E) FRET channel F) YFP channel (G-H) FRET/CFP ratio. G) ECATS2 Ratio at time=0 minutes H) ECATS2 Ratio at time=6 minutes 40 seconds at peak of response indicated by the green triangle in A and B. I) ECATS2 Ratio at time=13 minutes 20 seconds as response to 20 μ M ATP began to peak. J) ECATS2 Ratio at time=20 minutes during perfusion washout of ATP with 50% osmotic shock imaging solution after having reached a stable baseline. (K-R) Consist of all control NB-mutant channels of a representative astrocyte. K) DIC channel L) CFP channel M) FRET channel N) YFP channel (O-R) Time-matched NB-control representations of the FRET/CFP ratio to the same conditions as ECATS2 shown in (G-H).

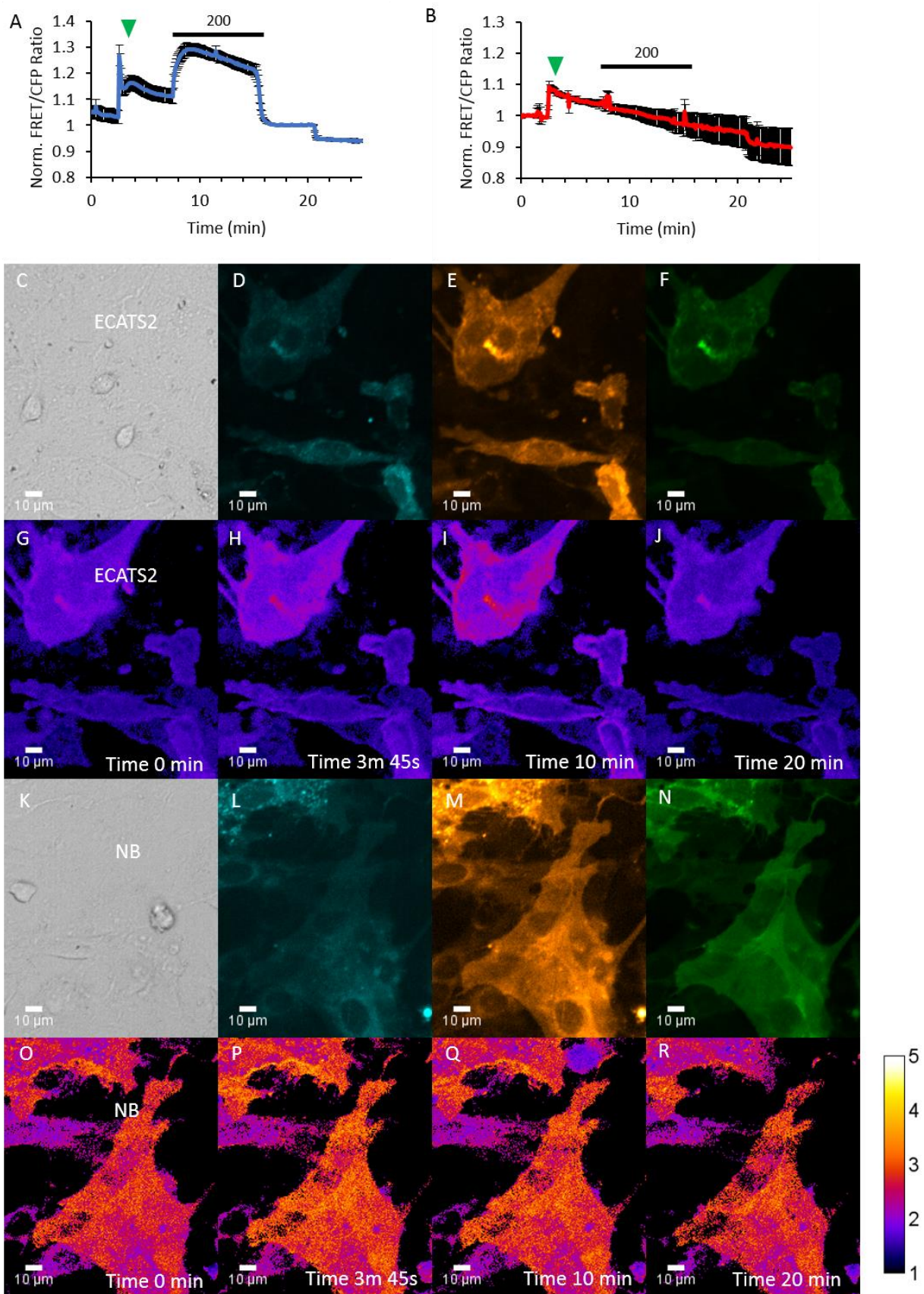


Our third experiment tested if ectonucleotidases inhibited by ARL in our first two experiments would dampen or prevent the ATP release. In Figure 5.6, we repeated our observation of ATP release in primary cortical mouse astrocytes following a fifty-percent reduction in osmolality in the absence of the ectonucleotidase inhibitor ARL. ECATS2 was calibrated by the addition of 200 μ M ATP in these experiments and functional sensor was present in all three replicates. The imaging artifact upon HOS was observed in all ECATS2 and NB-control experiments thus far.

To test if the change in osmolality was affecting the ECATS2 dynamic range and FRET/CFP ratio, we added an additional wash step in experiment three. The additional wash step perfuses out the 50% osmotic shock imaging solution and replaces it with 1X aCSF isotonic imaging solution. In Figure 5.6, we observed that this washout did provide a reduction in FRET/CFP ratio upon returning the osmolality of the solution to normal. This supports our hypothesis that the imaging artifact observed using ECATS2 during osmotic shock experiments is a result of the osmolality changing the dynamic range of the sensor. Further testing of this hypothesis in solution may further validate the hypothesis that osmolality affects the dynamic range, and possibly the ATP binding affinity of ECATS2.

Figure 5.6 Third Experiment using ECATS2 Detects ATP Release in Cortical Astrocytes in Response to 50% HOS without ARL

A) FRET/CFP ratio signal of ECATS2 signal mean \pm 95% confidence interval where n=13 astrocytes. B) NB mutant mean \pm 95% confidence interval where n=11 astrocytes. A pH matched osmotic shock solution was added at a 1:1 volume ratio at time=2 minutes 30 seconds to cause a 50% reduction in osmolality. Addition of 200 μ M ATP was made at time=7 minutes 30 seconds as indicated by the black bar and 200 over A and B. (C-J) Consist of all ECATS2 channels of a representative responding astrocyte. C) DIC channel D) CFP channel E) FRET channel F) YFP channel (G-H) FRET/CFP ratio. G) ECATS2 Ratio at time=0 minutes H) ECATS2 Ratio at time=3 minutes 45 seconds at peak of response indicated by the green triangle in A and B. I) ECATS2 Ratio at time=10 minutes as response to 200 μ M ATP began to peak. J) ECATS2 Ratio at time=20 minutes during perfusion washout of ATP with 50% osmotic shock imaging solution after having reached a stable baseline. At ~21 minutes perfusion with 1x aCSF normal imaging solution reduces ratio in both A and B. (K-R) Consist of all control NB-mutant channels of a representative astrocyte. K) DIC channel L) CFP channel M) FRET channel N) YFP channel (O-R) Time-matched NB-control representations of the FRET/CFP ratio to the same conditions as ECATS2 shown in (G-H).



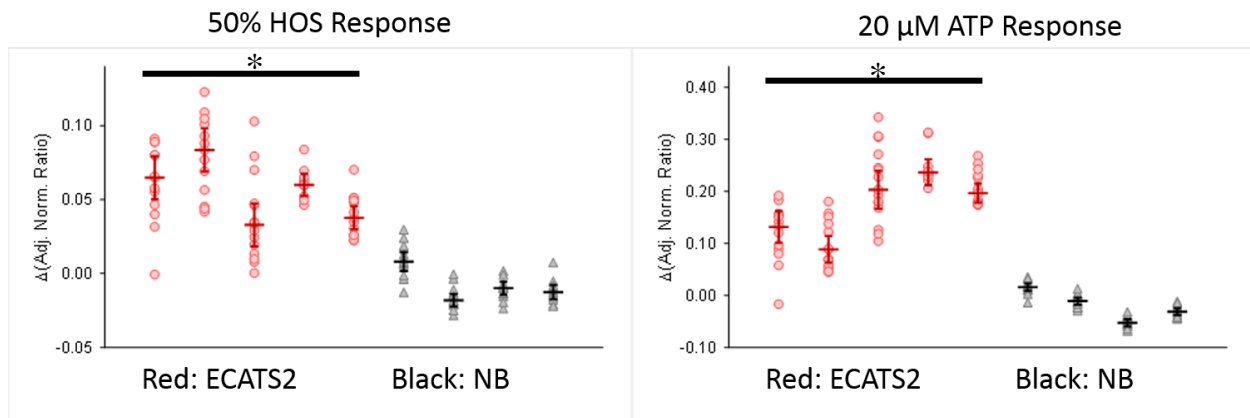


Figure 5.7 50% HOS Reveals ATP Release by use of the ECATS2 Sensor

Left: ECATS2 (red) shows a significant response to a 50% HOS when compared to the nonbinding (NB; black) control in cortical astrocytes. In all experiments $p<0.001$ when comparing ECATS2 to a NB experiment using an unpaired 2-tailed student's t-test. Right: ECATS2 (red) shows significant increased ratio to 20 μM ATP ($p<0.001$) when compared to the NB control (black) by unpaired 2-tailed student's t-test. The y-axis represents the artifact adjusted normalized CYFRET/CFP ratio, while each column represents an individual experiment in cortical astrocytes expressing ECATS2 or the NB control. Bars represent the median \pm 95% confidence interval.

In Figure 5.7 we compared the ECATS2 datapoints following the 50% hypo-osmotic shock in mouse cortical astrocytes to the nonbinding control and found that ECATS2 does detect an ATP release when compared to the control ($p<0.001$ when comparing individual experiment ECATS2 mean of HOS datapoints vs individual experiment NB mean of HOS datapoints; $p<0.001$ when comparing pooled ECATS2 HOS response mean ($n=5$) vs pooled NB HOS response mean ($n=4$) via an unpaired 2-tailed t-test). We also demonstrate that the ECATS2 responds to the calibrating addition of 20 μM ATP when compared to the nonbinding control ($p<0.001$ unpaired 2-tailed t-test).

Cultured cortical mouse astrocytes expressing ECATS2 validate our proof-of-concept that astrocyte purinergic signaling events can be detected using live-cell fluorescent microscopy and ECATS2. Multiple experiments from different dissections repeated the same phenotype of ATP-release with a delayed release of roughly one to two minutes following a fifty percent reduction in solution osmolality. Interestingly, calibration with 20 versus 200 μM ATP reveals that the

magnitude of ATP release is much closer to 20 μM ATP. This is ideal since the ATP release estimated is on the order of several micromolar, making ECATS2 an ideal sensor for studying purinergic signaling events in edema models.

Cortical astrocytes cultured alone in our hands only transduced reliably with sensor DNA packaged in adenovirus and not lentivirus. Lentivirus does reliably transduce neurons, and we sought to further validate ECATS2 using neuron-astrocyte co-culture and dual-sensor imaging. A spectrally compatible red sensor packaged in lentivirus was mixed with ECATS2 adenovirus. Next, we aimed to show that neuron-astrocyte co-culture releases ATP in the micromolar range detectable by ECATS2 in response to hypo-osmotic shock.

5.3.3 Hypo-osmotic shock of Neuron-Astrocyte Co-culture

We moved into the more physiological model of neuron-astrocyte co-culture (Hasel et al.), and aimed to test the hypothesis that HOS causes an ATP release in the low micromolar range from astrocytes. To further validate release of ATP and excitatory amino acids in response to osmotic shock, the intensiometric jRGECO1a sensor was chosen as a red calcium sensor (Dana et al.). Our sensor choice allowed visualization of excitation of neurons in response to osmotic shock by detecting intracellular calcium signals in neurons transduced with lentivirus.

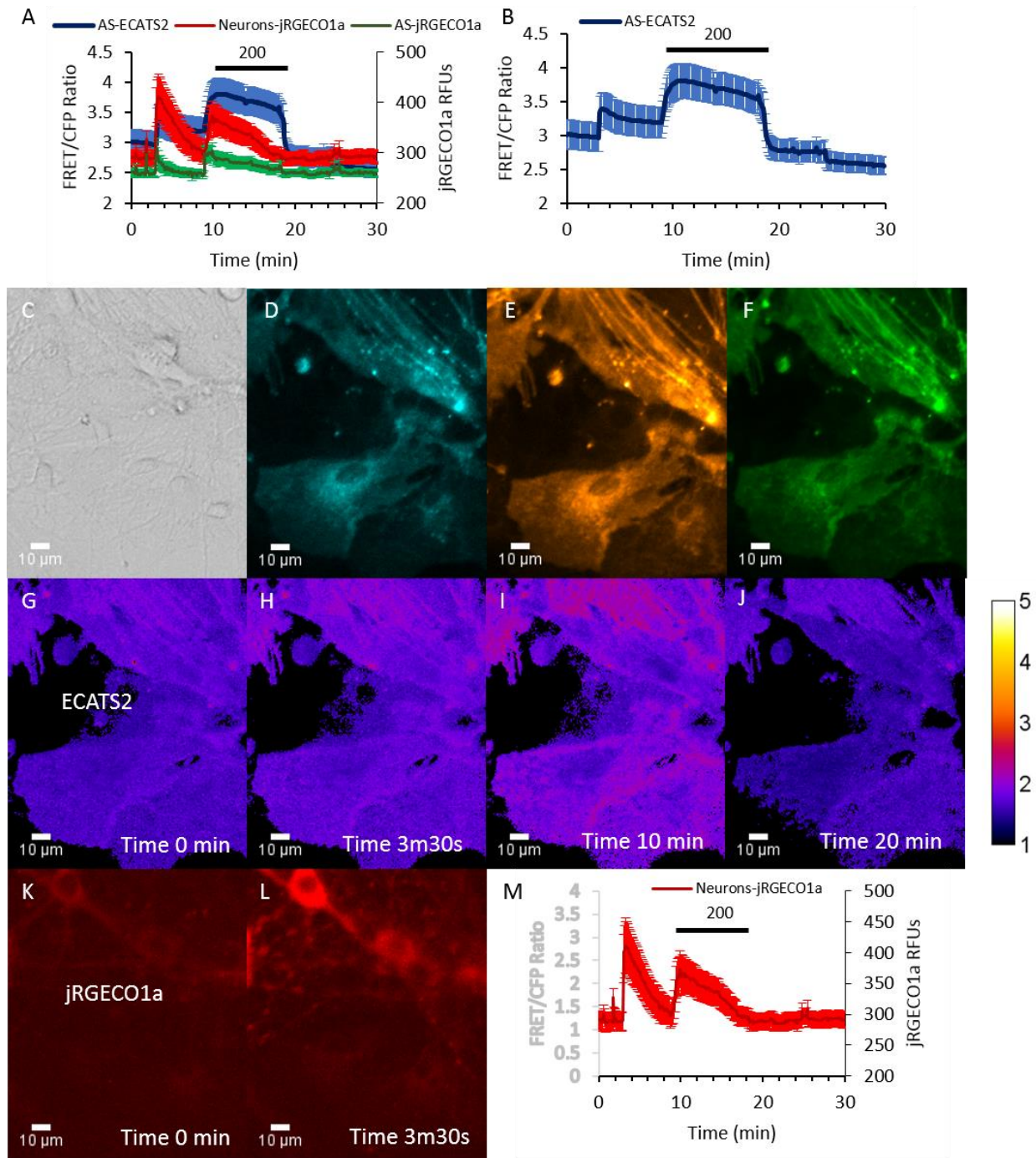
Previously in our hands, lentivirus has not transduced cortical astrocytes cultured alone. In neuron-astrocyte co-culture we noticed that the jRGECO1a lentivirus transduced not only the neurons, but to a limited extent several astrocytes as well. This could be due to the changes in receptor expression profile of astrocytes when co-cultured with neurons being more physiological (Hasel et al.). Therefore, several of the co-culture experiments yielded more data than we originally expected, allowing us to view cytosolic calcium signals in astrocytes with jRGECO1a that are also expressing ECATS2. The primary function of jRGECO1a was to verify neuron activation following osmotic shock and to visualize excitotoxicity as collapse of the nuclear envelope by monitoring cytosolic calcium (Dana et al.).

In Figure 5.8, we demonstrate that astrocytes and neurons both respond with intracellular calcium signals following a fifty percent osmotic shock with jRGECO1a. We also showed in all nine experiments with or without ARL that there was no detectable ATP release with ECATS2, proving our hypothesis that ATP released in response to osmotic shock is in the micromolar range false. This suggests that a more physiological model of neuron-astrocyte co-culture dampens or prevents the ATP release we observed in astrocytes cultured alone. This could be due to a change in surface protein expression profile, where VRACs that release ATP and glutamate are possibly

less abundant. Alternatively, the ATP release event could be reduced to nanomolar levels, requiring further ATP affinity increase in the next generation ECATS3.

Figure 5.8 HOS in Neuron-Astrocyte Co-culture

A) Data represents the mean \pm 95% confidence interval for the ECATS2 astrocytes where n=24 astrocytes, jRGECO1a neurons where n=29 neurons, and jRGECO1a astrocytes where n=24 astrocytes. All ECATS2 astrocytes analyzed were also jRGECO1a positive. B) Shows the mean \pm 95% confidence interval for the ECATS2 astrocytes. (C-J) represents all the ECATS2 channels C) DIC channel D) CFP channel E) FRET channel F) YFP channel and G-J showing the FRET/CFP ratio over time. G) Ratio at time=0 minutes as baseline H) Ratio at time=3 minutes 30 seconds after 50% HOS I) Ratio at time=10 minutes as response to 200 μ M ATP began to peak J) Ratio at time=20 minutes. K) Shows jRGECO1a at time=0 minutes during baseline recording. L) Shows jRGECO1a at time=3 minutes 30 seconds after 50% HOS J) Shows the mean \pm 95% confidence interval for all neuron ROIs of jRGECO1a signal. The 50% HOS was made at time=3 minutes and addition of 200 μ M ATP at time=9 minutes. ATP wash washed out by perfusion with 50% shock imaging solution before being switched to 1X aCSF normal imaging solution at time=24 minutes.



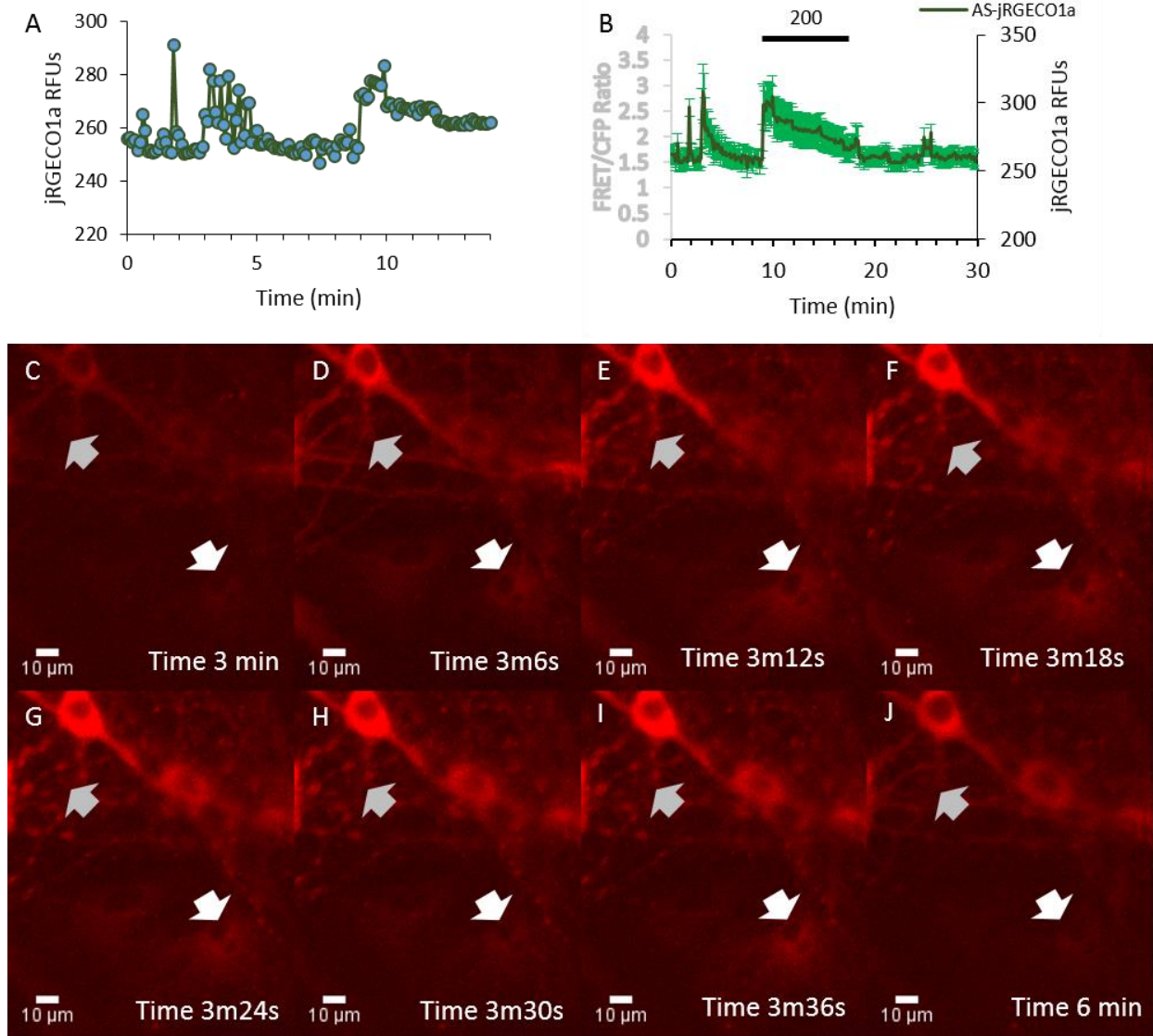


Figure 5.9 HOS causes calcium oscillations in neurons and astrocytes

A) Individual astrocyte trace of the astrocyte indicated by the white arrow in C-J time scale zoomed in to the view intracellular calcium signals following 50% HOS at time=3 minutes. B) Data shown is jRGECO1a astrocytes mean \pm 95% confidence interval show oscillating Ca-responses to both 50% HOS and 200 μ M ATP. The gray arrow in C-J points to blebbing axons following HOS and their clear recovery 3 minutes later in (J). Scalebars are 10 μ m.

In Figure 5.9 we focused in on the jRGECO1a signal in astrocytes as indicated by the white arrows. Following osmotic shock, we observed cytosolic calcium signals in several astrocytes expressing jRGECO1a. Due to the lack of ECATS2 signal, the calcium signals were not caused by ATP that could be detected with our sensor. It is possible that glutamate receptors are

responsible for the calcium signals observed. Strong calcium responses within astrocytes also were observed after addition of ATP, indicating activation of P2X and P2Y receptors (Darby et al.; Jacobson and Muller). We also hypothesized that a fifty percent hypo-osmotic shock would cause excitotoxicity due to the direct effect of the shock itself on neurons combined with the ATP and excitatory amino acid release when VRACs open. Remarkably, we see the neuronal projections begin to bleb within twelve seconds of the shock, and almost completely recover three minutes later indicated by the gray arrows.

Overall, neuron-astrocyte co-culture provides a dampening effect against the ATP release seen in cortical astrocytes when cultured alone. The loss of the ATP responses we observed in cultured astrocytes alone may indicate better water regulation of astrocytes in co-culture with neurons due to an increase in aquaporin expression in co-culture (Hasel et al.). Our tests with and without ARL made little difference indicating this protective effect is not likely from ectonucleotidases. ATP release could very well still be occurring within co-culture at levels below the detection limit of ECATS2, but further increases in affinity need to be made to study purinergic signaling mechanisms in the nanomolar magnitudes of concentration.

5.3.4 KCN Ischemia

Since it is known that chemical ischemia causes an ATP release in astrocytes (Rossi et al.), we sought to test the hypothesis that ATP released by KCN-induced ischemia is detectable by ECATS2 using live-cell microscopy. Cortical astrocytes in Figure 5.10 show a mixed population of responders and non-responders across three different fields of view in a 12-well plate. However, we only performed n=1 experiment and did not subject this data to statistical analysis. The astrocytes were imaged as fast as possible, which was ~30 seconds to complete the XY-scan between ROIs and re-focus. Previous studies have suggested that due to the ATP-starving conditions of ischemia, diffusion and CD39 activity, ATP release due to ischemia is small and cleared quickly (Rossi et al.). While other studies have reported lysosomal exocytosis of ATP in response to ischemia using media based luciferase methods in astrocytes and brain slices (Z. Zhang et al.). This further validates the need for membrane tethered sensors that can detect local signaling dynamics. Therefore, further increases in ATP-binding affinity and the creation of an ECATS3 with nanomolar to hundreds of nanomolar ATP affinity is needed to further study ATP signaling during ischemia.

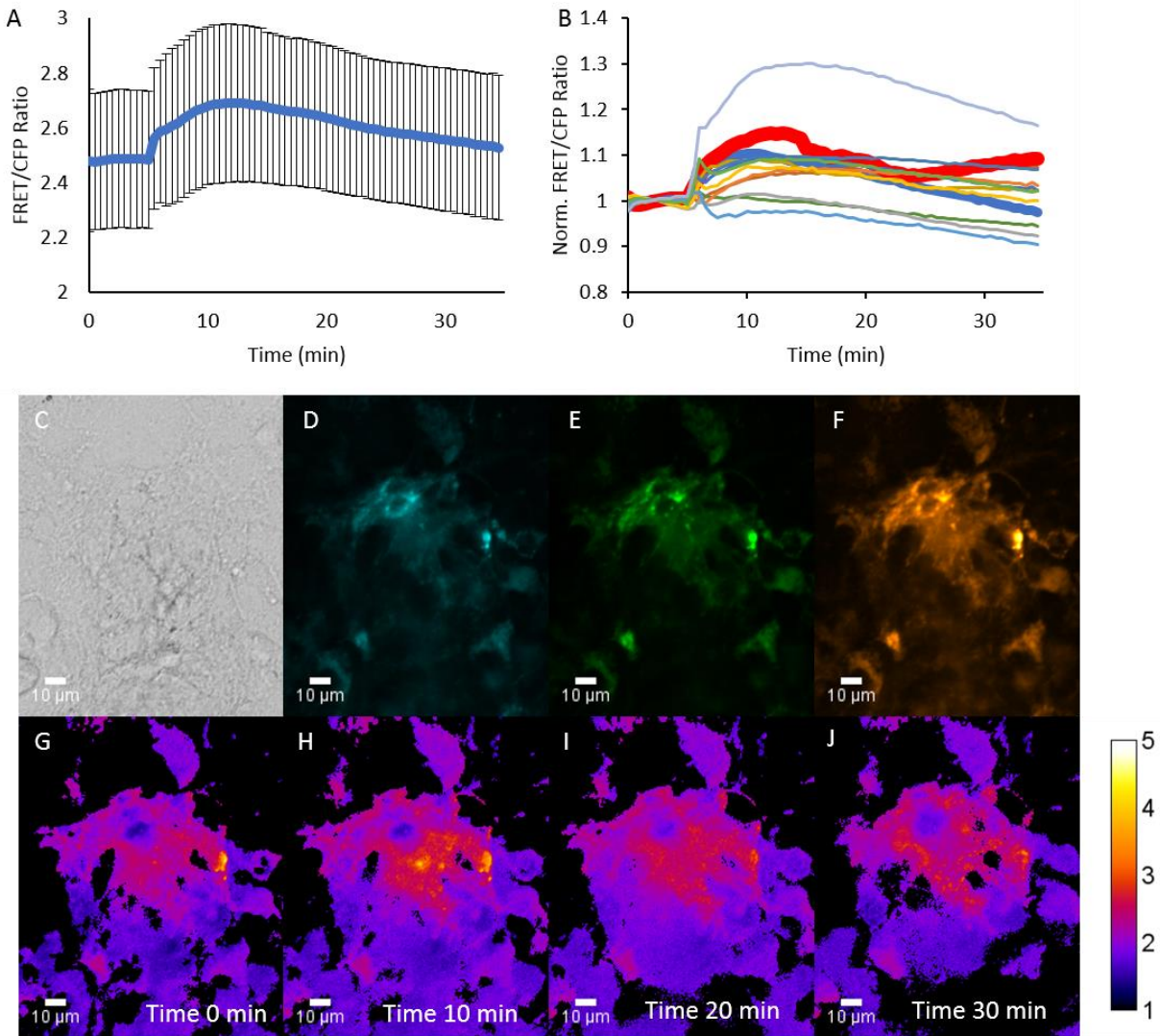


Figure 5.10 KCN Induced Ischemia shows ATP release detected by ECATS2 in Cortical Astrocytes

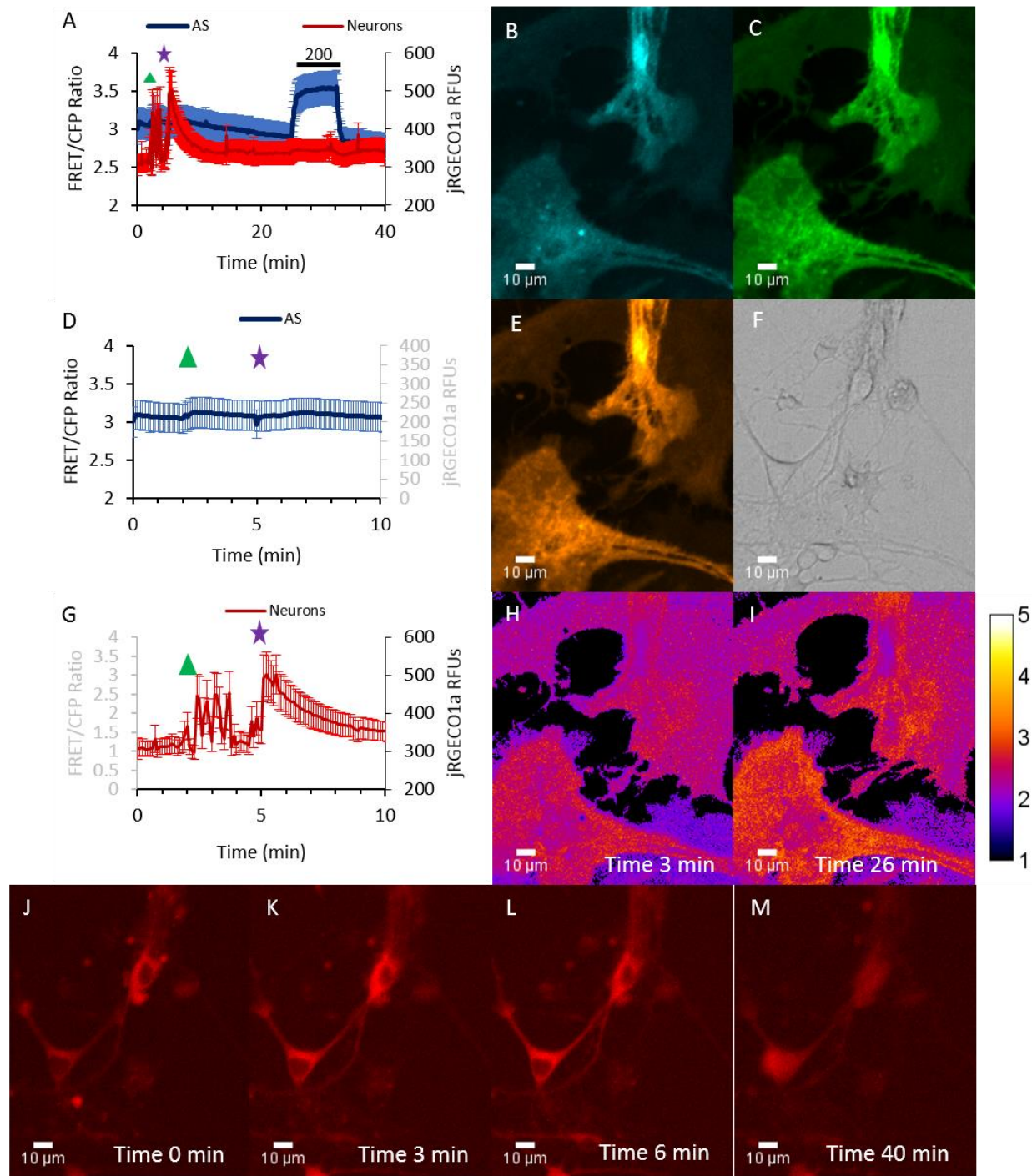
A) Average of all ROIs \pm 95% confidence interval shows potential ATP release. Addition of 10mM KCN at time = 5 minutes. B) Individual cell ROI traces show populations of responders and non-responders n=X cells total. C) DIC channel D) CFP channel E) YFP channel F) FRET channel. G-J FRET/CFP ratio over time of the highlighted red trace responding astrocyte in (B). G) Ratio time=0 minutes shows baseline ratio H) Ratio time=10 minutes shows increase in ratio in response to 10mM KCN after 5 minutes of exposure I) Ratio time=20 elevated ratio continues J) Ratio time=30 minutes. Scalebars are 10 μ m.

5.3.5 Seizure-like Excitotoxicity Models cause no detectable ATP release

Finally, we attempted to test the hypothesis that excitotoxic signaling will lead to ATP release. Large variations in responses across experiments largely showed little or no detectable ATP response by ECATS2 following addition of 100 μ M glutamate and picrotoxin in most experiments. One experiment (not shown) demonstrated a dramatic ATP release from cells, but the neurons and astrocytes withered and died within 10 minutes, and ECATS2 could not be calibrated with an addition of a known ATP concentration. Addition of an excitotoxic mixture of glutamate and picrotoxin did not provide instances of ATP release in most cases. This indicates that if ATP is released in response to an excitotoxic signal, it is below one micromolar and the detection limit of ECATS2. If CD39 were responsible for clearing ATP, we could repeat the experiments in the presence of ARL. A representative experiment is shown in Figure 5.11 where ECATS2 shows no significant changes.

Figure 5.11 Seizure-like Excitotoxicity Model does not show ATP signaling

A) ECATS2 astrocyte and jRGECO1a neuron data represent mean \pm 95% confidence interval overlapping traces showing Mg-free aCSF wash-in at time=2 minutes represented by the green triangle and addition of 100 μ M glutamate and picrotoxin at time=5 minutes represented by the purple star. B) CFP channel of ECATS2. C) YFP channel of ECATS2. D) Zoomed in timescale of ECATS2 ratio showing no significant ATP signals detected by FRET/CFP ratio of ECATS2 following Mg-free aCSF wash-in and addition of 100 μ M glutamate and picrotoxin. E) FRET channel of ECATS2. F) DIC channel of field of view. G) Zoomed in timescale of jRGECO1a signal in neurons to better see cytosolic calcium increases in neurons following Mg-free aCSF wash-in and persisted excitation following 100 μ M glutamate and picrotoxin addition shown by the purple star. H) FRET/CFP ratio at time=3 minutes as an example of baseline. I) FRET/CFP ratio at time=26 minutes as 200 μ M ATP response began to peak. (J-M) Shows jRGECO1a signal in neurons over time at J) time=0 minutes, K) time=3 minutes after Mg-free aCSF wash-in, L) time=6 minutes after 100 μ M glutamate and picrotoxin addition, and M) time=40 minutes after the nuclear envelope has disappeared in neurons.



5.4 Discussion

In this chapter we aimed to test the hypothesis that *in vitro* models of TBI cause an ATP release from cultured astrocytes and neuron-astrocyte co-culture in the micromolar range quantifiable by ECATS2. Our models included mechanical injury, edema, ischemia, and a seizure-like model. While largely successful as a proof-of-concept of ECATS2 function, neuron-astrocyte co-culture dampened or prevented the observed ATP released in cortical astrocytes alone in the edema model.

Hypo-osmotic shock (HOS) was used as a model of brain edema. During edema, astrocytes swell from water influx through aquaporins, then release chloride, ATP, and excitatory amino acids such that water will osmotically be obliged to exit the cell with the anions (Thrane et al.; Darby et al.). When we cultured cortical astrocytes alone, we saw a measurable ATP release nearly as large as twenty micromolar in response to HOS. A release this large would be capable of activating P2Y₂ (EC₅₀ ~ 100 nM) and P2Y₁₁ (EC₅₀ ~ 10 μM) receptors, causing increases in cytosolic Ca²⁺ and cAMP in astrocytes (Jacobson and Muller; Guzman and Gerevich).

However, when we transitioned into neuron-astrocyte co-culture, ATP release was either dampened below ECATS2 detection into nanomolar concentrations or was prevented entirely. The co-culture of neurons and astrocytes changes their expression profiles, increasing expression of aquaporins and astrocyte water regulation mechanisms, which may be responsible for the change in response we observed (Hasel et al.). It is interesting to note that the more physiological model reduces or entirely prevents the ATP signal, further demonstrating a need for greater improvements in ATP binding affinity in the next generation sensor. The need for nanomolar and hundreds of nanomolar dynamic detection by a high affinity extracellular ATP sensor is still required for

further study of purinergic signaling dynamics in the active ranges of the P2X₁ (EC₅₀ ~ 100-700 nM), P2X₅ (EC₅₀ ~500 nM) and P2Y₂ (EC₅₀ ~ 100 nM) receptors (Jacobson and Muller).

We hypothesized that a 50% HOS would be severe enough to kill neurons from outright osmotic shock, excitotoxicity from glutamate release during HOS or a combination of both. Our studies using two-sensor and multi-color imaging revealed calcium increases within neurons and astrocytes shown by jRGECO1a following HOS. Calcium increases within neurons and astrocytes indicate glutamate was released and is binding glutamate receptors on neurons and astrocytes in response to HOS (Guzman and Gerevich; Hasel et al.). Remarkably, the neuron-astrocyte co-cultures show blebbing for only fifteen seconds before recovering and blebbing is reduced. These observations align with the expectation that water management proteins are upregulated in astrocytes when co-cultured with neurons (Hasel et al.).

Mechanical injury was modeled by physically poking and scratching cultured astrocytes with a fire-polished borosilicate glass pipette. We hypothesized that physical disruption of the plasma membrane would cause a detectable ATP release by ECATS2. A direct poke showed ATP release in the upper range of ECATS2 detection, where previous methods with luciferase estimated millimolar level release (Y. Zhang et al.). Millimolar levels would need to be reached to trigger P2X₇ (EC₅₀ ~2-4 mM ATP) receptors that signal to apoptosis and necrosis pathways (Guzman and Gerevich; Jacobson and Muller; Y. Zhang et al.). Our tests using the poke model on a nearby astrocyte did not show ATP detection in ECATS2 expressing astrocytes ~100 μm away. This demonstrates that diffusion is one of the key contributors to clearing ATP signals as observed with membrane attached luciferase methods, and demonstrates the need for high affinity ATP sensors tethered to the cell surface (Y. Zhang et al.). The scratch model yielded an acute ATP release with a fast recovery on only the cell traumatized, while none of the surrounding cells showed a

detectable ATP release. Other groups have used antagonist studies to indicate scratch and stretch models release ATP and activate P2X₂ and P2Y₁ receptors in astrocytes (Neary et al.), and the ratio increase in ECATS2 implies a micromolar increase in ATP capable of driving P2X, P2Y₂ and P2Y₁₁ responses (Jacobson and Muller).

Ischemia was modeled by applying KCN to inhibit cytochrome c oxidase and aerobic respiration. It has been previously reported using a medium-based luciferase method that ATP release from lysosome occurs in response to acute ischemic insult from KCN (Z. Zhang et al.). While several astrocytes responded, indicating micromolar release of ATP, many astrocytes did not show an ATP release as detected by ECATS2. Given the low energy state of ischemia, it is possible that the majority of ATP signaling dynamics occurs in the nanomolar to hundreds of nanomolar ranges. We also modeled seizure-like excitotoxicity in neuron-astrocyte co-culture, since it has been reported that increases in neuronal activity lead to sharp elevations in extracellular ATP (Engel et al.). In our hands, we did not observe an ATP release, as detected by ECATS2, in response to seizure-like excitotoxicity in any cells, indicating that if ATP is released it is on the nanomolar order of magnitude. To better detect ATP signaling dynamics, further increases in ATP binding affinity are required to tailor ECATS2 into a nanomolar affinity sensor in ECATS3.

In conclusion, we aimed to increase the affinity of ECATS1 to create a sensor with a binding affinity for extracellular ATP near nanomolar concentrations to study purinergic signaling in neurons and astrocytes. ECATS2 is a product of two phases of sensor optimization from ECATS1, including increasing the ATP-binding affinity of the epsilon subunit and optimizing the extracellular membrane linker length. Future work to increase ATP affinity in ECATS sensors would be better focused on further increasing the epsilon subunit ATP affinity. Our work in Chapter 3 revealed that extracellular membrane linker optimization may not provide any further

beneficial outcomes and that the 20 nm ER/K linker is best suited for restoring sensor flexibility. Future work studying purinergic signaling events in response to ischemia and excitotoxic neuronal activity require further increases in ECATS ATP affinity. ECATS2 could be paired with sensors of second messengers such as cAMP and calcium as we have demonstrated, in addition to nuclear translocation probes that indicate kinase pathway activation. Upstream and downstream purinergic signaling events could be elucidated and used for therapeutics research in TBI models of edema and mechanical injury.

CHAPTER 6. CONCLUSIONS AND FUTURE PERSPECTIVES

6.1 Protein Engineering Perspectives

In the above studies we have provided the highest affinity extracellular ATP sensor that the field has available right now, ECATS2, as seen in Figure 6.1. Further increases in ATP binding affinity may be better focused on improving the *Bacillus sp PS3* F₀F₁-ATP synthase epsilon subunit ATP affinity, as our work with increasing linker length provided no relationship between linker length and improved affinity. Improvement of the binding site could be done by mutations further from the ATP-interacting residues to rearrange the electrostatics of the binding domain. Less likely, would be the use of an unknown alternative ATP binding domain from a different species of bacteria that has higher ATP affinities than *Bacillus sp PS3* while still providing a conformational change that yields a FRET signal. To our awareness, no such ATP binding domain has been identified.

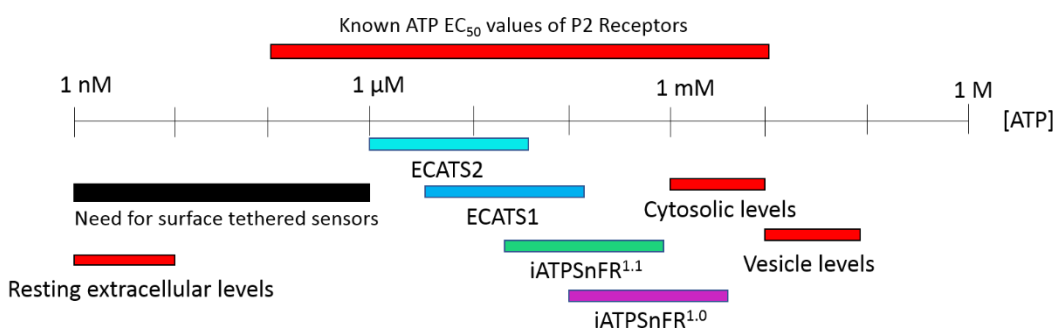


Figure 6.1 ATP Signaling Concentrations and Current Extracellular ATP Sensors

In red: Biological levels of ATP in cells ranging from nanomolar (nM) at resting extracellular levels increasing to hundreds of millimolar (mM) in secretory vesicles. Known EC₅₀ values of P2 receptors span hundreds of nM – tens of mM of ATP. In purple: iATPSnFR^{1.0} with a limit of detection near 100 μM ATP. In green: iATPSnFR^{1.1} with a limit of detection near 30 μM ATP. In blue: ECATS1 with a limit of detection near 4 μM ATP. In teal: ECATS2 with a limit of detection near 1 μM ATP produced by the work described in Chapters 2 and 3. In black: ATP magnitudes that still require sensors to study purinergic signaling dynamics capable of activating the highest affinity P2 receptors. Other sensors produced by: (Lobas et al.; Conley et al.).

It should be noted that despite our increase in extracellular ATP affinity by addition of the 20 nm ER/K linker, its respective R103A/R115A protein solution observed ATP binding affinity is still 18.5-fold higher. The remaining 18.5-fold difference in binding affinity between the sensor in solution and ECATS2 might be explained by the differences in the ionic strength and osmolality of the buffers used in protein solution versus live cells. As we observed in Chapter 4, changes in osmolality affects sensor function, but not enough to cause a near 20-fold shift in binding affinity. Alternatively, the semi-rigid α -helix ER/K linker may not be completely restoring freedom-of-movement to ECATS2, and long, flexible glycine/serine (G/S) linkers or the combination of ER/K and G/S linkers may further improve extracellular ATP binding affinity (Sivaramakrishnan and Spudich). Investigating these manipulations in ECATS2 may lead to a higher affinity ECATS3. Production of an even higher affinity sensor is still necessary to study dynamics of purinergic signaling at ATP concentrations capable of evoking responses in the highest affinity P2 receptors, P2X₁ and P2Y₂ (Table 4).

Table 4 Purinergic Receptors in the Brain

Receptor	ATP EC₅₀
P2X ₇	2-4 mM
P2Y ₁₁ *	10 μ M
P2X ₄	1-10 μ M
P2X ₂	2-8 μ M
P2X ₃	1 μ M
P2X ₁ [#]	100-700 nM
P2Y ₂ [#]	100 nM

* = no rodent homologue to study; [#] = no sensor available to study receptor signaling

6.2 Using ECATS2 to Study Purinergic Signaling

Surface-tethered fluorescent sensors capable of directly detecting the agonist (ATP) that binds P2 receptors (Table 4) have not been available until recently (Figure 6.1). Firefly luciferase-luciferin ATP detection methods paved the way for surface tethered sensors by describing which cell types are suspect of releasing ATP in response to insults and signals, however the magnitude of ATP release is not known (Gould and Subramani; Y. Zhang et al.; Beigi et al.; Praetorius and Leipziger; Darby et al.). The advantage of surface tethered sensors includes direct detection of the local ATP concentration at the membrane, targeting sensor expression to desired cell types, and they do not consume ATP to produce their signal. Previous work on purinergic signaling and P2 receptor roles in disease have been studied through knock-out animal models, measurement of ATP with luciferase methods, or prevention of ATP signaling by use of non-specific P2R antagonists or application of excess apyrase (Darby et al.; Y. Zhang et al.; Praetorius and Leipziger; Beigi et al.; Thrane et al.; Bender et al.).

ECATS2 provides direct visualization of ATP signaling at concentrations that activates receptors P2X₂-P2X₄ and P2Y₁₁, where previously ECATS1 could reliably study ATP concentrations capable of activating P2X₄ and P2Y₁₁ signaling. All four of these P2 receptors are present in the central nervous system in humans and the knock-out animals for P2X₃ and P2X₄ suggest these receptors play a role in hippocampal long-term depression. ATP and adenosine are known to play a role in hippocampal long-term potentiation (LTP) and long-term depression (LTD), but previous studies have had to rely on the indirect ATP measurements described above or rely solely on inhibitors (Duster et al.). Now that the tools exist to directly observe local ATP signaling events at concentrations capable of activating these P2 receptors, researchers can pair sensors like ECATS2 with pharmacological studies to elucidate purinergic signaling mechanisms of learning and memory without relying on indirect detection of ATP.

The issue with indirect detection of ATP lies on the assumption that several of these receptors studied are activated by ATP alone. While we know this is not the case since receptors have multiple potential ligands, and the purinergic receptors are no different. For example, P2Y₂ can be activated by UTP ($EC_{50} = 10 \text{ nM}$) at concentrations 10-fold lower than ATP (Jacobson and Muller). Studies that rely on indirect methods to assume that ATP is responsible for driving these receptor signals may be studying the wrong ligands as the intracellular response often reported are converging response pathways that can be activated by a large variety of signaling molecules. In our hands, we never observed ATP release at concentrations 1 μM or higher in neuron-astrocyte co-culture using ECATS2. This indicates that either ATP signaling is occurring at lower magnitudes or other agonists are responsible for driving these responses and not ATP. If ATP is not responsible for these signaling events, what other ligands could be binding these receptors to drive these responses? The most likely candidates are other purines such as ADP, AMP, adenosine, UTP and UDP which currently have no high-affinity extracellular sensors to study their signaling dynamics.

REFERENCES

- Beigi, Reza, et al. "Detection of Local ATP Release from Activated Platelets Using Cell Surface-Attached Firefly Luciferase." *American Journal of Physiology-Cell Physiology*, vol. 276, no. 1, 1999, pp. C267–78, doi:10.1016/s0002-7138(09)61913-0.
- Bender, A. S., et al. "Involvement of Second Messengers and Protein Phosphorylation in Astrocyte Swelling." *Canadian Journal of Physiology and Pharmacology*, vol. 70, no. S1, 1991, pp. S362–66, doi:10.1139/y92-284.
- Burda, Joshua E., et al. "Astrocyte Roles in Traumatic Brain Injury." *Experimental Neurology*, vol. 275, Elsevier Inc., 2016, pp. 305–15, doi:10.1016/j.expneurol.2015.03.020.
- Burnstock, Geoffrey. "An Introduction to the Roles of Purinergic Signalling in Neurodegeneration, Neuroprotection and Neuroregeneration." *Neuropharmacology*, vol. 104, 2016, pp. 4–17.
- Coloma, M. Josefina, et al. "Novel Vectors for the Expression of Antibody Molecules Using Variable Regions Generated by Polymerase Chain Reaction." *Journal of Immunological Methods*, vol. 152, no. 1, 1992, pp. 89–104, doi:10.1016/0022-1759(92)90092-8.
- Conley, Jason M., et al. "Imaging Extracellular ATP with a Genetically-Encoded, Ratiometric Fluorescent Sensor." *PLoS ONE*, vol. 12, no. 11, 2017, pp. 1–24, doi:10.1371/journal.pone.0187481.
- Dana, Hod, et al. "Sensitive Red Protein Calcium Indicators for Imaging Neural Activity." *Elife*, vol. 5, 2016.
- Darby, Mark, et al. "ATP Released From Astrocytes During Swelling Activates Chloride Channels." *Journal of Neurophysiology*, vol. 89, no. 4, 2006, pp. 1870–77, doi:10.1152/jn.00510.2002.
- Duster, Robert, et al. "Purinergic Signaling and Hippocampal Long-Term Potentiation." *Current Neuropharmacology*, vol. 12, no. 1, 2013, pp. 37–43, doi:10.2174/1570159x113119990045.
- Engel, Tobias, et al. "ATPergic Signalling during Seizures and Epilepsy." *Neuropharmacology*, vol. 104, Elsevier Ltd, 2016, pp. 140–53, doi:10.1016/j.neuropharm.2015.11.001.
- Gao, Kai, et al. "Traumatic Scratch Injury in Astrocytes Triggers Calcium Influx to Activate the JNK/c-Jun/AP-1 Pathway and Switch on GFAP Expression." *Glia*, vol. 61, no. 12, 2013, pp. 2063–77, doi:10.1002/glia.22577.

- Gould, Stephen J., and Suresh Subramani. "Firefly Luciferase as a Tool in Molecular and Cell Biology." *Analytical Biochemistry*, vol. 175, no. 1, 1988, pp. 5–13, doi:10.1016/0003-2697(88)90353-3.
- Gronwald, R. G., et al. "Cloning and Expression of a cDNA Coding for the Human Platelet-Derived Growth Factor Receptor: Evidence for More than One Receptor Class." *Proceedings of the National Academy of Sciences*, vol. 85, no. 10, 1988, pp. 3435–39, doi:10.1073/pnas.85.10.3435.
- Guzman, Segundo J., and Zoltan Gerevich. "P2Y Receptors in Synaptic Transmission and Plasticity: Therapeutic Potential in Cognitive Dysfunction." *Neural Plasticity*, vol. 2016, 2016, pp. 1–12, doi:10.1155/2016/1207393.
- Harada, Kazuki, et al. "Red Fluorescent Protein-Based cAMP Indicator Applicable to Optogenetics and in Vivo Imaging." *Scientific Reports*, vol. 7, no. 1, Springer US, 2017, pp. 1–9, doi:10.1038/s41598-017-07820-6.
- Hasel, Philip, et al. "Neurons and Neuronal Activity Control Gene Expression in Astrocytes to Regulate Their Development and Metabolism." *Nature Communications*, vol. 8, no. May, 2017, p. 15132, doi:10.1038/ncomms15132.
- Hélix, N., et al. "Inhibition of the Endogenous Volume-Regulated Anion Channel (VRAC) in HEK293 Cells by Acidic Di-Aryl-Ureas." *Journal of Membrane Biology*, vol. 196, no. 2, 2003, pp. 83–94, doi:10.1007/s00232-003-0627-x.
- Hoffmann, Else K., et al. "Physiology of Cell Volume Regulation in Vertebrates." *Physiological Reviews*, vol. 89, no. 1, 2009, pp. 193–277, doi:10.1152/physrev.00037.2007.
- Horovitz, Amnon. "Double-Mutant Cycles: A Powerful Tool for Analyzing Protein Structure and Function." *Folding and Design*, vol. 1, no. 6, 1996, pp. 121–26, doi:10.1016/S1359-0278(96)00056-9.
- Imamura, Hiromi, et al. "Visualization of ATP Levels inside Single Living Cells with Fluorescence Resonance Energy Transfer-Based Genetically Encoded Indicators." *Proceedings of the National Academy of Sciences of the United States of America*, vol. 106, no. 37, 2009, pp. 15651–56, doi:10.1073/pnas.0904764106.
- Jacobson, Kenneth A., and Christa E. Muller. "Medicinal Chemistry of Adenosine, P2Y and P2X Receptors." *Neuropharmacology*, vol. 104, 2016, pp. 31–49, doi:10.1002/cnrc.27633.Percutaneous.

- James, Greg, and Arthur M. Butt. "P2Y and P2X Purinoceptor Mediated Ca²⁺ Signalling in Glial Cell Pathology in the Central Nervous System." *European Journal of Pharmacology*, vol. 447, no. 2–3, 2002, pp. 247–60, doi:10.1016/S0014-2999(02)01756-9.
- Kato-Yamada, Yasuyuki. "High Affinity Nucleotide-Binding Mutant of the ε Subunit of Thermophilic F1-ATPase." *Biochemical and Biophysical Research Communications*, vol. 469, no. 4, 2016, pp. 1129–32, doi:10.1016/j.bbrc.2015.12.121.
- Kimelberg, Harold K., et al. "Anion Channels in Astrocytes: Biophysics, Pharmacology, and Function." *Glia*, vol. 54, 2006, pp. 747–57.
- Krah, Alexander, et al. "The Structural Basis of a High Affinity ATP Binding e Subunit from a Bacterial ATP Synthase." *PLoS ONE*, vol. 12, no. 5, 2017, pp. 1–15, doi:10.1371/journal.pone.0177907.
- Lacin, Emre, et al. "Construction of Cell-Based Neurotransmitter Fluorescent Engineered Reporters (CNiFERs) for Optical Detection of Neurotransmitters In Vivo." *Journal of Visualized Experiments*, no. 111, 2016, pp. 1–13, doi:10.3791/53290.
- Lobas, Mark A., et al. "A Genetically Encoded Single-Wavelength Sensor for Imaging Cytosolic and Cell Surface ATP." *Nature Communications*, vol. 10, no. 1, Springer US, 2019, doi:10.1038/s41467-019-08441-5.
- Mulligan, Sean J., and Brian A. MacVicar. "VRACs CARVe a Path for Novel Mechanisms of Communication in the CNS." *Science's STKE : Signal Transduction Knowledge Environment*, vol. 2006, no. 357, 2006, pp. 1–4, doi:10.1126/stke.3572006pe42.
- Neary, Joseph T., et al. "Activation of Extracellular Signal-Regulated Kinase by Stretch-Induced Injury in Astrocytes Involves Extracellular ATP and P2 Purinergic Receptors." *The Journal of Neuroscience : The Official Journal of the Society for Neuroscience*, vol. 23, no. 6, 2003, pp. 2348–56, <http://www.ncbi.nlm.nih.gov/pubmed/12657694>.
- Pérez-Ortiz, José M., et al. "Mechanical Lesion Activates Newly Identified NFATc1 in Primary Astrocytes: Implication of ATP and Purinergic Receptors." *European Journal of Neuroscience*, vol. 27, no. 9, 2008, pp. 2453–65, doi:10.1111/j.1460-9568.2008.06197.x.
- Praetorius, Helle A., and Jens Leipziger. "ATP Release from Non-Excitable Cells." *Purinergic Signalling*, vol. 5, no. 4, 2009, pp. 433–46, doi:10.1007/s11302-009-9146-2.
- Rossi, David J., et al. "Astrocyte Metabolism and Signaling during Brain Ischemia." *Nature Reviews Neuroscience*, vol. 10, no. 11, 2007, pp. 1–4, doi:10.1038/xxxx.

- Schachter, Joel B., et al. "HEK293 Human Embryonic Kidney Cells Endogenously Express the P2Y1 and P2Y2 Receptors." *Neuropharmacology*, vol. 36, no. 9, 1997, pp. 1181–87, doi:10.1016/S0028-3908(97)00138-X.
- Schwiebert, Erik M., et al. "CFTR Regulates Outwardly Rectifying Chloride Channels through an Autocrine Mechanism Involving ATP." *Cell*, vol. 81, no. 7, 1995, pp. 1063–73, doi:10.1016/S0092-8674(05)80011-X.
- Sivaramakrishnan, S., and J. A. Spudich. "Systematic Control of Protein Interaction Using a Modular ER/K -Helix Linker." *Proceedings of the National Academy of Sciences*, vol. 108, no. 51, 2011, pp. 20467–72, doi:10.1073/pnas.1116066108.
- Swanson, Carter J., and Sivaraj Sivaramakrishnan. "Harnessing the Unique Structural Properties of Isolated α -Helices." *Journal of Biological Chemistry*, vol. 289, no. 37, 2014, pp. 25460–67, doi:10.1074/jbc.R114.583906.
- Tantama, Mathew, et al. "Imaging Energy Status in Live Cells with a Fluorescent Biosensor of the Intracellular ATP-to-ADP Ratio." *Nature Communications*, vol. 4, no. May, 2013, doi:10.1038/ncomms3550.
- Thrane, A. S., et al. "Critical Role of Aquaporin-4 (AQP4) in Astrocytic Ca²⁺ Signaling Events Elicited by Cerebral Edema." *Proceedings of the National Academy of Sciences*, vol. 108, no. 2, 2011, pp. 846–51, doi:10.1073/pnas.1015217108.
- Trautmann, Alain. "Extracellular ATP in the Immune System: More than Just a 'Danger Signal.'" *Science Signaling*, vol. 2, no. 56, 2009, pp. 1–4, doi:10.1126/scisignal.256pe6.
- Wang, Y., et al. "Autocrine Signaling through ATP Release Represents a Novel Mechanism for Cell Volume Regulation." *Proceedings of the National Academy of Sciences of the United States of America*, vol. 93, no. 21, 1996, pp. 12020–25, doi:10.1073/pnas.93.21.12020.
- Yagi, Hiromasa, et al. "Conformational Change of H⁺-ATPase β Monomer Revealed on Segmental Isotope Labeling NMR Spectroscopy." *Journal of the American Chemical Society*, vol. 126, no. 50, 2004, pp. 16632–38, doi:10.1021/ja045279o.
- Yuen, Alan W. C., and Josemir W. Sander. "Can Magnesium Supplementation Reduce Seizures in People with Epilepsy? A Hypothesis." *Epilepsy Research*, vol. 100, no. 1–2, 2012, pp. 152–56, doi:10.1016/j.eplepsyres.2012.02.004.
- Zhang, Yun, et al. "Imaging Localized Astrocyte ATP Release with Firefly Luciferase Beads Attached to the Cell Surface." *Analytical Chemistry*, vol. 80, no. 23, 2008, pp. 9316–25, doi:10.1021/ac801701w.

Zhang, Zhijun, et al. "Regulated ATP Release from Astrocytes through Lysosome Exocytosis." *Nature Cell Biology*, vol. 9, no. 8, 2007, pp. 945–53, doi:10.1038/ncb1620.

Zhao, Hai, et al. "What Else Can CD39 Tell Us?" *Frontiers in Immunology*, vol. 8, no. JUN, 2017, pp. 310–17, doi:10.3389/fimmu.2017.00727.

Zhao, Yuzheng, and Yi Yang. "Profiling Metabolic States with Genetically Encoded Fluorescent Biosensors for NADH." *Current Opinion in Biotechnology*, vol. 31, Elsevier Ltd, 2015, pp. 86–92, doi:10.1016/j.copbio.2014.08.007.

VITA

HONORS & AWARDS

Second Place Best Ph.D. Poster, Ohio Valley Society of Toxicology Annual Meeting (\$100)	
November 2015	
Grand Finish Grant, Grand Valley State University (\$1000)	November 2012
Moomer's Homemade Ice Cream Scholarship (\$250)	June 2010

POSTERS & CONFERENCE PROCEEDINGS

-
1. Dan Cholger, Steve....., and Mathew Tantama “*poster*” – The Protein Society 2018 Annual Meeting in Boston – July X 2019
 2. Dan Cholger, Xue Fu, and Wei Zheng “*Increased Interactive Toxicities on the Blood-CSF-Barrier Following Co-Exposure to Mangangese (Mn) and Lead (Pb), in vitro*” – Ohio Valley of Toxicology 2016 Student meeting platform presentation – June 20th 2016
 3. Dan Cholger, Xue Fu, and Wei Zheng “*Increased Interactive Toxicities on the Blood-CSF-Barrier Following Co-Exposure to Mangangese (Mn) and Lead (Pb), in vitro*” – Purdue Office of Interdisciplinary Graduate Studies (OIGP) Spring Reception Poster session – May 2nd 2016
 4. Dan Cholger, Xue Fu, and Wei Zheng “*Increased Interactive Toxicities on the Blood-CSF-Barrier Following Co-Exposure to Mangangese (Mn) and Lead (Pb), in vitro*” – Purdue Public Health Symposium Poster – April 5th 2016
 5. Dan Cholger, Xue Fu, and Wei Zheng “*Increased Interactive Toxicities on the Blood-CSF-Barrier Following Co-Exposure to Mangangese (Mn) and Lead (Pb), in vitro*” – Purdue Health and Disease Research Poster – March 28th 2016

6. Dan Cholger, Xue Fu, and Wei Zheng “*Increased Interactive Toxicities on the Blood-CSF-Barrier Following Co-Exposure to Mangangese (Mn) and Lead (Pb), in vitro*” – Society of Toxicology 55th Annual Meeting in New Orleans – March 15th 2016
7. Dan Cholger, Xue Fu, and Wei Zheng “*Increased Interactive Toxicities on the Blood-CSF-Barrier Following Co-Exposure to Mangangese (Mn) and Lead (Pb), in vitro*” – PULSe Spring Research Symposium Poster – February 25th 2016
8. Dan Cholger, Xue Fu, and Wei Zheng “*Increased Interactive Toxicities on the Blood-CSF-Barrier Following Co-Exposure to Mangangese (Mn) and Lead (Pb), in vitro*” – Ohio Valley of Toxicology 2015 Annual Meeting – November 13th 2015
9. Dan Cholger, Jason Connely, and Mathew Tantama “*Fluorescent Protein Biosensors to Study Purinergic Signaling from Astrocytes*” – PULSe Spring Awards Reception Poster – April 20th 2015
10. Dan Cholger, Albert Dionese, Nick Poirier, Avery Andrus, Randi Curtis, and Eric S. Ramsson “*Paraffin Wax Sealing of Carbon Fiber Microelectrodes is a Comparable Electrode Sealing Agent to Epoxy*” - West Michigan Regional Undergraduate Science Research Conference Poster – November 16th 2013
11. Dan Cholger and Albert Dionese, Randi Curtis, Renah Farhan, and Eric S. Ramsson “*Tryptophan Modification Enhances Neurotransmitter Recordings*” Grand Valley State University Undergraduate Research Fair Poster - October 1st 2013
12. Dan Cholger and Albert Dionese, Randi Curtis, Renah Farhan, and Eric S. Ramsson “*Tryptophan Modification Enhances Neurotransmitter Recordings*” Society for Neuroscience-Michigan Chapter Poster - May 13th 2013

13. Dan Cholger and Albert Dionese, Randi Curtis, Renah Farhan, and Eric S. Ramsson

"Tryptophan Modification Enhances Neurotransmitter Recordings" Grand Valley State

University Undergraduate Research Fair Poster - October 2nd 2012

SEMINARS AND PRESENTATIONS GIVEN

Purdue University School of Health Sciences Seminar, hosted by Dr. Wei Zheng – February 7th, 2017

Ohio Valley of Toxicology 2016 Student meeting platform presentation – June 20th 2016

Grand Valley State University Biomedical Sciences Seminar, invited by Dr. Eric Ramsson – April 29th, 2016

CONFERENCES ATTENDED

The Protein Society Annual Meeting – Boston, MA	2018
Ohio Valley Society of Toxicology Annual Meeting (OVSoT) – Indianapolis, IN	2016
Ohio Valley Society of Toxicology Student Meeting (OVSoT) – Cincinnati, OH	2016
Society of Toxicology 55 th Annual Meeting – New Orleans, LA	2016
Ohio Valley Society of Toxicology Annual Meeting (OVSoT) – Highland Heights, KY	2015
West Michigan Regional Undergraduate Science Research Conference—Grand Rapids, MI	2013
Society for Neuroscience-Michigan Chapter—Ann Arbor, MI	2013

PUBLICATIONS

1. Cholger, Dan, Jason Conley, Steve Valentino, Saranya Radhakrishnan, Elaine Colomb, and Mathew Tantama. "Engineering A High Affinity Extracellular ATP Sensor for the Study of Purinergic Signaling." *Manuscript prepared for submission* (2019).
2. Fu, Sherleen, Wendy Jiang, Xiang Gao, Andrew Zeng, **Daniel Cholger**, Jason Cannon, Jinhui Chen, and Wei Zheng. "Aberrant adult Neurogenesis in the subventricular zone-rostral migratory stream-olfactory bulb system following subchronic manganese exposure." *Toxicological Sciences* (2016)
3. Fu, Sherleen, **Daniel Cholger**, and Wei Zheng. "Approaches in Evaluating In Vivo Mn Effect on Adult Neurogenesis Response." *Toxicological Sciences* 152, no. 2 (2016): 260-261.
4. Ramsson, Eric S., **Daniel Cholger**, Albert Dionise, Nicholas Poirier, Avery Andrus, and Randi Curtiss. "Characterization of fast-scan cyclic voltammetric electrodes using paraffin as an effective sealant with in vitro and in vivo applications." *PloS one* 10, no. 10 (2015)